APPENDIX A: INDIVIDUAL SITE AND BOREHOLE LOCATIONS

As noted in Table A1: Lowland Boring IDs CHUMR-1, CHUMR-2 and CHUMR-3 (Table A.1) refer to Test Site #3 (Figures 2.6 and 5.2); Upland Boring IDs CHUMR-1, CHUMR-2 and CHUMR-3 refer to Test Site #15 (Figures 2.6 and A.1); Boring ID BHUMR-1 refers to Test Site #19 (Figures 2.6 and A.2); Boring ID BHUMR-2 refers to Test Site #25 (Figures 2.6 and A.3); Boring ID BHUMR-5 refers to Test Site #31 (Figures 2.6 and 5.11); Boring ID BHUMR-6 refers to Test Site #25 (Figures 2.6 and A.3); Boring ID BHUMR-5 refers to Test Site #10 (Figures 2.6 and 5.9).

Boring ID	Site ID	Struct. ID	Subsurface Exploration & Sampling Requirements
---------- Upland Locations ----------			
BHUMR-1	19	A37230	SPT and tube sampling to 100’ max (see above)
BHUMR-2	25	none	SPT and tube sampling to 100’ max (see above)
CHUMR-1	15	A2572W	SPT and tube sampling for CH test, 150’max (see above)
CHUMR-2	15	A2572W	Hole for Crosshole test – 150’ cased with 3”- PVC pipe
CHUMR-3	15	A2572W	Hole for Crosshole test – 150’ cased with 3”- PVC pipe
---------- Lowland Locations ----------			
BHUMR-5	31	A2201U	SPT and tube sampling to 100’ max (see above)
BHUMR-6	10	A32440	SPT and tube sampling to 100’ max (see above)
CHUMR-1	3	A3683U	SPT and tube sampling for CH test, 150’max (see above)
CHUMR-2	3	A3683U	Hole for Crosshole test – 150’ cased with 3”- PVC pipe
CHUMR-3	3	A3683U	Hole for Crosshole test – 150’ cased with 3”- PVC pipe

Table A1: Drilling and borehole detailed plan (site, structure and sampling).

Figure A.1: Soil samples with Upland Boring IDs CHUMR-1, CHUMR-2 and CHUMR-3 were extracted from the borehole at Test Site #15 (Figure 2.6).

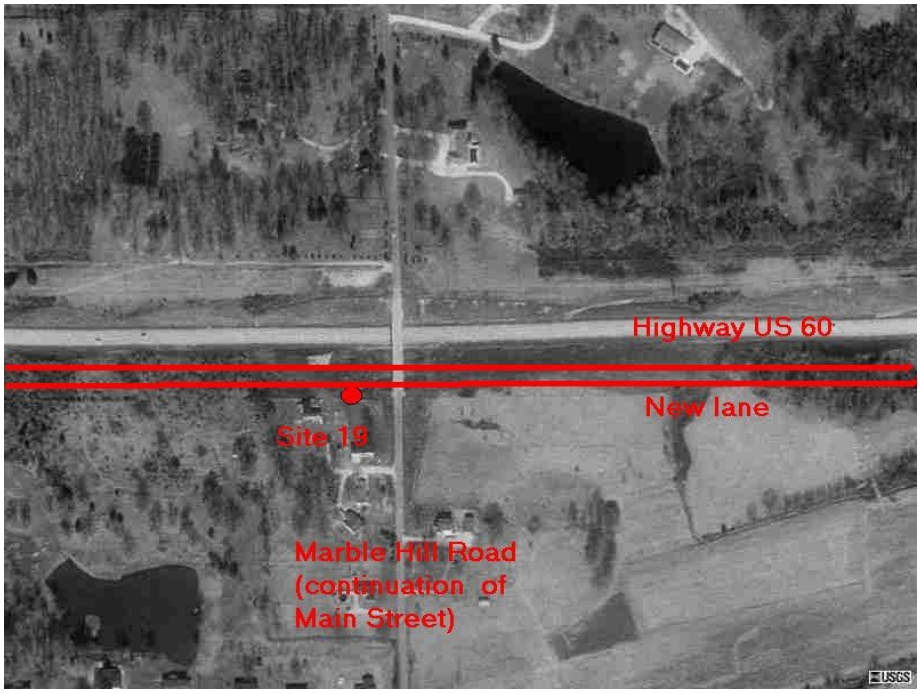

Figure A.2: Soil samples with Boring ID BHUMR-1 were extracted from the borehole at Test Site #19 (Figure 2.6).

Figure A.3: Soil samples with Boring ID BHUMR-2 were extracted from the borehole at Test Site #25 (Figure 2.6).

APPENDIX B: GEOTECHNICAL BOREHOLE LOGS

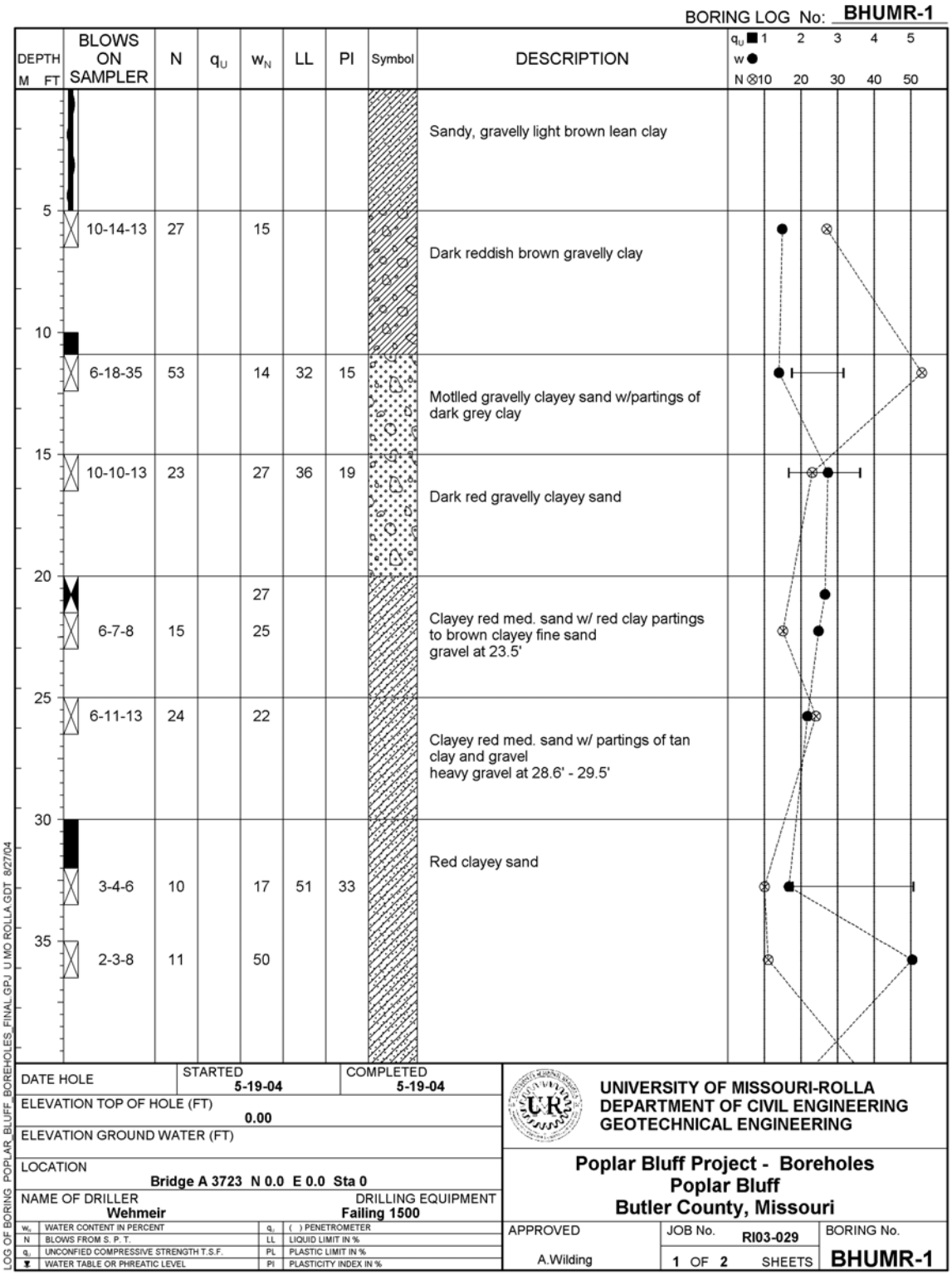

Figure B.1: Geotechnical borehole log for Boring ID BHUMR-1 (Appendix A).

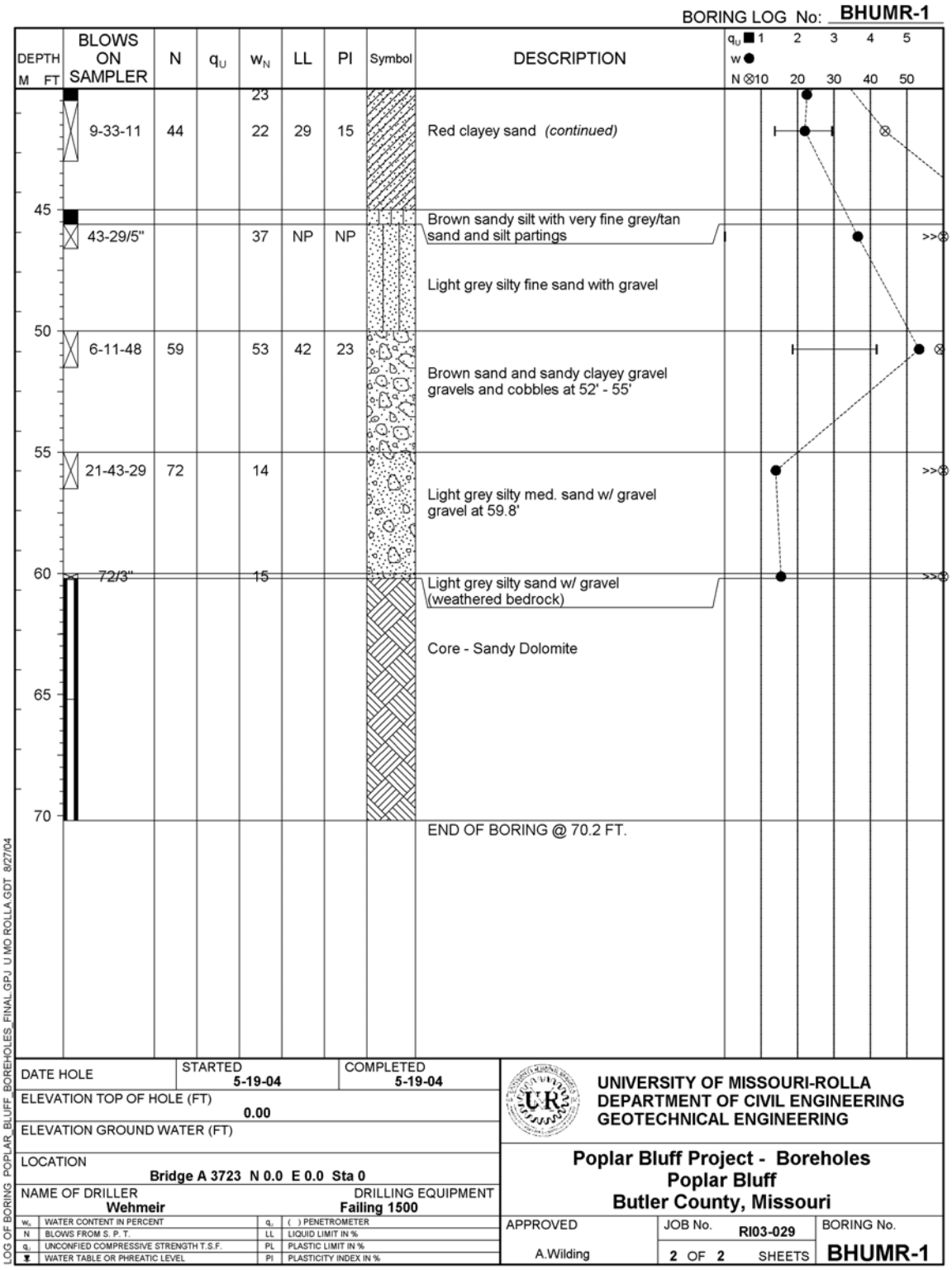

Figure B.2: Geotechnical borehole log for Boring ID BHUMR-1 (Appendix A).

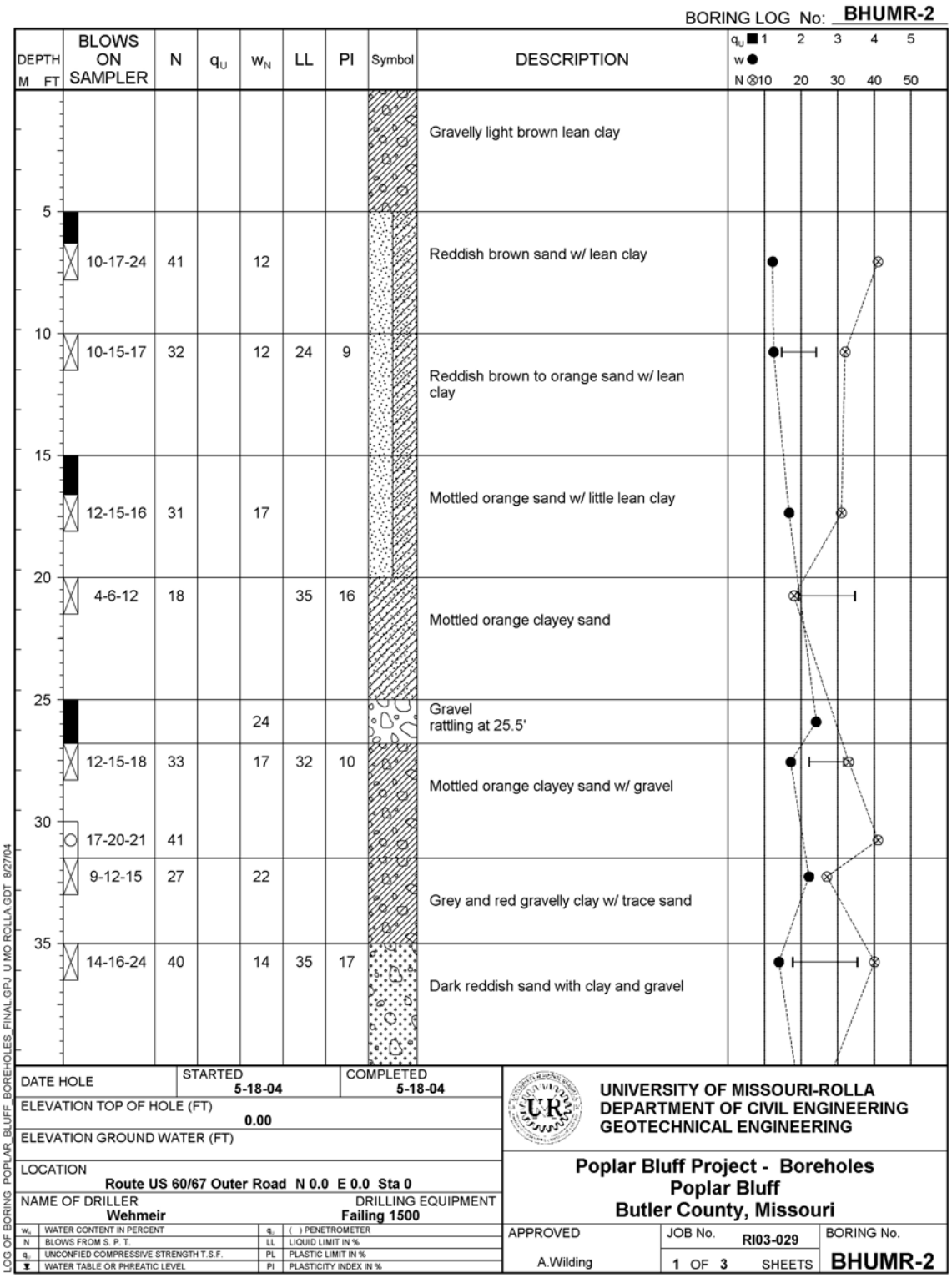

Figure B.3: Geotechnical borehole log for Boring ID BHUMR-2 (Appendix A).

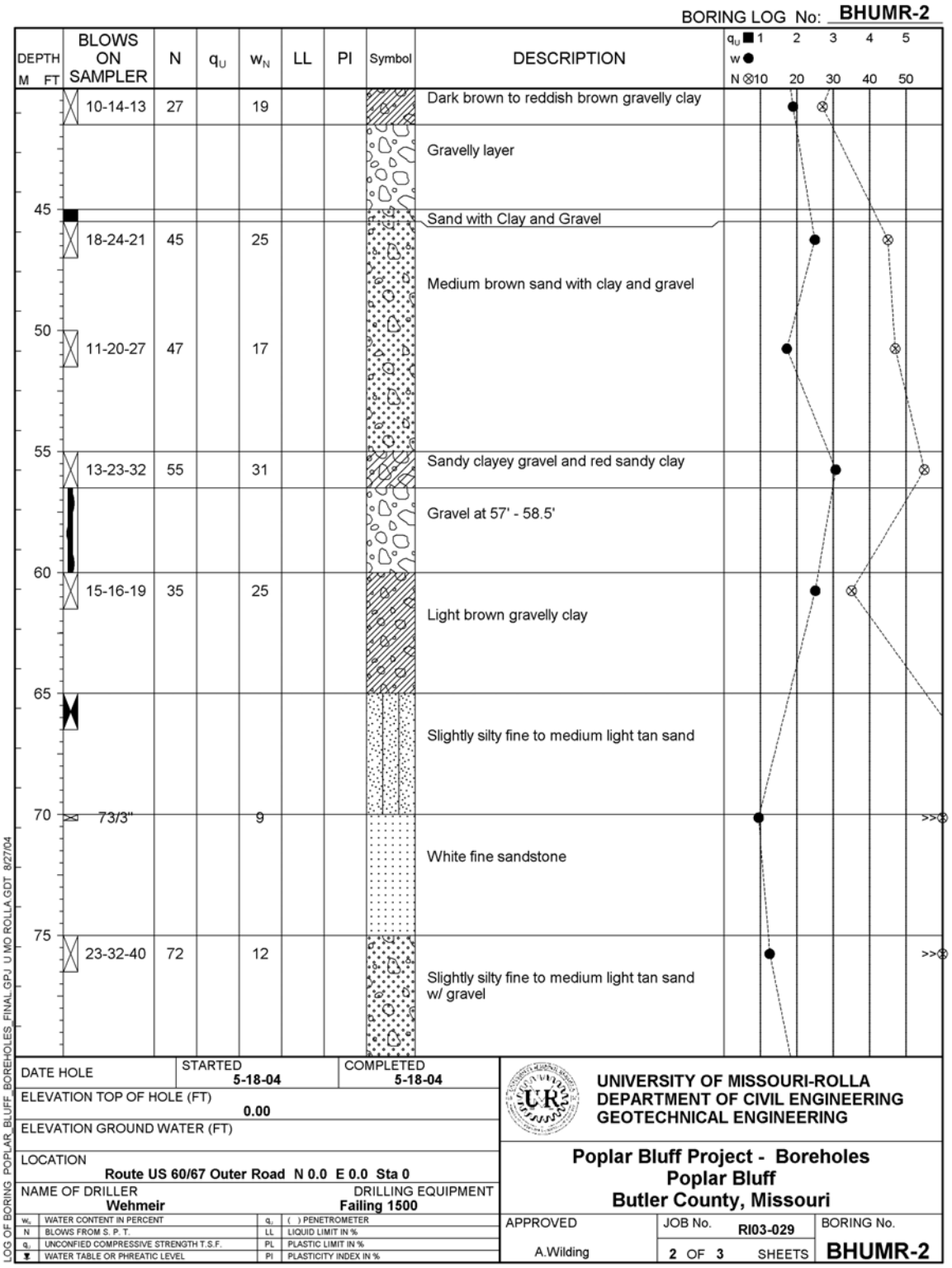

Figure B.4: Geotechnical borehole log for Boring ID BHUMR-2 (Appendix A).

BORING LOG No: **BHUMR-2**

DEPTH M FT	BLOWS ON SAMPLER	N	q_U	w_N	LL	PI	Symbol	DESCRIPTION
	78/10"			19				Brown silty fine to medium sand w/ gravel
85	25-22-28	50		25				Mottled silty fine to medium sand w/ gravel
90	40-19-20	39		28				
95	20-21-29	50		17				Mottled silty fine to medium, sand w/ gravel
100	27-23-20	43		18	28	10		Mottled silty fine to medium sand w/ gravel and trace red clay
								END OF BORING @ 101.5 FT.

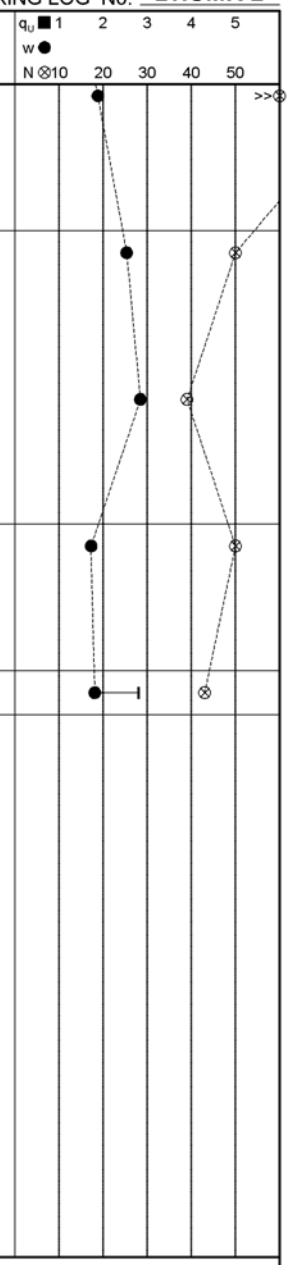

DATE HOLE	STARTED 5-18-04	COMPLETED 5-18-04
ELEVATION TOP OF HOLE (FT)	0.00	
ELEVATION GROUND WATER (FT)		
LOCATION	Route US 60/67 Outer Road N 0.0 E 0.0 Sta 0	
NAME OF DRILLER	Wehmeir	DRILLING EQUIPMENT Failing 1500

w_c	WATER CONTENT IN PERCENT	q_p	( ) PENETROMETER
N	BLOWS FROM S. P. T.	LL	LIQUID LIMIT IN %
q_u	UNCONFIED COMPRESSIVE STRENGTH T.S.F.	PL	PLASTIC LIMIT IN %
▼	WATER TABLE OR PHREATIC LEVEL	PI	PLASTICITY INDEX IN %

UNIVERSITY OF MISSOURI-ROLLA
DEPARTMENT OF CIVIL ENGINEERING
GEOTECHNICAL ENGINEERING

Poplar Bluff Project - Boreholes
Poplar Bluff
Butler County, Missouri

APPROVED	JOB No.	BORING No.
A.Wilding	RI03-029	BHUMR-2
	3 OF 3 SHEETS	

LOG OF BORING POPLAR_BLUFF_BOREHOLES_FINAL.GPJ U MO ROLLA.GDT 8/27/04

Figure B.5: Geotechnical borehole log for Boring ID BHUMR-2 (Appendix A).

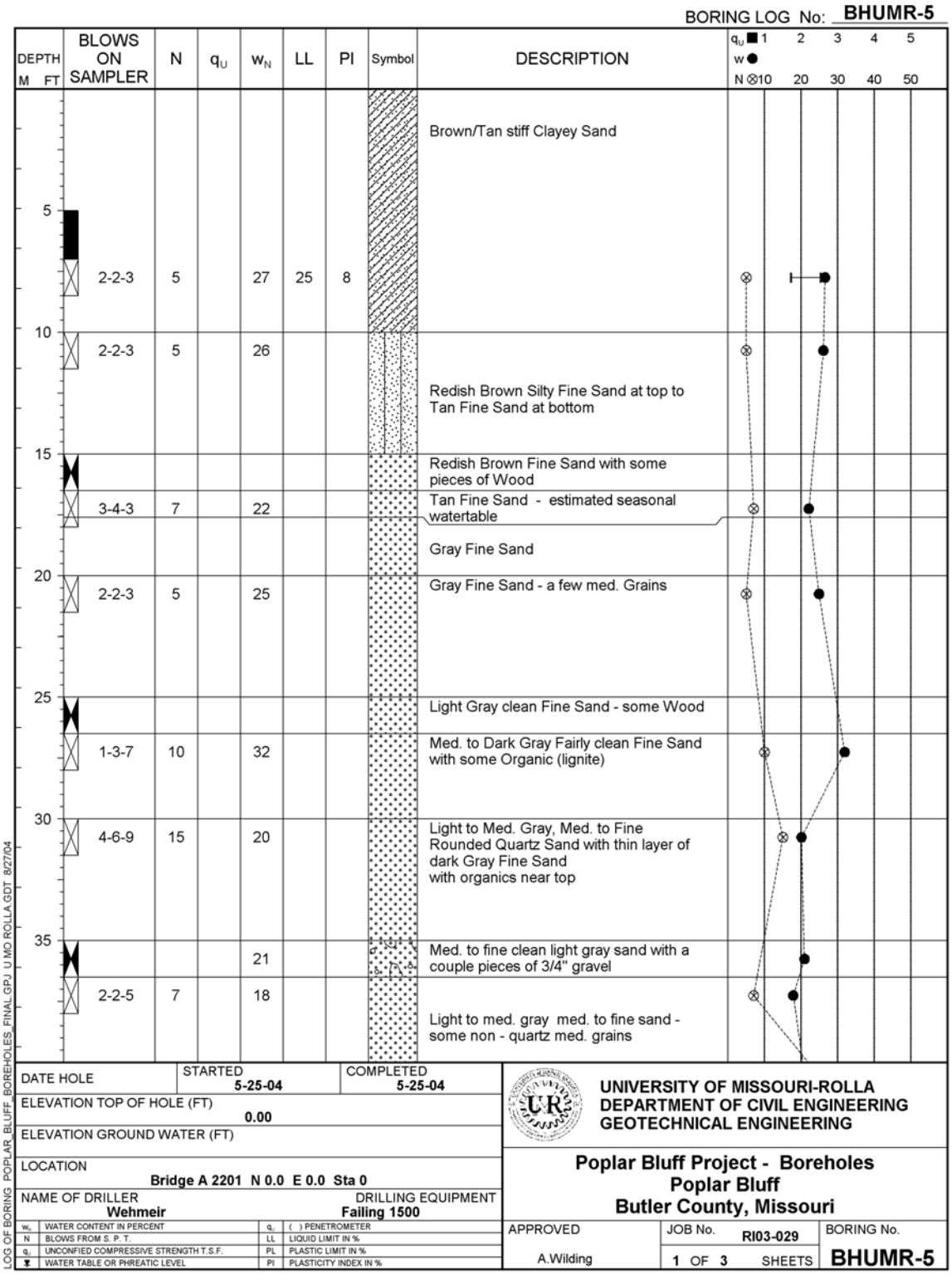

Figure B6: Geotechnical borehole log for Boring ID BHUMR-5 (Appendix A).

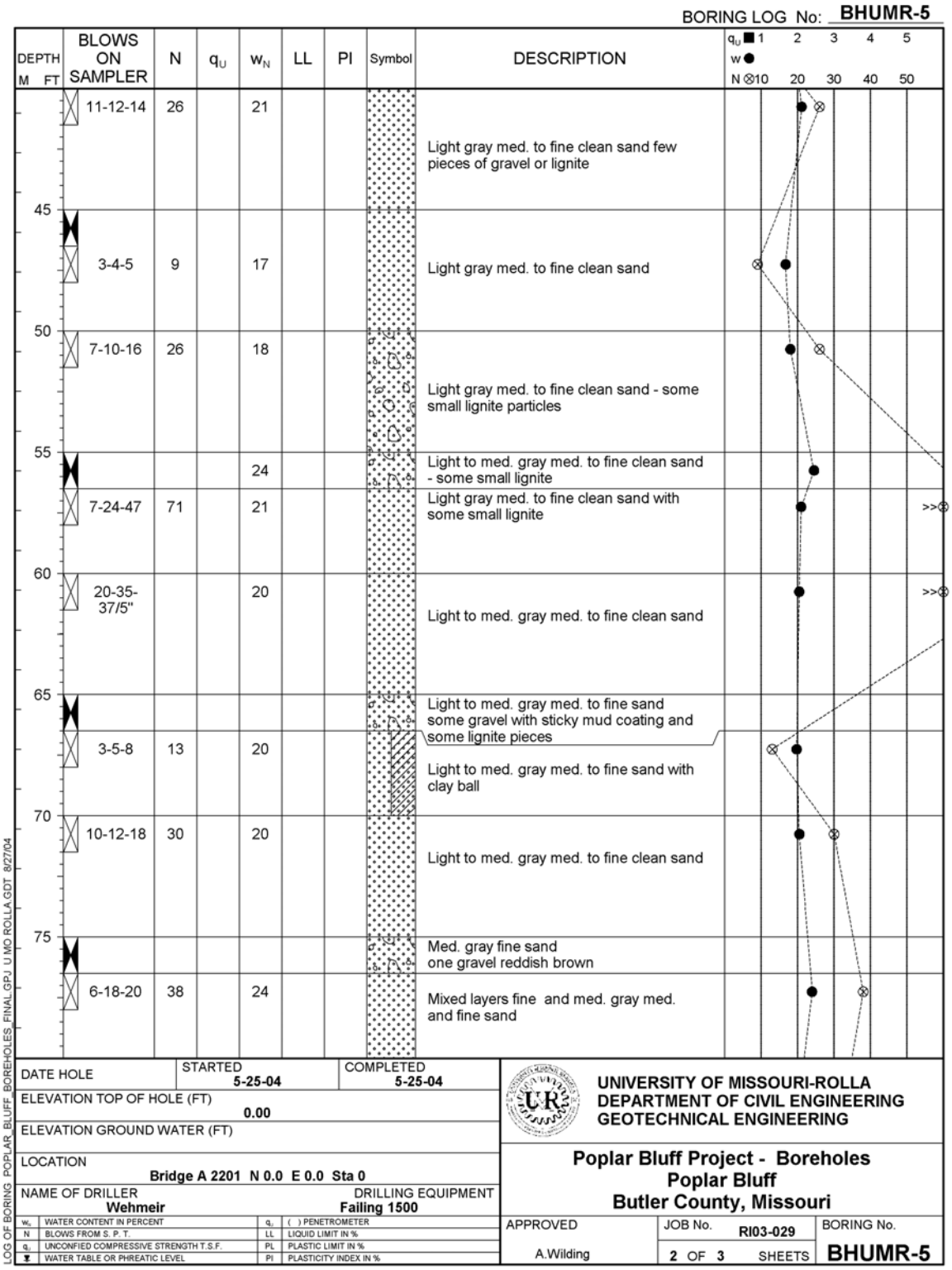

Figure B.7: Geotechnical borehole log for Boring ID BHUMR-5 (Appendix A).

BORING LOG No: **BHUMR-5**

DEPTH M FT	BLOWS ON SAMPLER	N	q_U	w_N	LL	PI	Symbol	DESCRIPTION
	7-15-19	34		21				Mixed layers light to med. gray med. to fine sand with lignite and fine sand layers
85	6-10-13	23		20				Light gray med. to fine clean sand one metamorphic gravel 1"
90	13-18-22	40		22				Light gray med. to fine clean sand
95				25				Alternating thin layers med. to fine light gray sand and black lignite (upper part) - (lower part) med. and some coarse light gray sand
	7-8-12	20		17				Light to med. gray sand - med. to fine in upper 2/3 and med. to coarse in lower 1/3 , one 1/2" gravel in lower part
100	9-16-15	31		12				Light to med. gray sand - fine to med. in upper part and coarse to med. with some small gravel in lower part
105								
110								END OF BORING @ 110 FT.

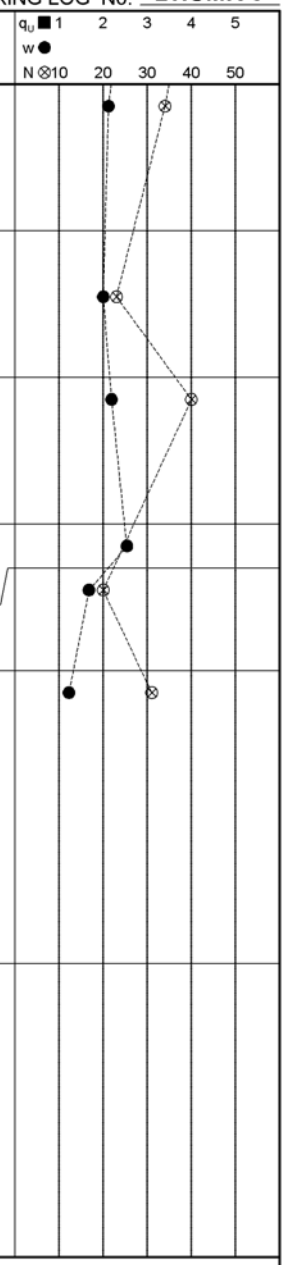

DATE HOLE	STARTED 5-25-04	COMPLETED 5-25-04
ELEVATION TOP OF HOLE (FT)	0.00	
ELEVATION GROUND WATER (FT)		
LOCATION	Bridge A 2201 N 0.0 E 0.0 Sta 0	
NAME OF DRILLER	Wehmeir	DRILLING EQUIPMENT Failing 1500

w_c	WATER CONTENT IN PERCENT	q_p	( ) PENETROMETER
N	BLOWS FROM S. P. T.	LL	LIQUID LIMIT IN %
q_u	UNCONFIED COMPRESSIVE STRENGTH T.S.F.	PL	PLASTIC LIMIT IN %
▼	WATER TABLE OR PHREATIC LEVEL	PI	PLASTICITY INDEX IN %

UNIVERSITY OF MISSOURI-ROLLA
DEPARTMENT OF CIVIL ENGINEERING
GEOTECHNICAL ENGINEERING

Poplar Bluff Project - Boreholes
Poplar Bluff
Butler County, Missouri

APPROVED	JOB No.	BORING No.
A.Wilding	RI03-029	BHUMR-5
	3 OF 3 SHEETS	

LOG OF BORING POPLAR_BLUFF_BOREHOLES_FINAL.GPJ U MO ROLLA.GDT 8/27/04

Figure B.8: Geotechnical borehole log for Boring ID BHUMR-5 (Appendix A).

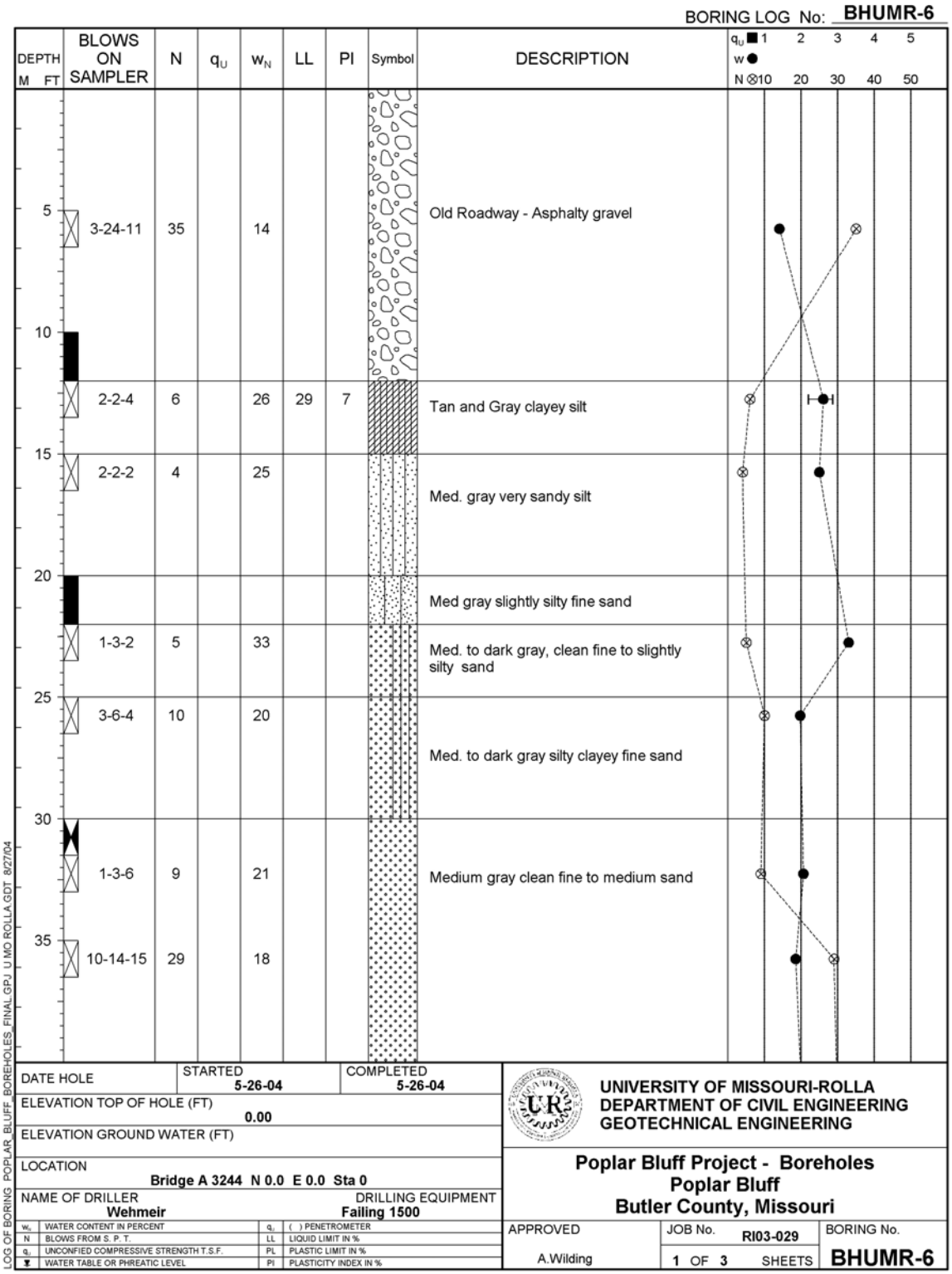

Figure B.9: Geotechnical borehole log for Boring ID BHUMR-6 (Appendix A).

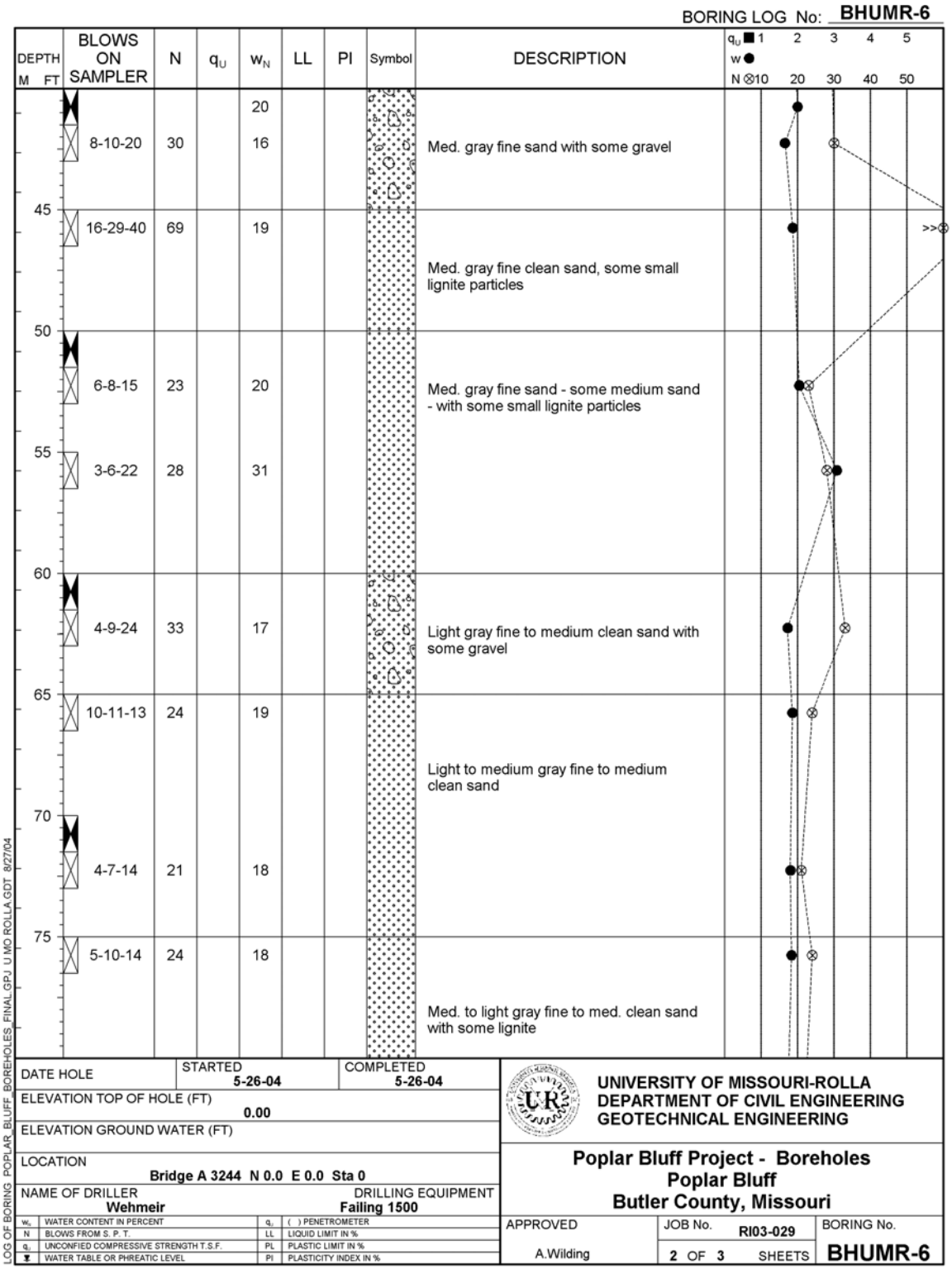

Figure B.10: Geotechnical borehole log for Boring ID BHUMR-6 (Appendix A).

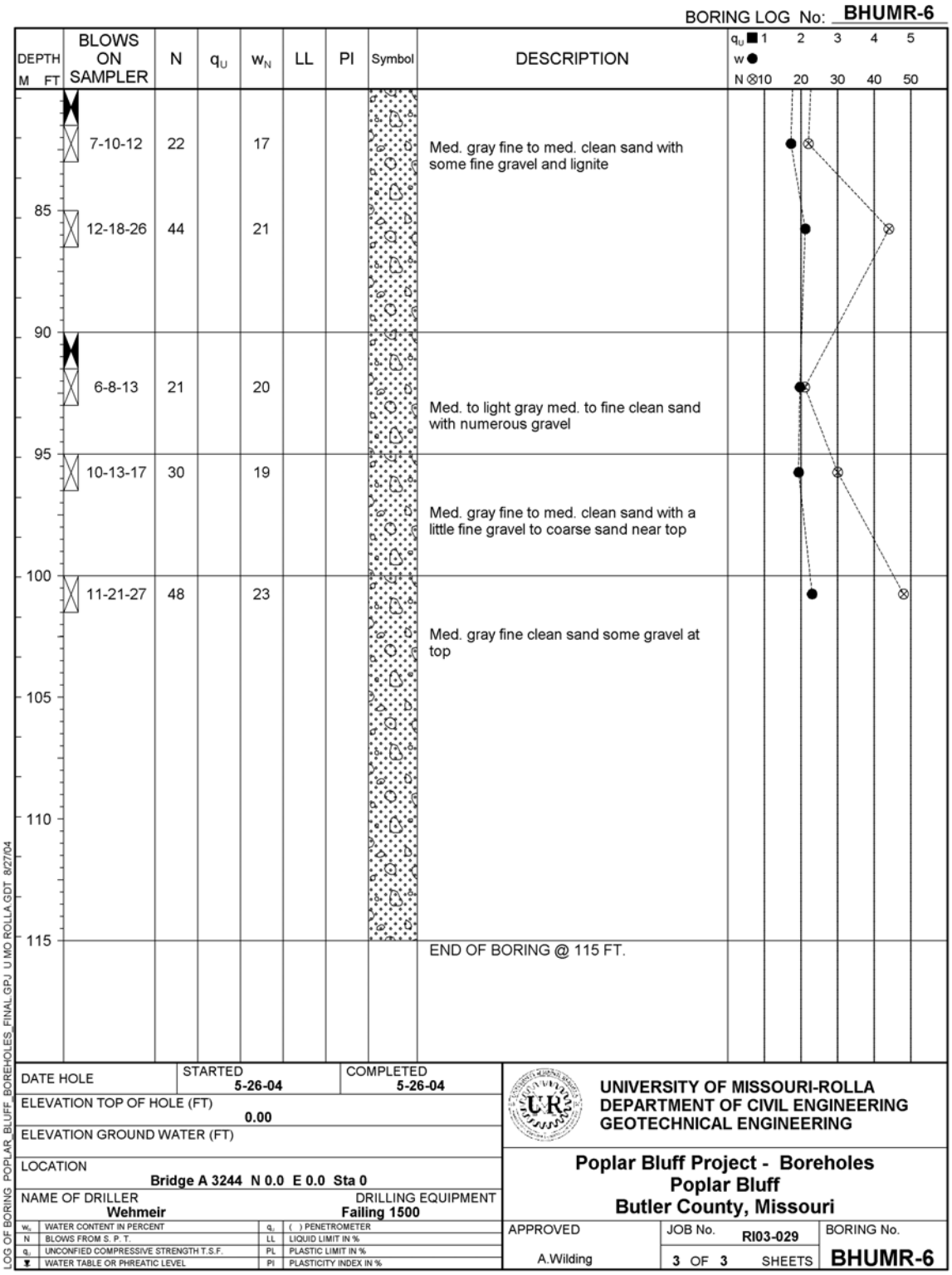

Figure B.11: Geotechnical borehole log for Boring ID BHUMR-6 (Appendix A).

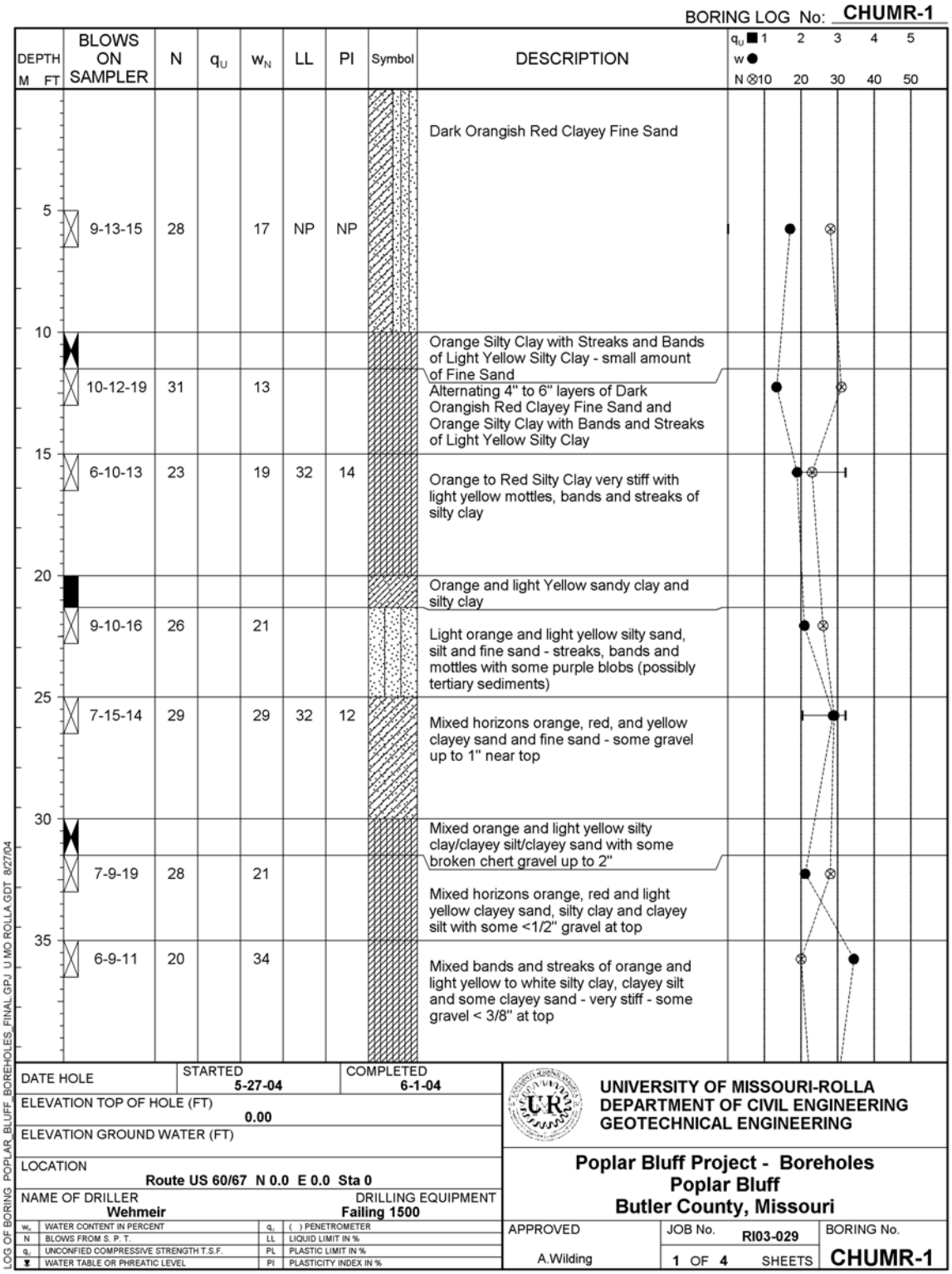

Figure B.12: Geotechnical borehole log for Upland Boring ID CHUMR-1 (Appendix A).

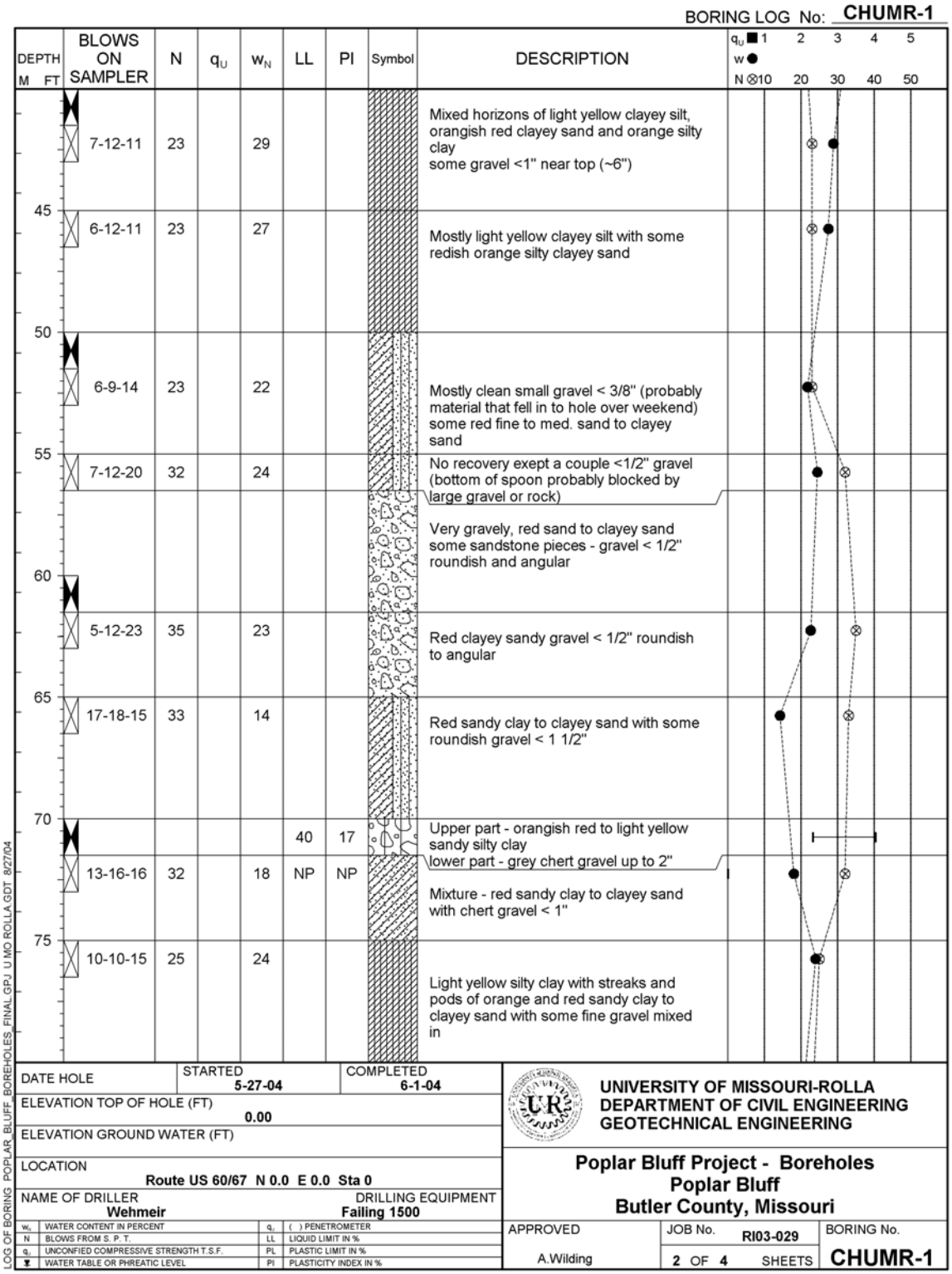

Figure B.13: Geotechnical borehole log for Upland Boring ID CHUMR-1 (Appendix A).

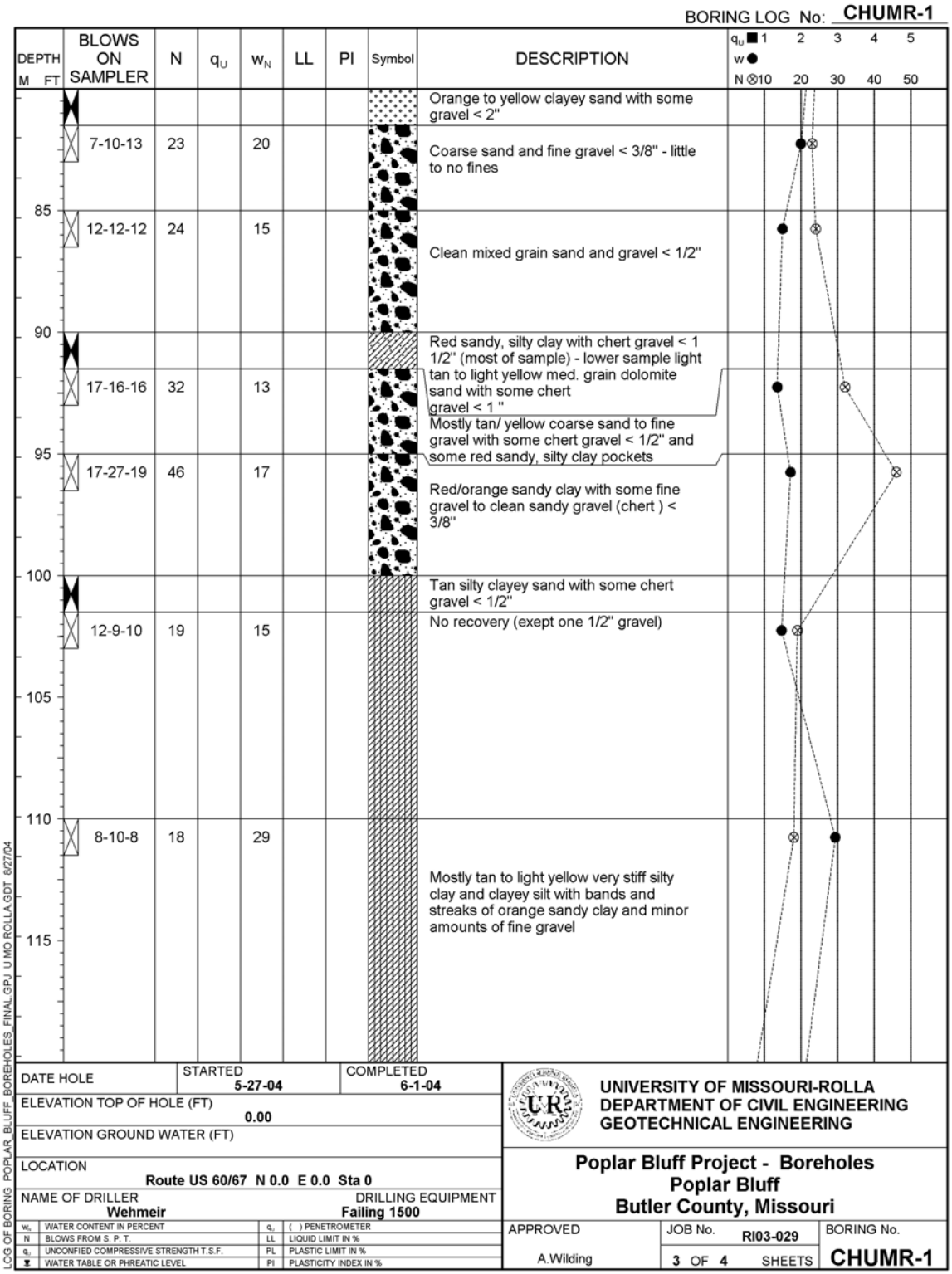

Figure B.14: Geotechnical borehole log for Upland Boring ID CHUMR-1 (Appendix A).

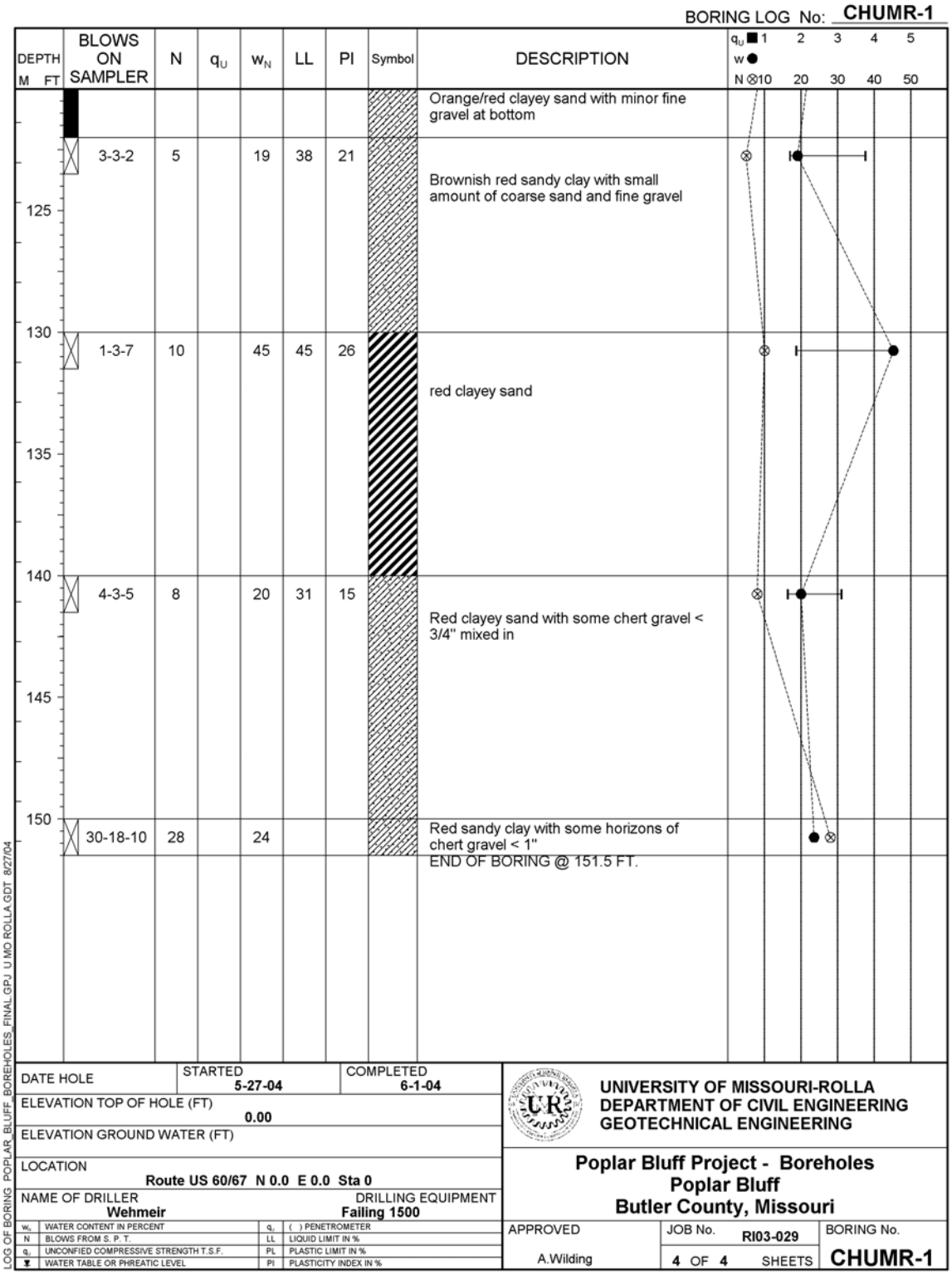

Figure B.15: Geotechnical borehole log for Upland Boring ID CHUMR-1 (Appendix A).

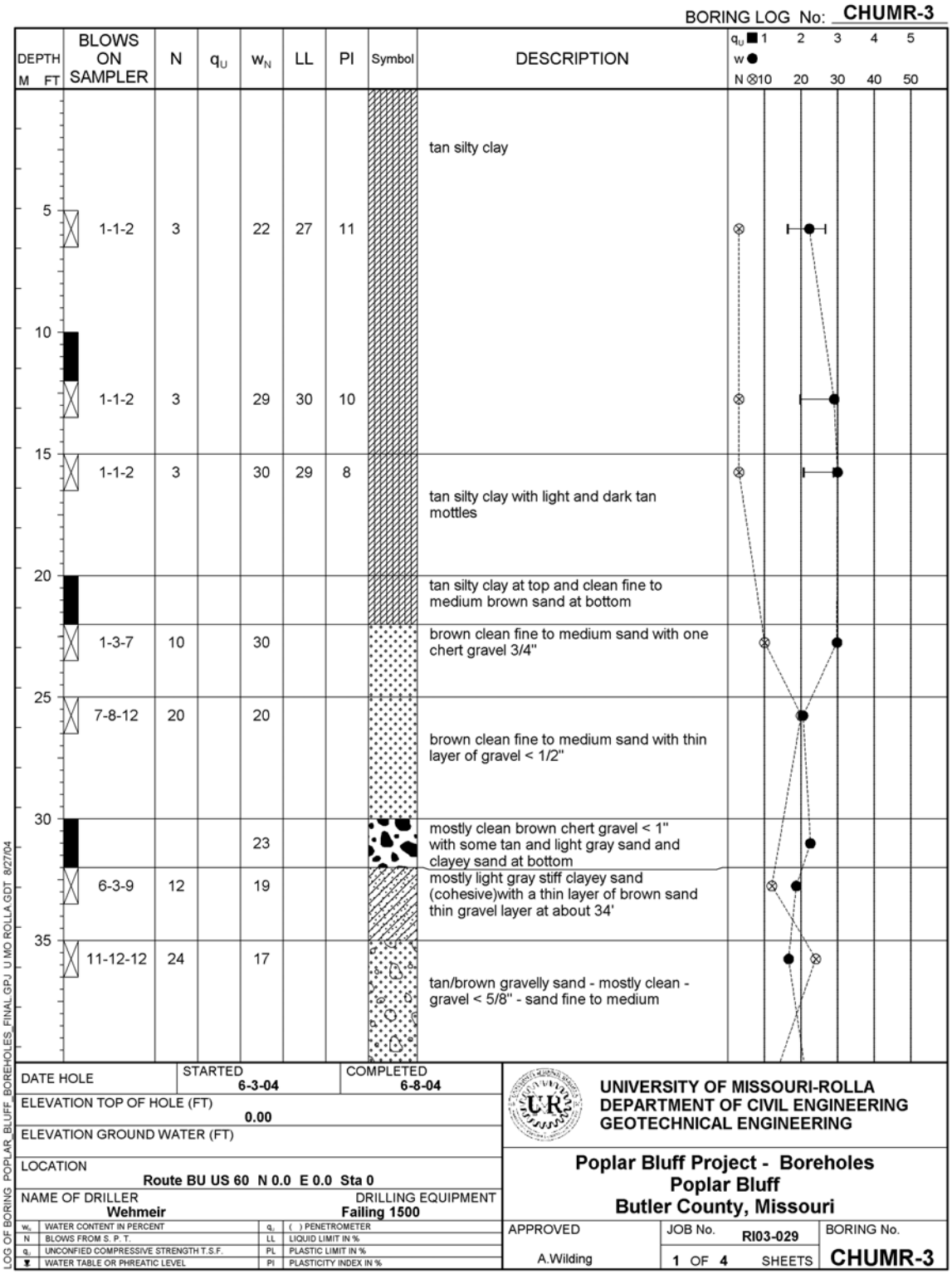

Figure B.16: Geotechnical borehole log for Lowland Boring ID CHUMR-3 (Appendix A).

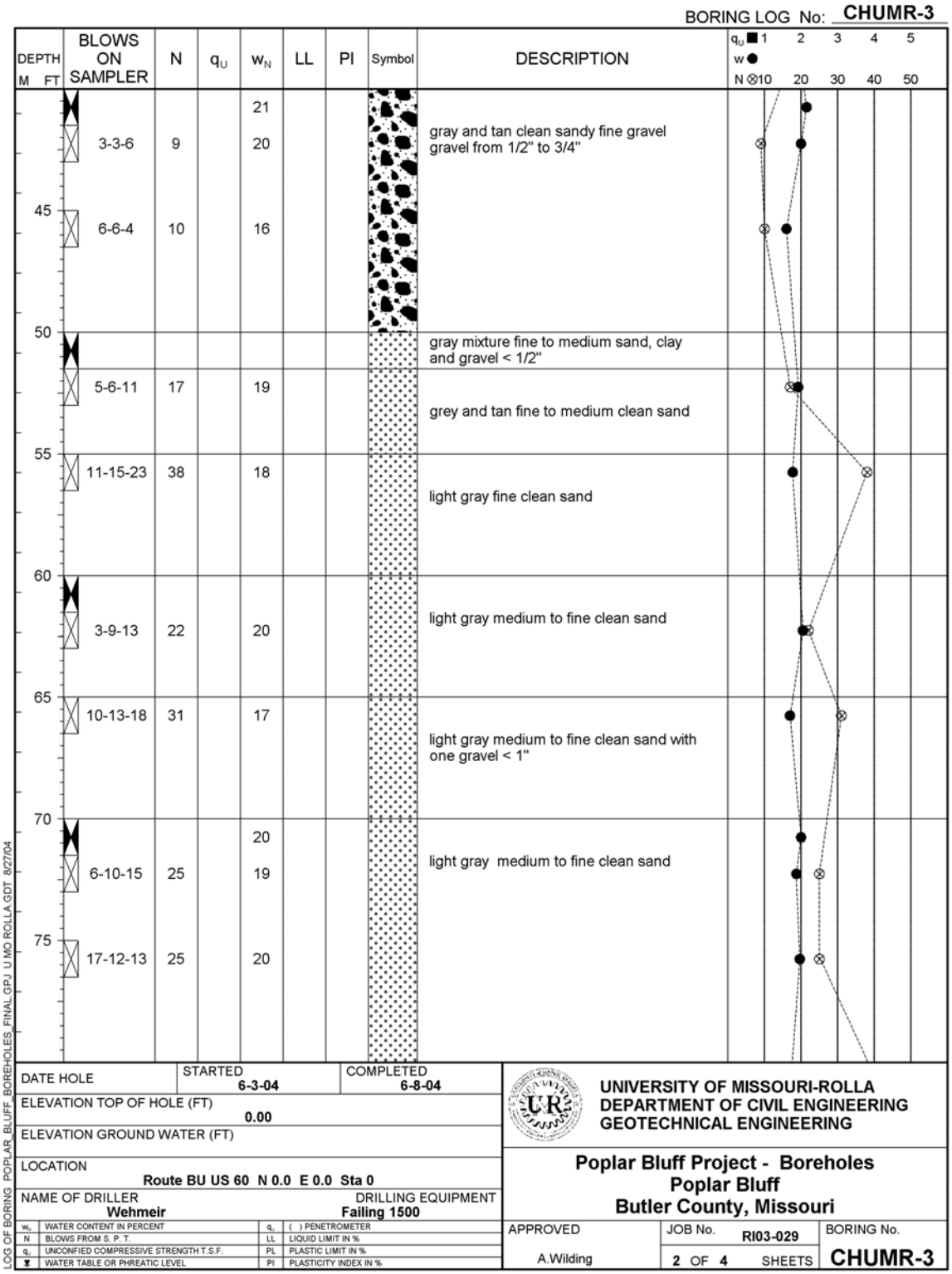

Figure B.17: Geotechnical borehole log for Lowland Boring ID CHUMR-3 (Appendix A).

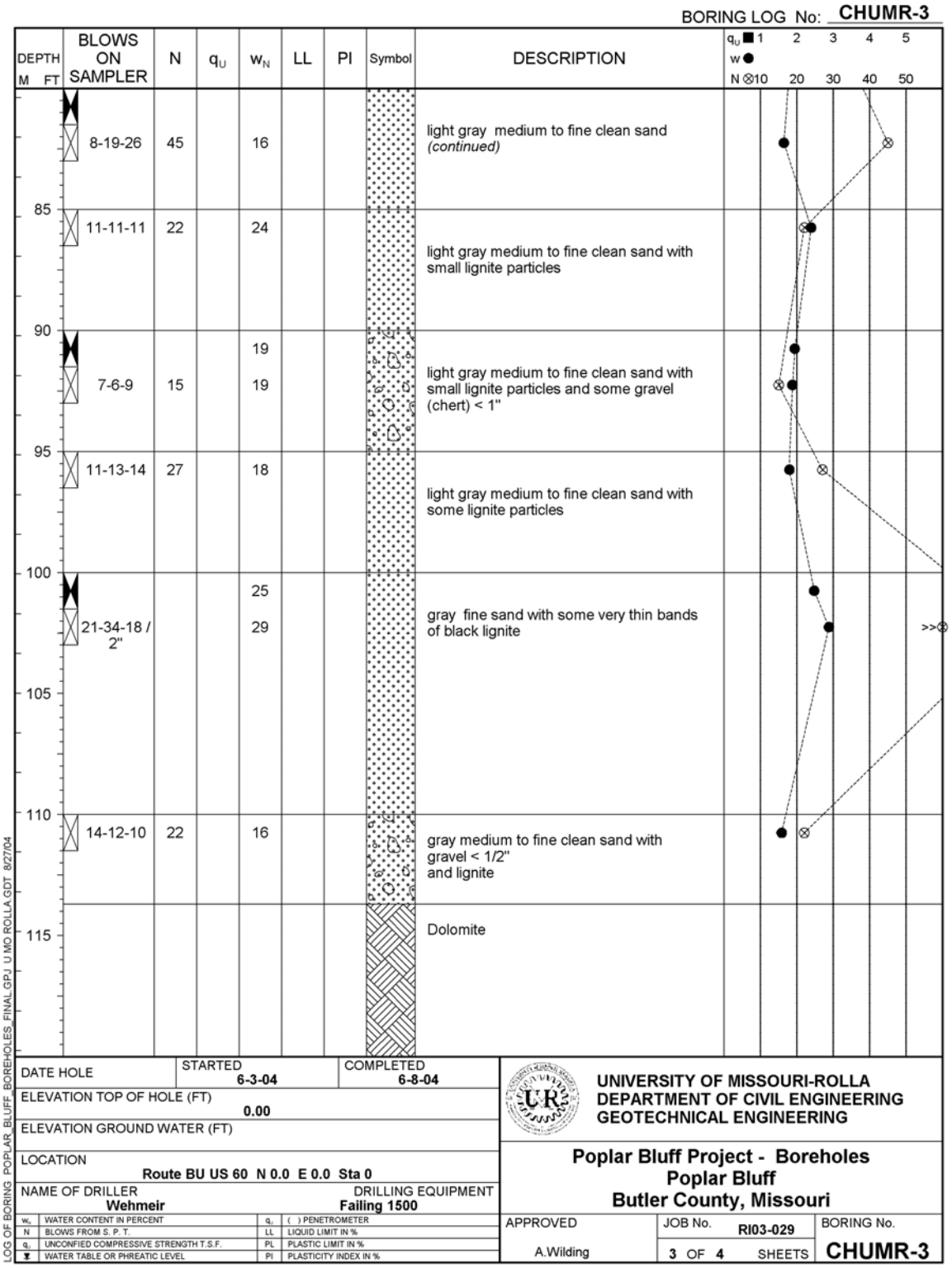

Figure B.18: Geotechnical borehole log for Lowland Boring ID CHUMR-3 (Appendix A).

BORING LOG No: CHUMR-3

DEPTH M FT	BLOWS ON SAMPLER	N	q_U	w_N	LL	PI	Symbol	DESCRIPTION	q_U ■ 1 2 3 4 5 / w ● / N ⊗10 20 30 40 50
								Dolomite *(continued)*	
								END OF BORING @ 123.7 FT.	

DATE HOLE	STARTED 6-3-04	COMPLETED 6-8-04
ELEVATION TOP OF HOLE (FT) 0.00		
ELEVATION GROUND WATER (FT)		
LOCATION Route BU US 60 N 0.0 E 0.0 Sta 0		
NAME OF DRILLER Wehmeir	DRILLING EQUIPMENT Failing 1500	

w_N	WATER CONTENT IN PERCENT	q_p	( ) PENETROMETER
N	BLOWS FROM S. P. T.	LL	LIQUID LIMIT IN %
q_U	UNCONFIED COMPRESSIVE STRENGTH T.S.F.	PL	PLASTIC LIMIT IN %
▼	WATER TABLE OR PHREATIC LEVEL	PI	PLASTICITY INDEX IN %

UNIVERSITY OF MISSOURI-ROLLA
DEPARTMENT OF CIVIL ENGINEERING
GEOTECHNICAL ENGINEERING

Poplar Bluff Project - Boreholes
Poplar Bluff
Butler County, Missouri

APPROVED	JOB No.	BORING No.
A.Wilding	RI03-029	CHUMR-3
	4 OF 4 SHEETS	

LOG OF BORING POPLAR_BLUFF_BOREHOLES_FINAL.GPJ U MO ROLLA.GDT 8/27/04

Figure B.19: Geotechnical borehole log for Lowland Boring ID CHUMR-3 (Appendix A).

APPENDIX C: LABORATORY SOIL INDEX PROPERTIES TEST RESULTS

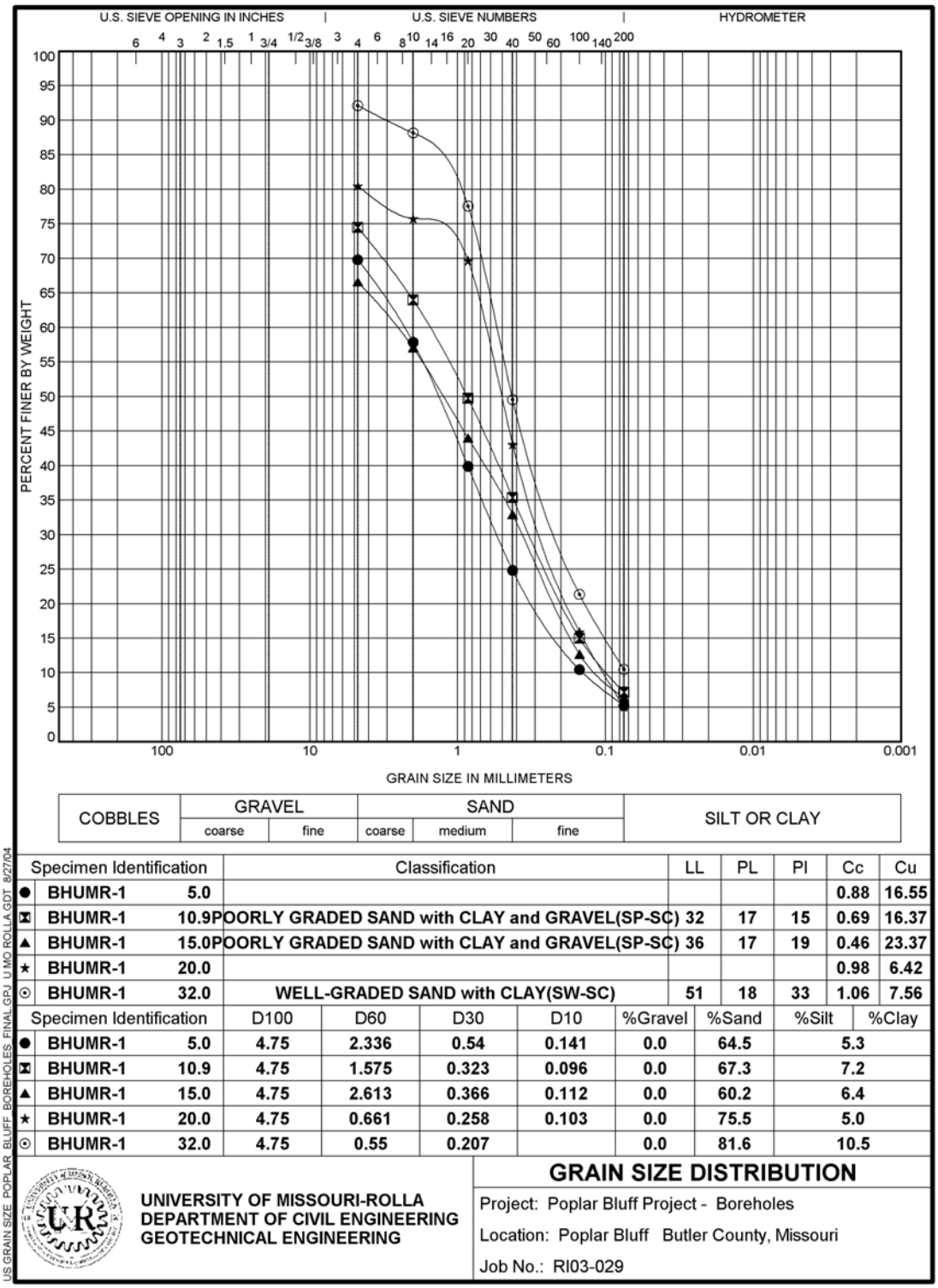

Specimen Identification			Classification	LL	PL	PI	Cc	Cu
●	BHUMR-1	5.0					0.88	16.55
⊠	BHUMR-1	10.9	POORLY GRADED SAND with CLAY and GRAVEL(SP-SC)	32	17	15	0.69	16.37
▲	BHUMR-1	15.0	POORLY GRADED SAND with CLAY and GRAVEL(SP-SC)	36	17	19	0.46	23.37
★	BHUMR-1	20.0					0.98	6.42
⊙	BHUMR-1	32.0	WELL-GRADED SAND with CLAY(SW-SC)	51	18	33	1.06	7.56

Specimen Identification			D100	D60	D30	D10	%Gravel	%Sand	%Silt	%Clay
●	BHUMR-1	5.0	4.75	2.336	0.54	0.141	0.0	64.5	5.3	
⊠	BHUMR-1	10.9	4.75	1.575	0.323	0.096	0.0	67.3	7.2	
▲	BHUMR-1	15.0	4.75	2.613	0.366	0.112	0.0	60.2	6.4	
★	BHUMR-1	20.0	4.75	0.661	0.258	0.103	0.0	75.5	5.0	
⊙	BHUMR-1	32.0	4.75	0.55	0.207		0.0	81.6	10.5	

Figure C.1: Grain size distribution curves for Boring ID BHUMR-1 (Appendix A).

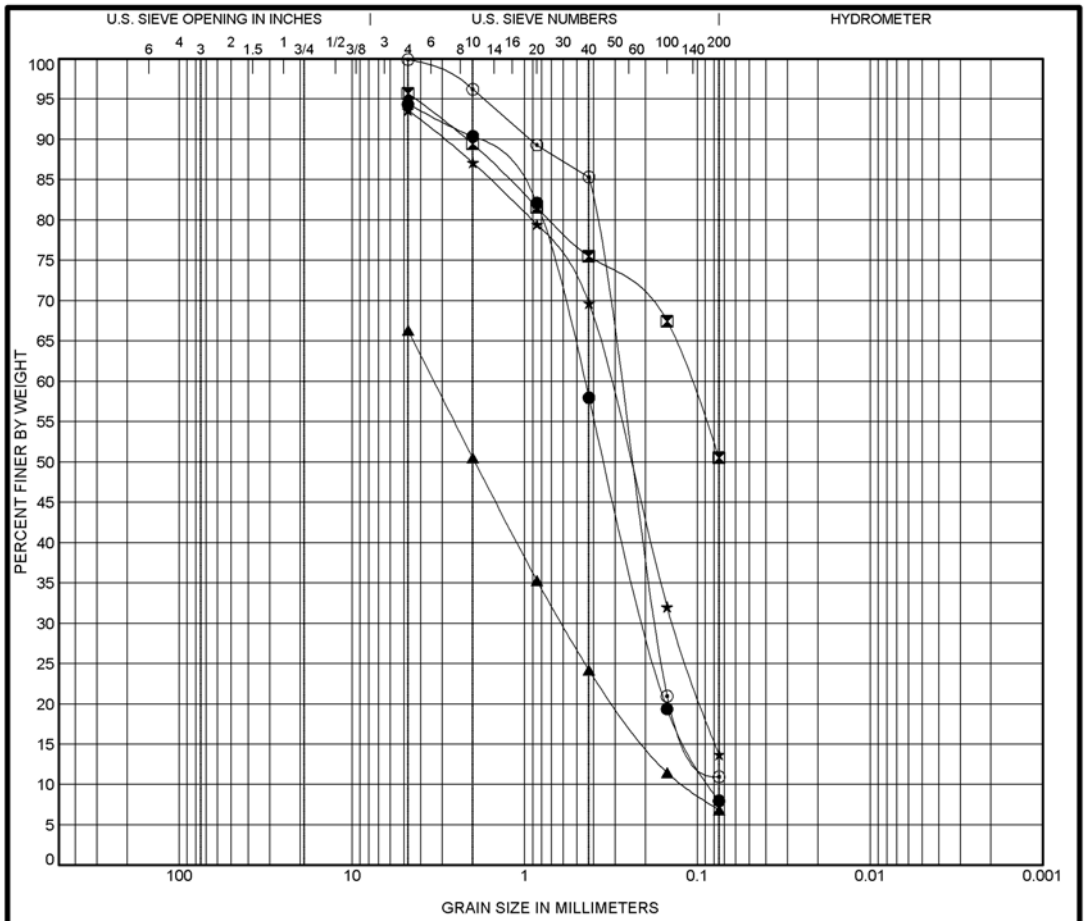

Specimen Identification			Classification	LL	PL	PI	Cc	Cu
●	BHUMR-1	40.5	POORLY GRADED SAND with CLAY(SP-SC)	29	14	15	1.05	5.31
⊠	BHUMR-1	45.6	SANDY SILT(ML)	NP	NP	NP		
▲	BHUMR-1	50.0	POORLY GRADED SAND with CLAY and GRAVEL(SP-SC)	42	19	23	0.92	27.94
★	BHUMR-1	55.0						
⊙	BHUMR-2	10.0	POORLY GRADED SAND with CLAY(SP-SC)	24	15	9	1.52	4.02

Specimen Identification			D100	D60	D30	D10	%Gravel	%Sand	%Silt	%Clay
●	BHUMR-1	40.5	4.75	0.451	0.2	0.085	0.0	86.4	8.0	
⊠	BHUMR-1	45.6	4.75	0.111			0.0	45.2	50.5	
▲	BHUMR-1	50.0	4.75	3.361	0.611	0.12	0.0	59.5	6.9	
★	BHUMR-1	55.0	4.75	0.325	0.139		0.0	79.9	13.7	
⊙	BHUMR-2	10.0	4.75	0.282	0.174		0.0	88.9	11.0	

UNIVERSITY OF MISSOURI-ROLLA
DEPARTMENT OF CIVIL ENGINEERING
GEOTECHNICAL ENGINEERING

GRAIN SIZE DISTRIBUTION

Project: Poplar Bluff Project - Boreholes
Location: Poplar Bluff Butler County, Missouri
Job No.: RI03-029

US GRAIN SIZE POPLAR BLUFF BOREHOLES FINAL.GPJ U.MO ROLLA.GDT 8/27/04

Figure C.2: Grain size distribution curves for Boring IDs BHUMR-1 and BHUMR-2 (Appendix A).

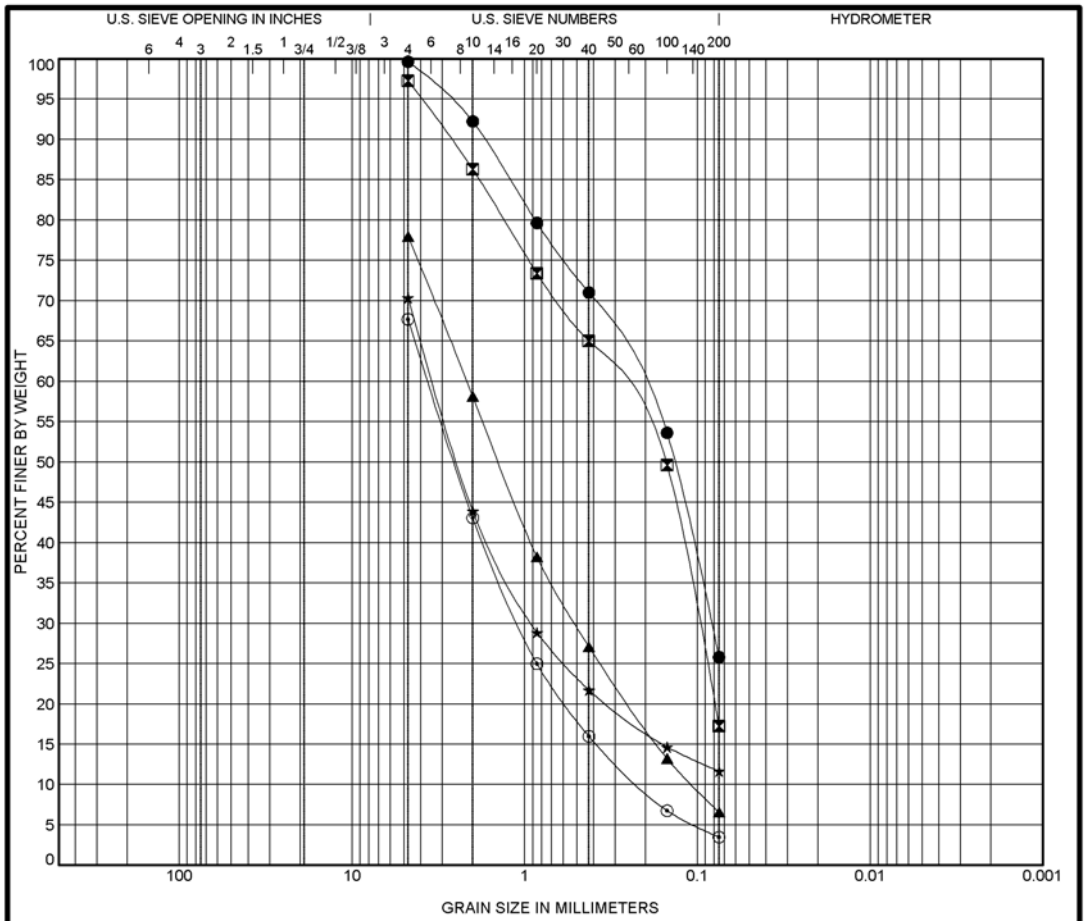

	Specimen Identification		Classification	LL	PL	PI	Cc	Cu
●	BHUMR-2	20.0	CLAYEY SAND(SC)	35	19	16		
⧗	BHUMR-2	26.8	CLAYEY SAND(SC)	32	22	10		
▲	BHUMR-2	35.0	WELL-GRADED SAND with CLAY and GRAVEL(SW-SC)	35	18	17	1.12	20.21
★	BHUMR-2	40.0					4.75	66.12
⊙	BHUMR-2	45.5	WELL-GRADED SAND with GRAVEL(SW)				1.48	16.76

	Specimen Identification		D100	D60	D30	D10	%Gravel	%Sand	%Silt	%Clay
●	BHUMR-2	20.0	4.75	0.22	0.083		0.0	73.8	25.8	
⧗	BHUMR-2	26.8	4.75	0.303	0.099		0.0	80.0	17.3	
▲	BHUMR-2	35.0	4.75	2.17	0.51	0.107	0.0	71.4	6.6	
★	BHUMR-2	40.0	4.75	3.385	0.907		0.0	58.7	11.7	
⊙	BHUMR-2	45.5	4.75	3.626	1.078	0.216	0.0	64.2	3.5	

UNIVERSITY OF MISSOURI-ROLLA
DEPARTMENT OF CIVIL ENGINEERING
GEOTECHNICAL ENGINEERING

GRAIN SIZE DISTRIBUTION

Project: Poplar Bluff Project - Boreholes
Location: Poplar Bluff Butler County, Missouri
Job No.: RI03-029

US GRAIN SIZE POPLAR BLUFF BOREHOLES FINAL.GPJ U MO ROLLA.GDT 8/27/04

Figure C.3: Grain size distribution curves for Boring ID BHUMR-2 (Appendix A).

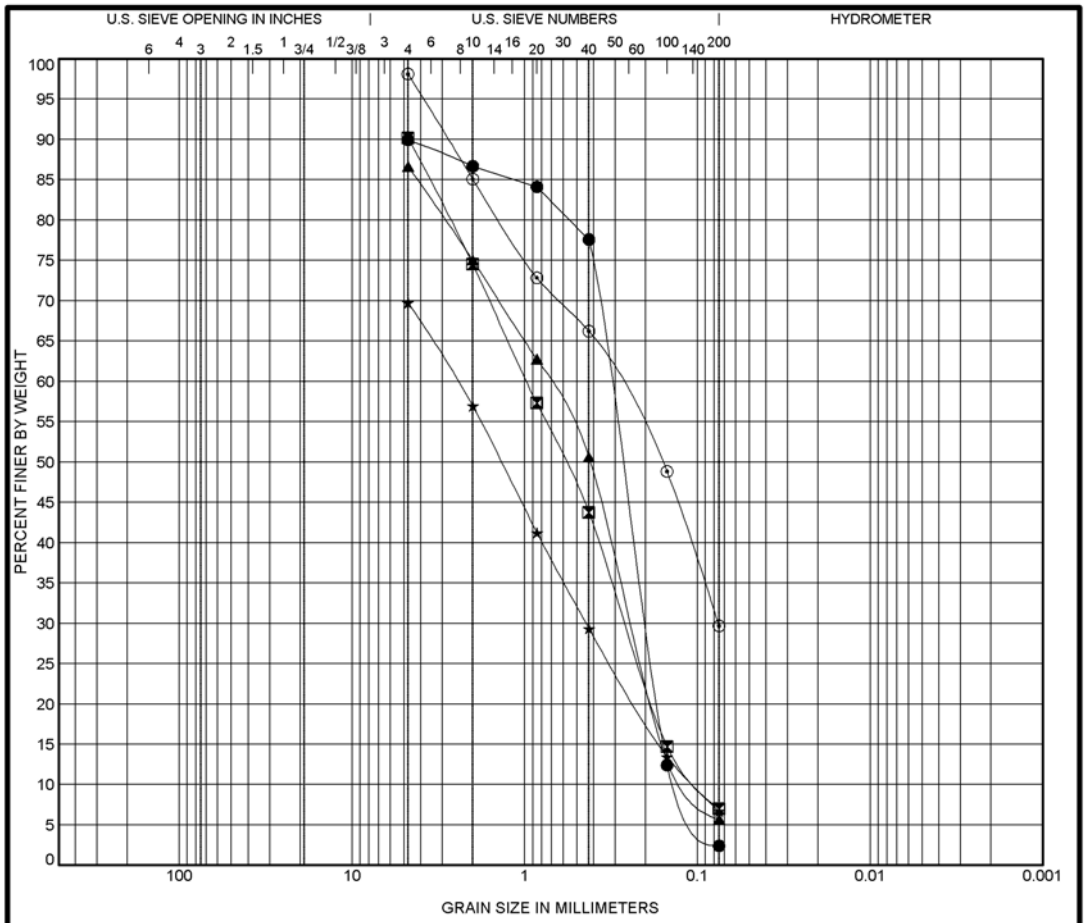

Specimen Identification			Classification	LL	PL	PI	Cc	Cu
●	BHUMR-2	65.0	POORLY GRADED SAND(SP)				0.97	2.53
⧗	BHUMR-2	75.0					0.71	9.92
▲	BHUMR-2	85.0					0.70	6.36
★	BHUMR-2	100.0	POORLY GRADED SAND with CLAY and GRAVEL(SP-SC)	28	18	10	0.76	23.36
⊙	BHUMR-5	7.0	CLAYEY SAND(SC)	25	17	8		

Specimen Identification			D100	D60	D30	D10	%Gravel	%Sand	%Silt	%Clay
●	BHUMR-2	65.0	4.75	0.321	0.199	0.127	0.0	87.5	2.4	
⧗	BHUMR-2	75.0	4.75	0.973	0.26	0.098	0.0	83.2	7.0	
▲	BHUMR-2	85.0	4.75	0.727	0.241	0.114	0.0	81.0	5.7	
★	BHUMR-2	100.0	4.75	2.457	0.442	0.105	0.0	63.0	6.7	
⊙	BHUMR-5	7.0	4.75	0.293	0.076		0.0	68.4	29.7	

UNIVERSITY OF MISSOURI-ROLLA
DEPARTMENT OF CIVIL ENGINEERING
GEOTECHNICAL ENGINEERING

GRAIN SIZE DISTRIBUTION

Project: Poplar Bluff Project - Boreholes
Location: Poplar Bluff Butler County, Missouri
Job No.: RI03-029

US GRAIN SIZE POPLAR BLUFF BOREHOLES FINAL.GPJ U MO ROLLA.GDT 8/27/04

Figure C.4: Grain size distribution curves for Boring IDs BHUMR-2 and BHUMR-5 (Appendix A).

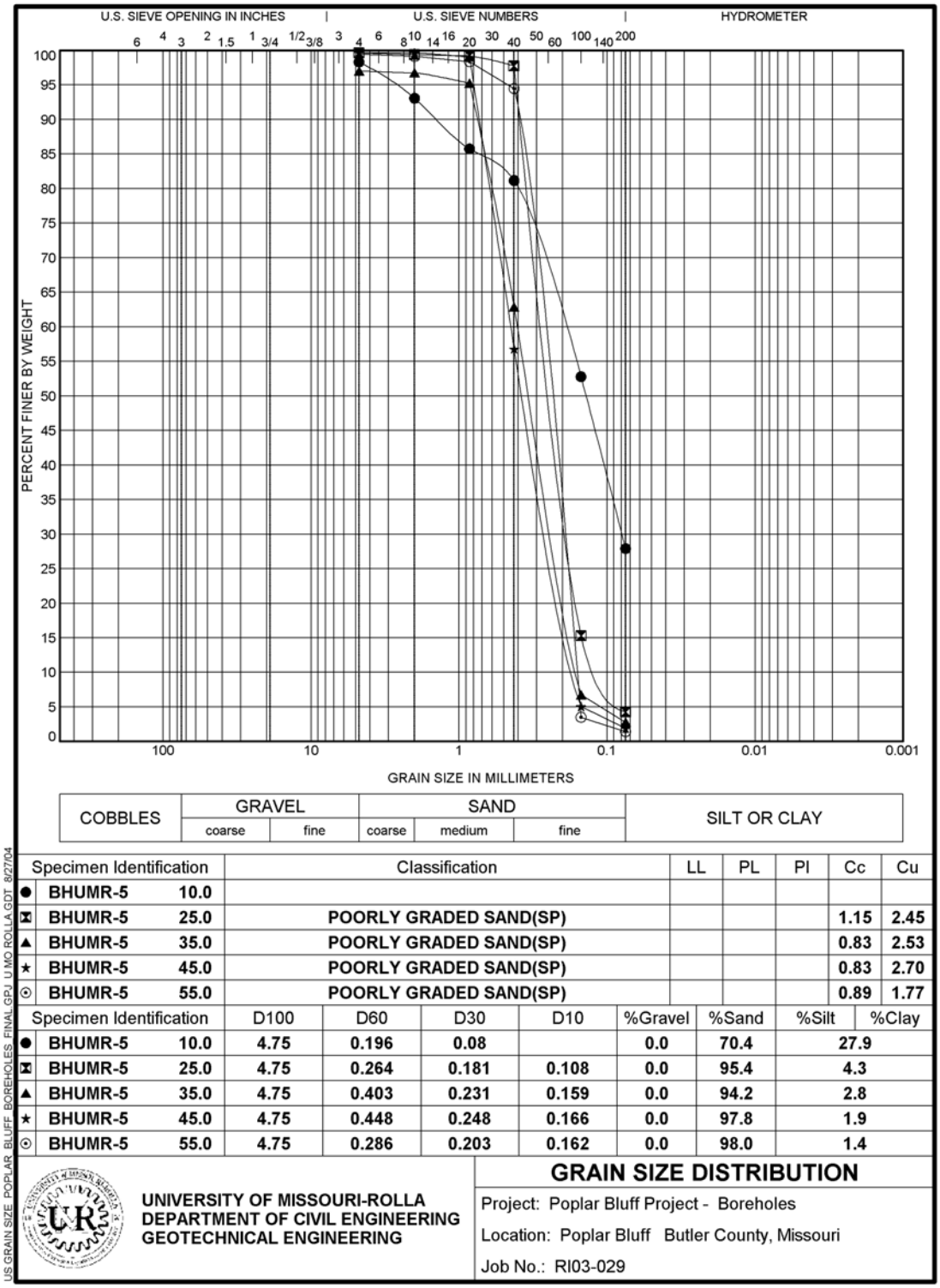

Figure C.5: Grain size distribution curves for Boring ID BHUMR-5 (Appendix A).

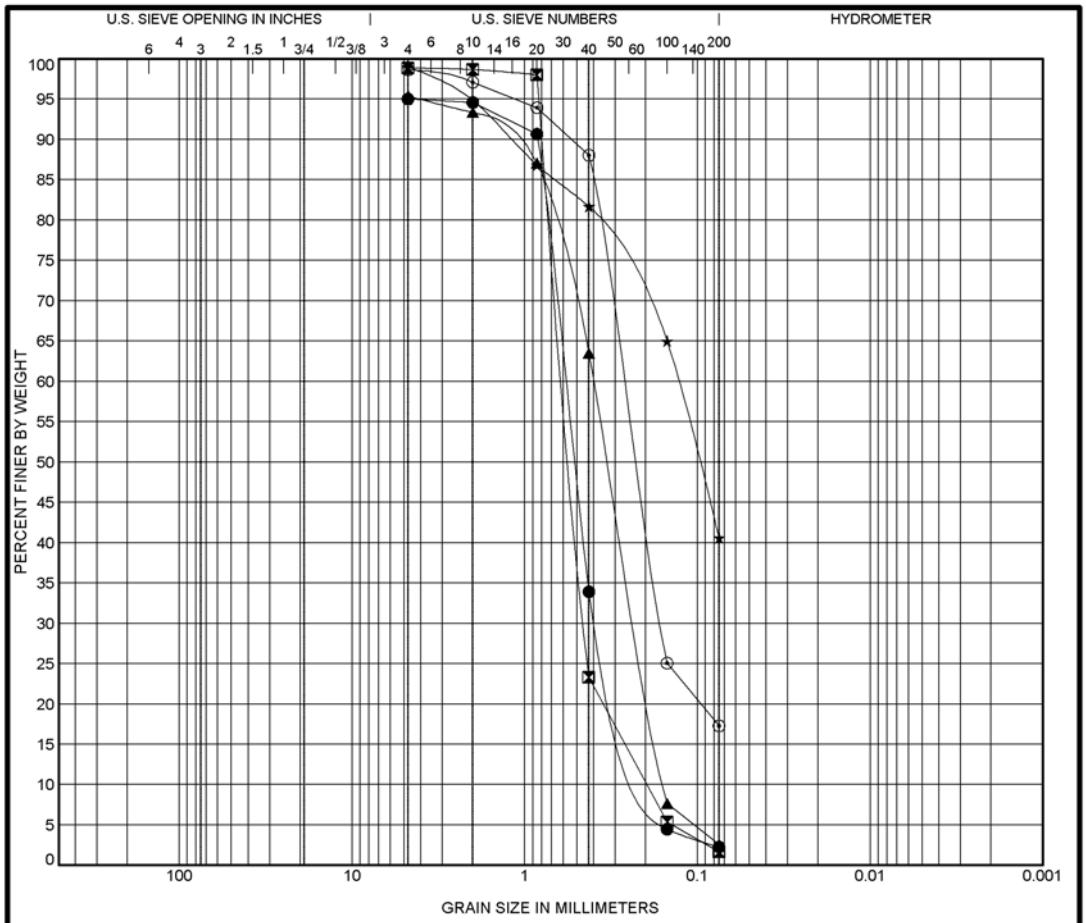

Specimen Identification			Classification	LL	PL	PI	Cc	Cu
●	BHUMR-5	65.0	POORLY GRADED SAND(SP)				1.28	3.20
⧗	BHUMR-5	85.0	POORLY GRADED SAND(SP)				1.74	3.04
▲	BHUMR-5	95.0	POORLY GRADED SAND(SP)				0.83	2.54
★	BHUMR-6	15.0						
⊙	BHUMR-6	25.0						

Specimen Identification			D100	D60	D30	D10	%Gravel	%Sand	%Silt	%Clay
●	BHUMR-5	65.0	4.75	0.585	0.37	0.182	0.0	92.7	2.3	
⧗	BHUMR-5	85.0	4.75	0.597	0.452	0.196	0.0	97.2	1.7	
▲	BHUMR-5	95.0	4.75	0.398	0.228	0.157	0.0	92.9	2.5	
★	BHUMR-6	15.0	4.75	0.13			0.0	58.4	40.6	
⊙	BHUMR-6	25.0	4.75	0.267	0.163		0.0	81.4	17.3	

UNIVERSITY OF MISSOURI-ROLLA
DEPARTMENT OF CIVIL ENGINEERING
GEOTECHNICAL ENGINEERING

GRAIN SIZE DISTRIBUTION

Project: Poplar Bluff Project - Boreholes
Location: Poplar Bluff Butler County, Missouri
Job No.: RI03-029

US GRAIN SIZE POPLAR BLUFF BOREHOLES FINAL.GPJ U.MO ROLLA.GDT 8/27/04

Figure C.6: Grain size distribution curves for Boring IDs BHUMR-5 and BHUMR-6 (Appendix A).

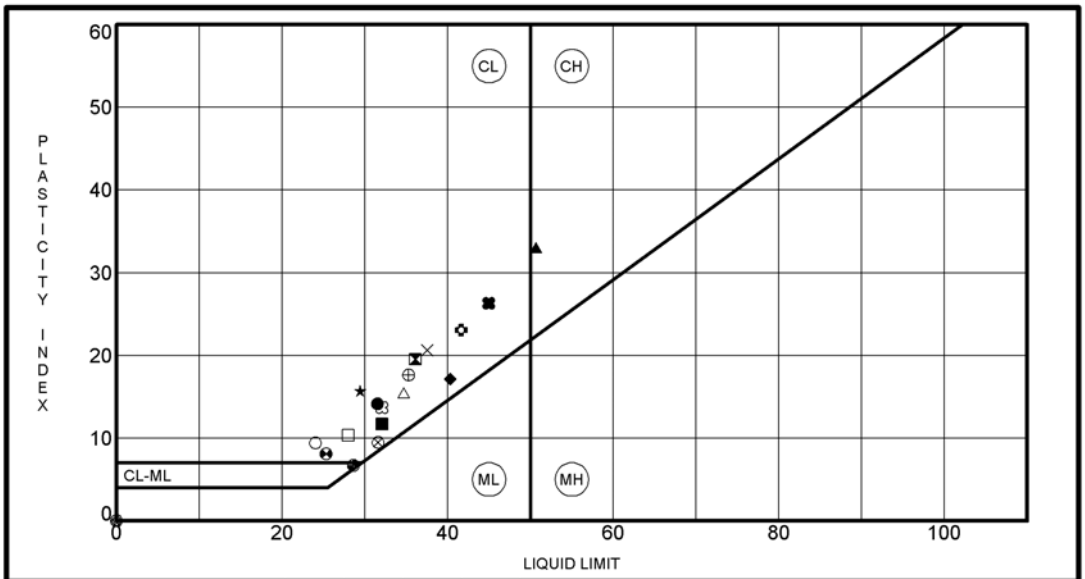

	Specimen Identification		LL	PL	PI	Fines	Classification
●	BHUMR-1	10.9	32	17	15	7	POORLY GRADED SAND with CLAY and GRAVEL(SP-SC)
⧗	BHUMR-1	15.0	36	17	19	6	POORLY GRADED SAND with CLAY and GRAVEL(SP-SC)
▲	BHUMR-1	32.0	51	18	33	10	WELL-GRADED SAND with CLAY(SW-SC)
★	BHUMR-1	40.5	29	14	15	8	POORLY GRADED SAND with CLAY(SP-SC)
⊙	BHUMR-1	45.6	NP	NP	NP	51	SANDY SILT(ML)
✿	BHUMR-1	50.0	42	19	23	7	POORLY GRADED SAND with CLAY and GRAVEL(SP-SC)
○	BHUMR-2	10.0	24	15	9	11	POORLY GRADED SAND with CLAY(SP-SC)
△	BHUMR-2	20.0	35	19	16	26	CLAYEY SAND(SC)
⊗	BHUMR-2	26.8	32	22	10	17	CLAYEY SAND(SC)
⊕	BHUMR-2	35.0	35	18	17	7	WELL-GRADED SAND with CLAY and GRAVEL(SW-SC)
□	BHUMR-2	100.0	28	18	10	7	POORLY GRADED SAND with CLAY and GRAVEL(SP-SC)
⊖	BHUMR-5	7.0	25	17	8	30	CLAYEY SAND(SC)
◕	BHUMR-6	12.0	29	22	7		
☆	CHUMR-1	5.0	NP	NP	NP	7	POORLY GRADED SAND with SILT(SP-SM)
⊠	CHUMR-1	15.0	32	18	14		
■	CHUMR-1	25.0	32	20	12	14	CLAYEY SAND(SC)
◆	CHUMR-1	70.0	40	23	17	7	POORLY GRADED SAND with CLAY and GRAVEL(SP-SC)
◇	CHUMR-1	71.5	NP	NP	NP	9	POORLY GRADED SAND with SILT and GRAVEL(SP-SM)
×	CHUMR-1	122.0	38	17	21	8	WELL-GRADED SAND with CLAY(SW-SC)
✖	CHUMR-1	130.0	45	19	26	11	POORLY GRADED SAND with CLAY(SP-SC)

UNIVERSITY OF MISSOURI-ROLLA
DEPARTMENT OF CIVIL ENGINEERING
GEOTECHNICAL ENGINEERING

ATTERBERG LIMITS' RESULTS

Project: Poplar Bluff Project - Boreholes
Location: Poplar Bluff Butler County, Missouri
Job No.: RI03-029

US ATTERBERG LIMITS POPLAR BLUFF BOREHOLES FINAL.GPJ U MO ROLLA.GDT 8/27/04

Figure C.7: Grain size distribution curves for Boring IDs BHUMR-1, BHUMR-2, BHUMR-5, BHUMR-6, and Upland CHUMR-1 (Appendix A).

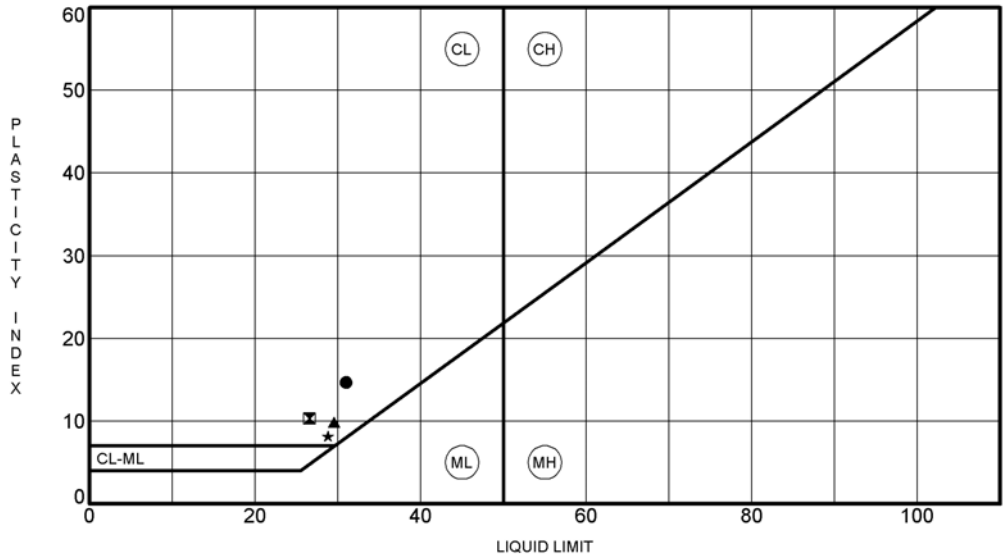

	Specimen Identification		LL	PL	PI	Fines	Classification
●	CHUMR-1	140.0	31	16	15	8	WELL-GRADED SAND with CLAY(SW-SC)
⧗	CHUMR-3	5.0	27	16	11		
▲	CHUMR-3	12.0	30	20	10		
★	CHUMR-3	15.0	29	21	8		

UNIVERSITY OF MISSOURI-ROLLA
DEPARTMENT OF CIVIL ENGINEERING
GEOTECHNICAL ENGINEERING

ATTERBERG LIMITS' RESULTS

Project: Poplar Bluff Project - Boreholes
Location: Poplar Bluff Butler County, Missouri
Job No.: RI03-029

US ATTERBERG LIMITS POPLAR BLUFF BOREHOLES FINAL.GPJ U MO ROLLA.GDT 8/27/04

Figure C.8: Grain size distribution curve for Upland Boring IDs CHUMR-1 and CHUMR-3 (Appendix A).

APPENDIX D: SEISMIC CONE PENETROMETER (SCPT) DATA

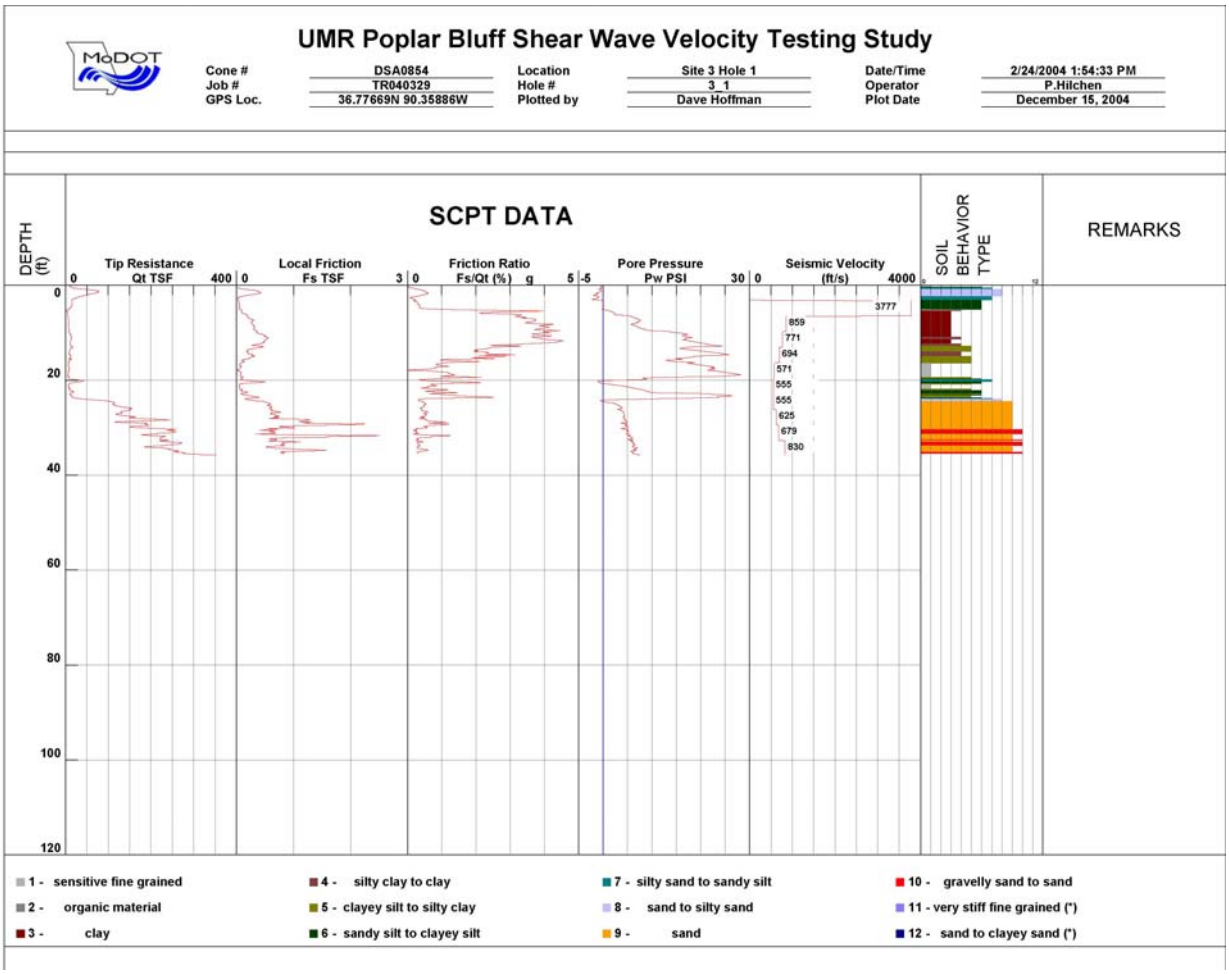

Figure D.1: SCPT data for SCPT Test Site #3-1 (Figure 2.4).

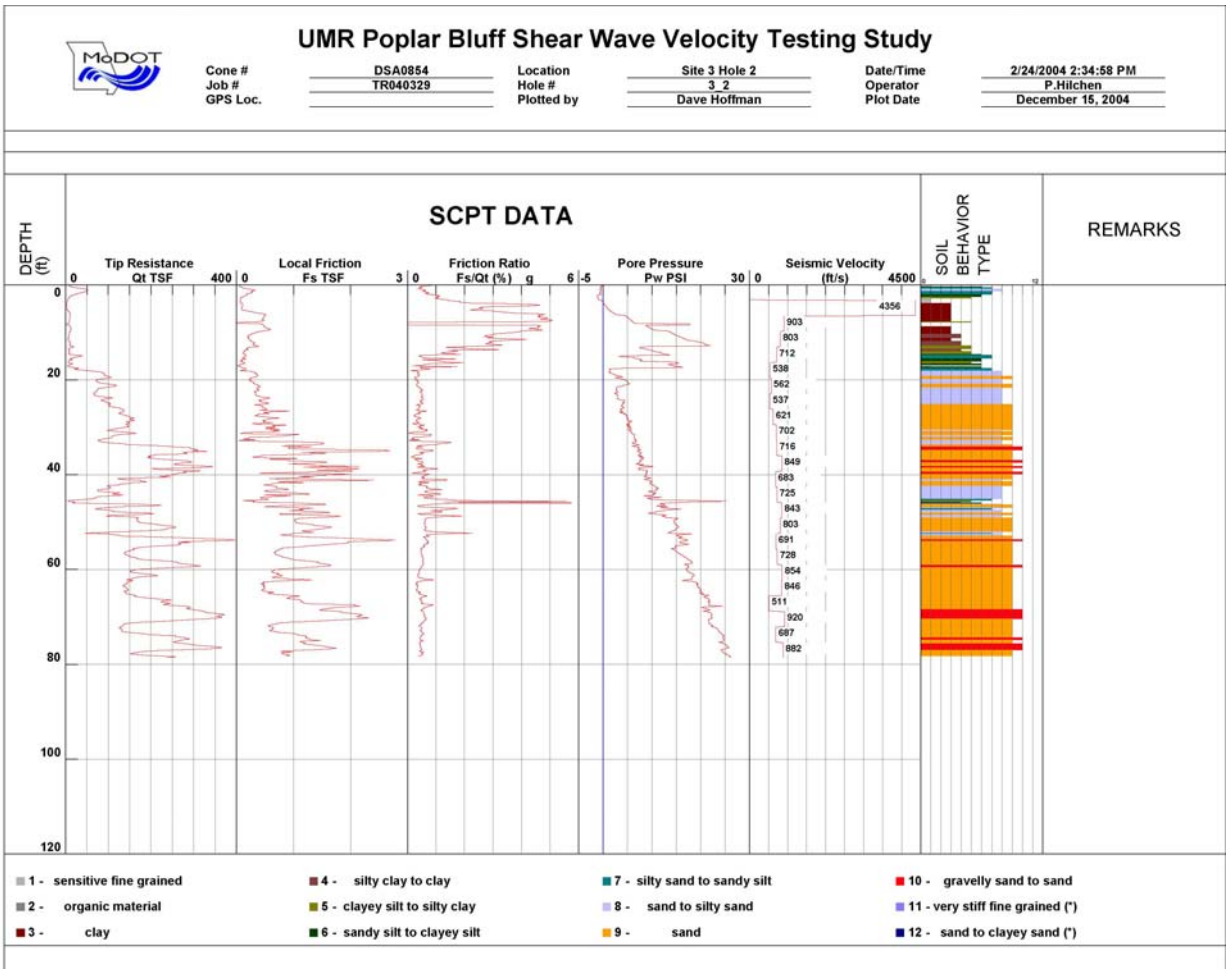

Figure D.2: SCPT data for SCPT Test Site #3-2 (Figure 2.4).

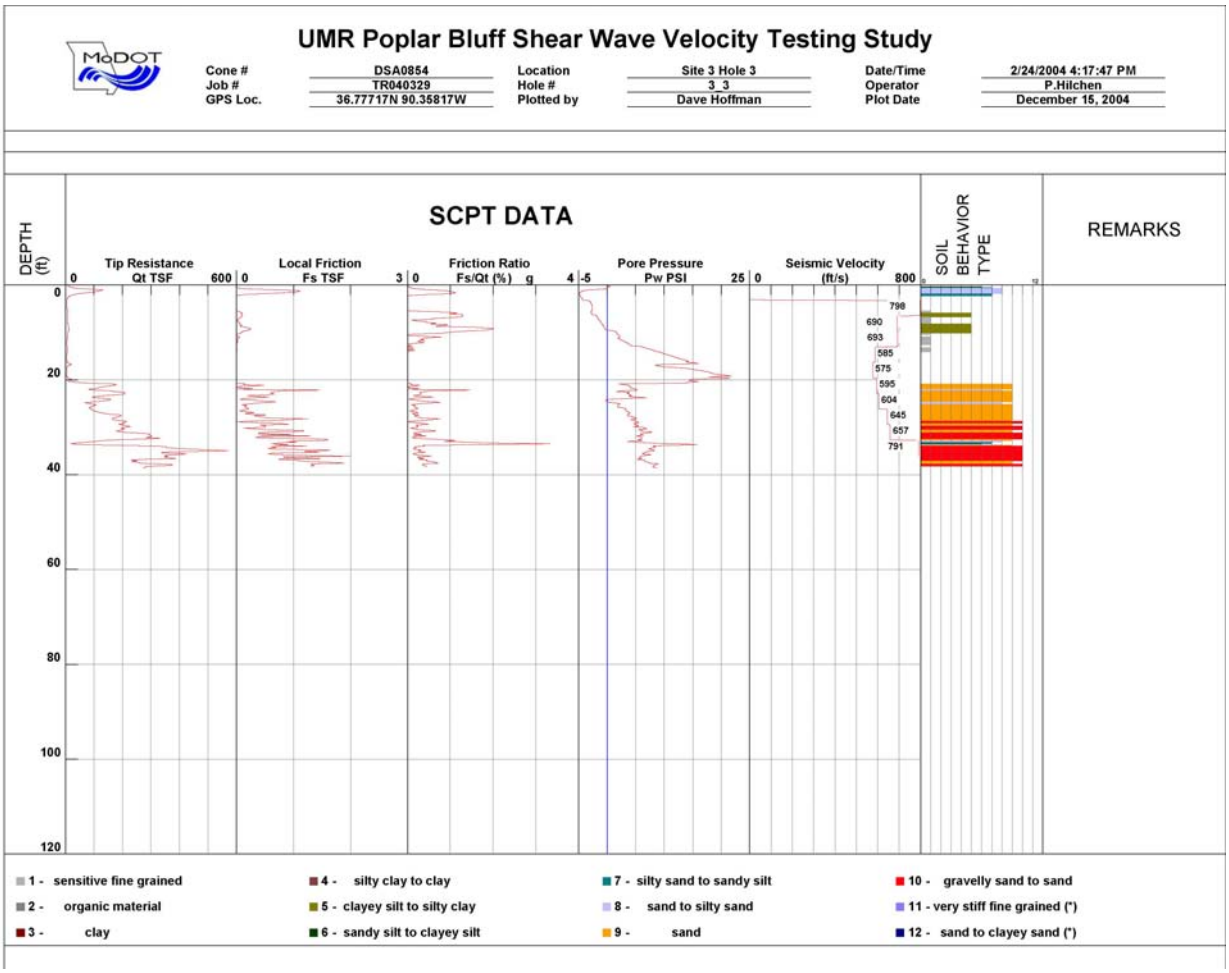

Figure D.3: SCPT data for SCPT Test Site #3-3 (Figure 2.4).

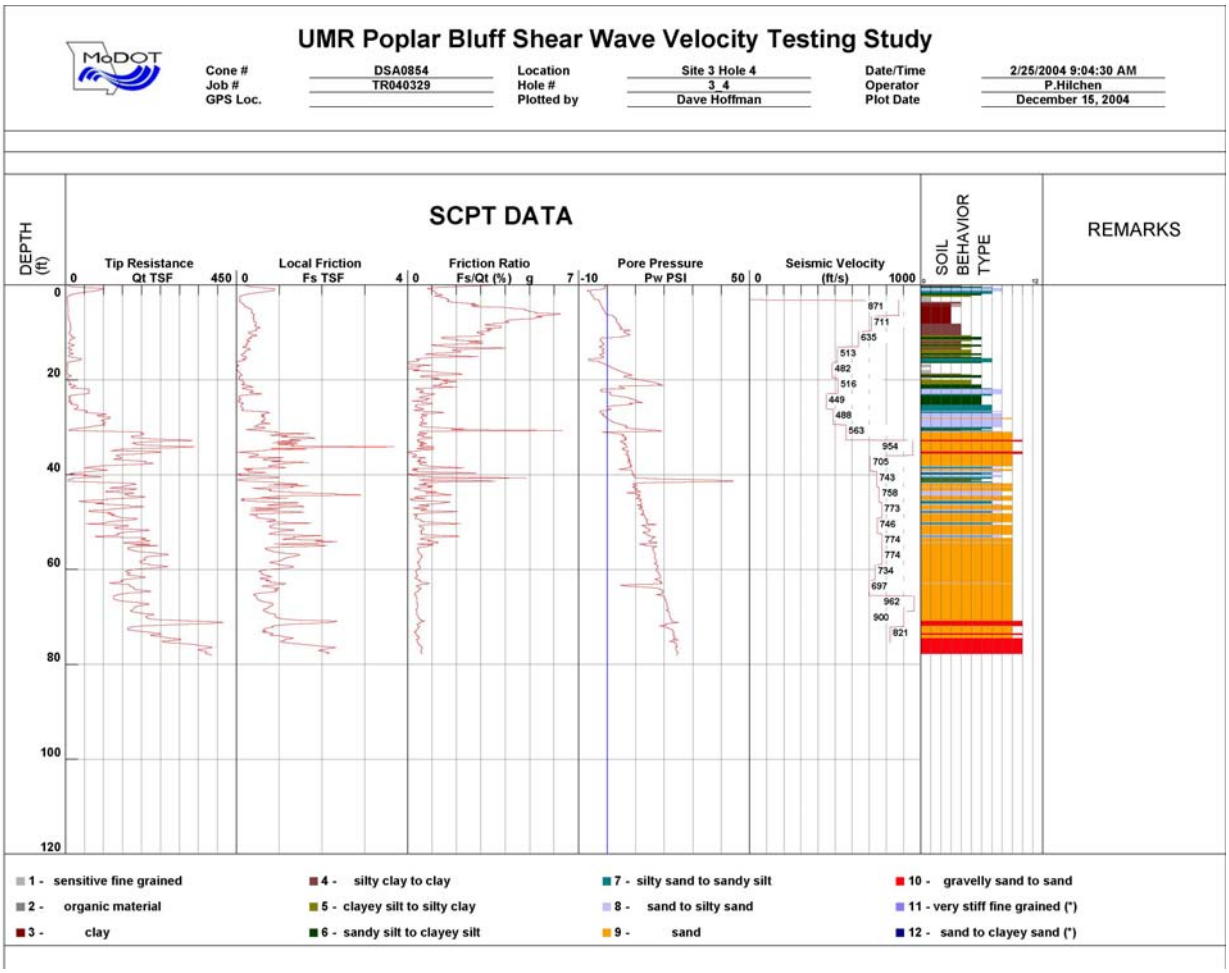

Figure D.4: SCPT data for SCPT Test Site #3-4 (Figure 2.4).

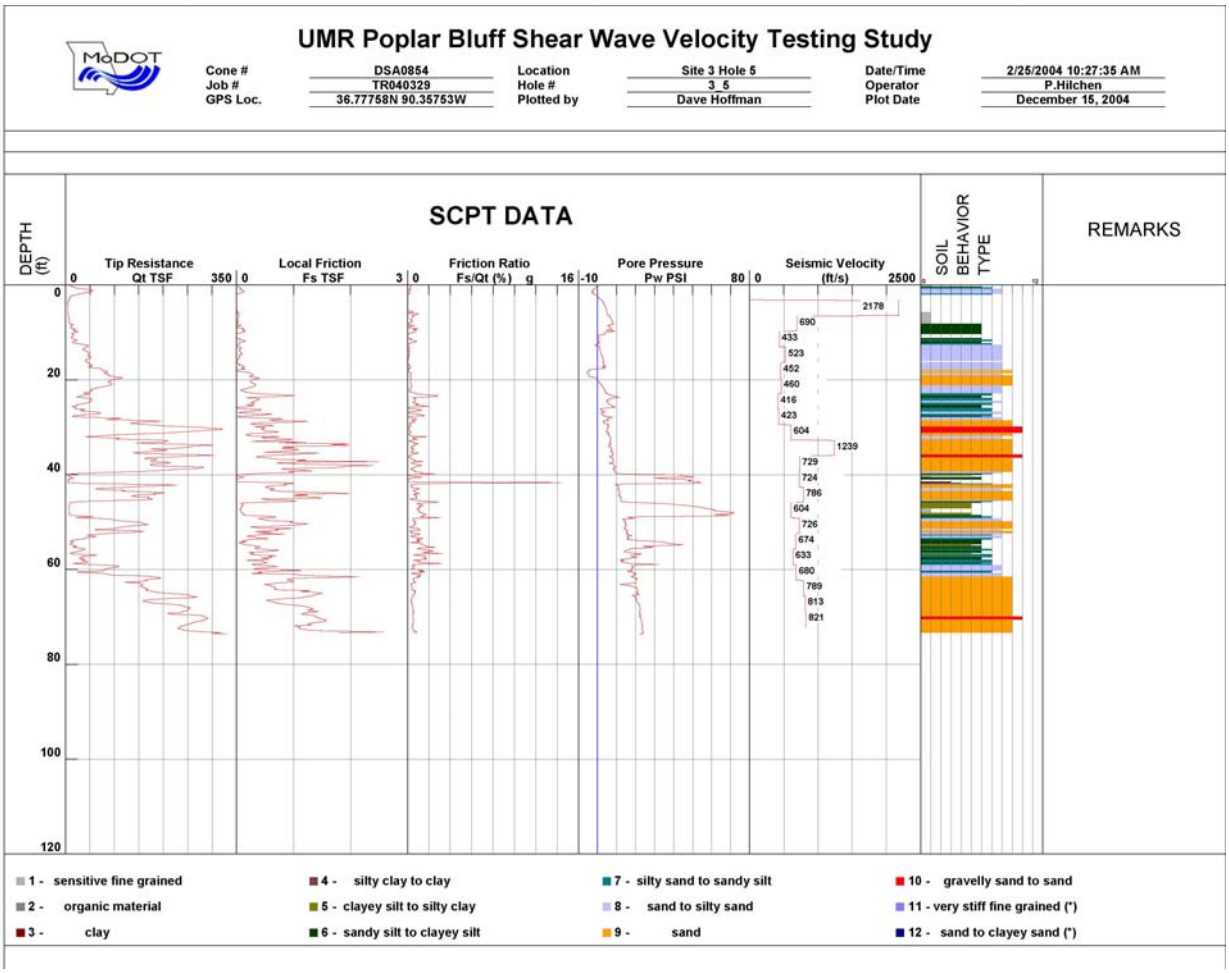

Figure D.5: SCPT data for SCPT Test Site #3-5 (Figure 2.4).

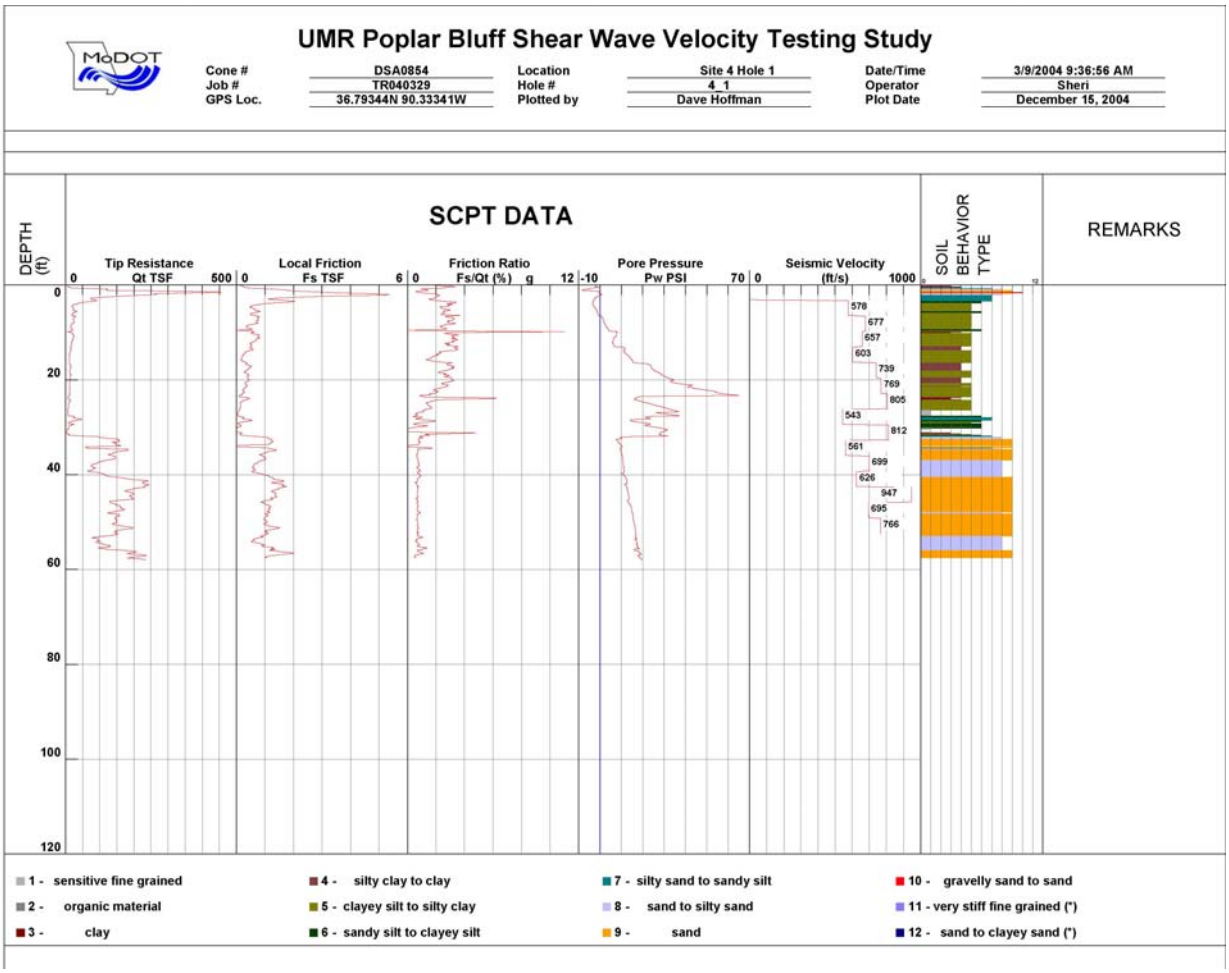

Figure D.6: SCPT data for SCPT Test Site #4-1 (Figure 2.4).

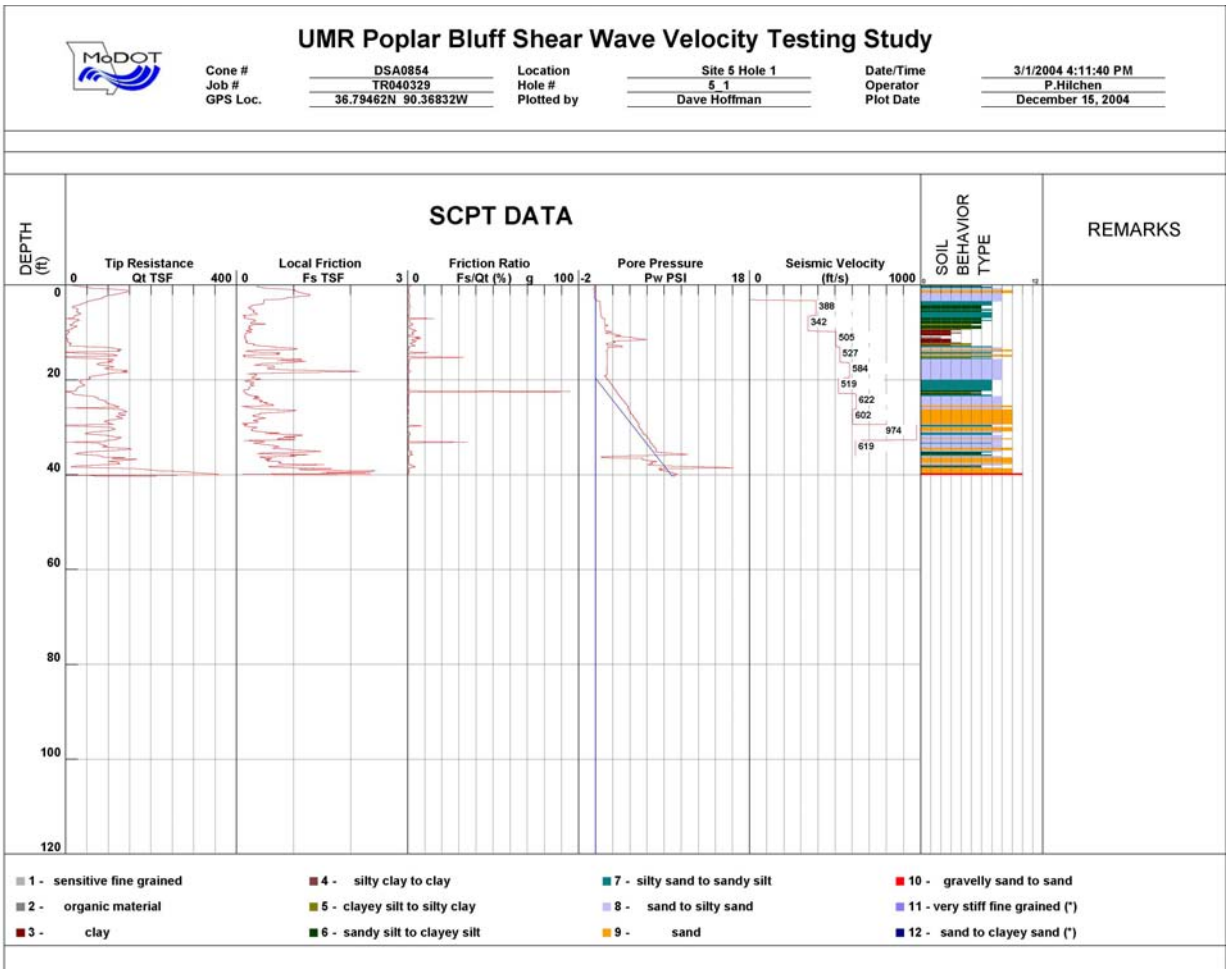

Figure D.7: SCPT data for SCPT Test Site #5-1 (Figure 2.4).

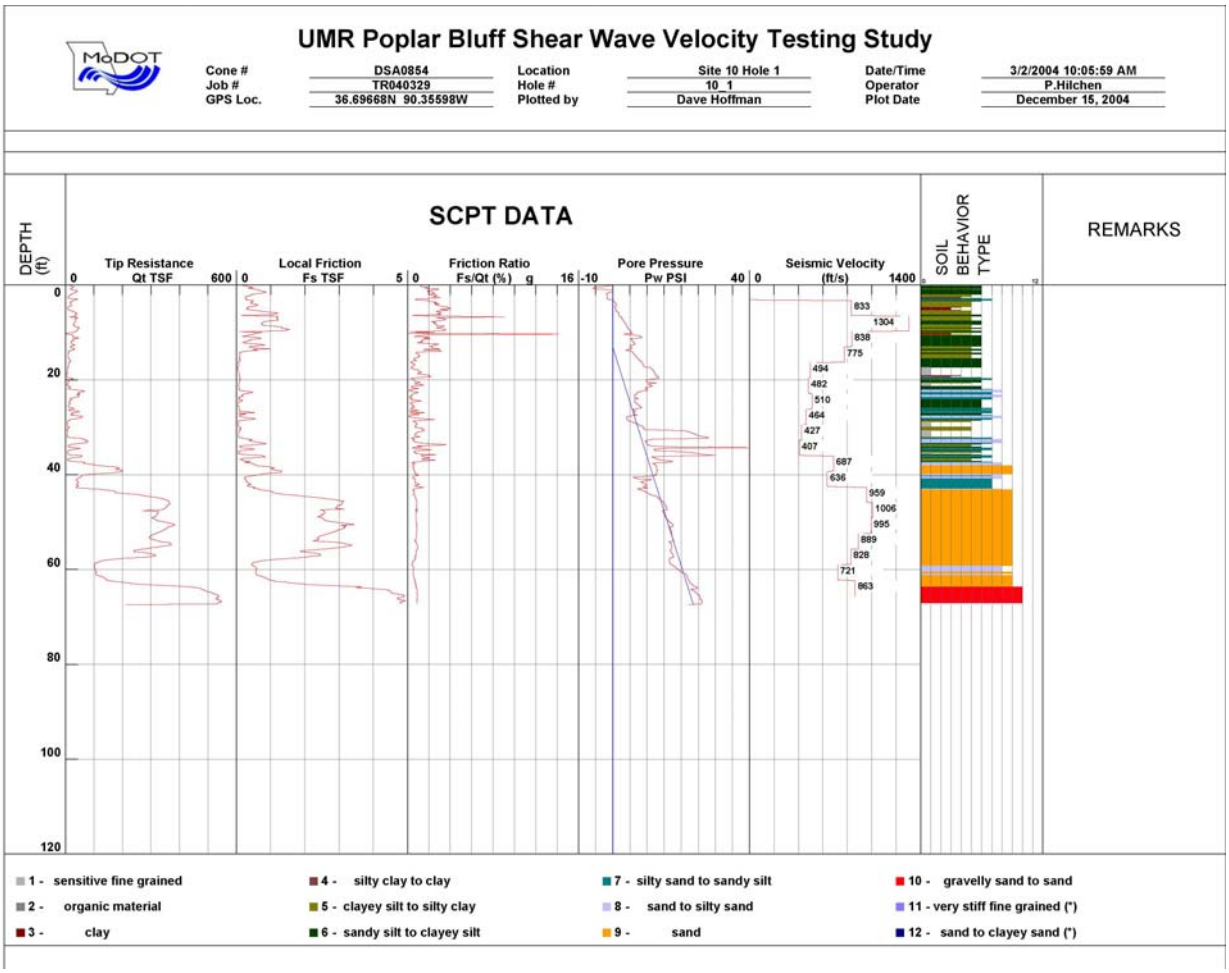

Figure D.8: SCPT data for SCPT Test Site #10-1 (Figure 2.4).

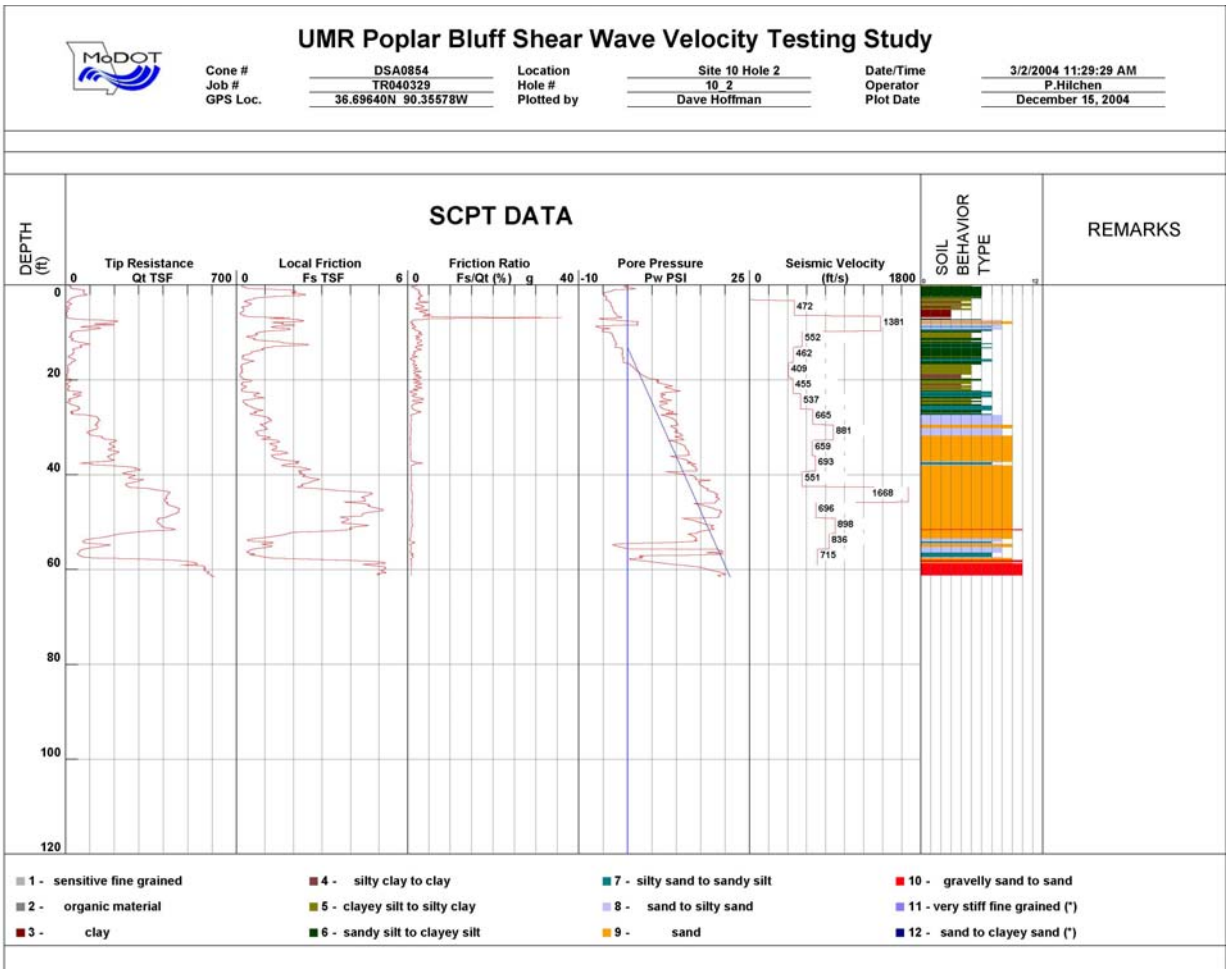

Figure D.9: SCPT data for SCPT Test Site #10-2 (Figure 2.4).

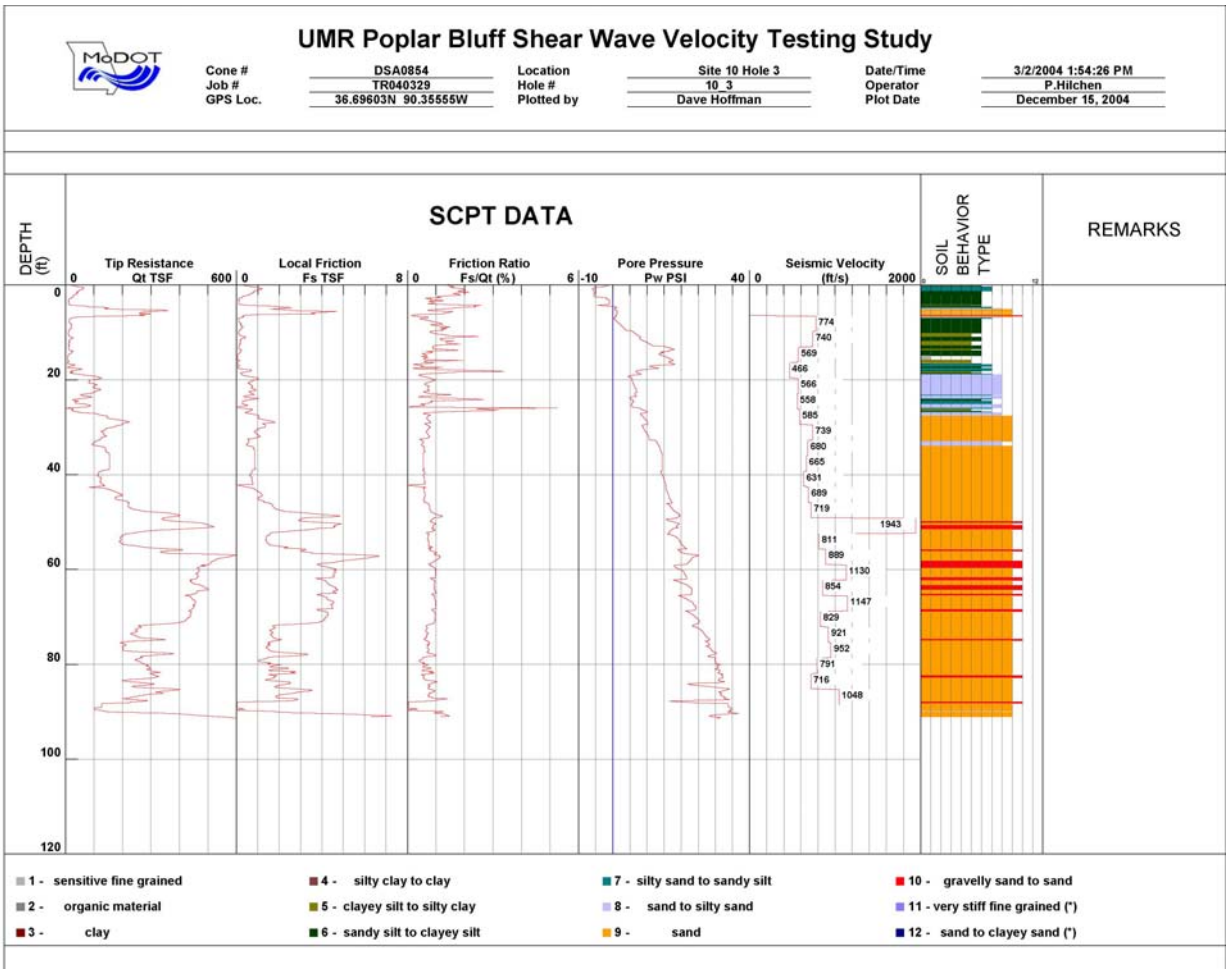

Figure D.10: SCPT data for SCPT Test Site #10-3 (Figure 2.4).

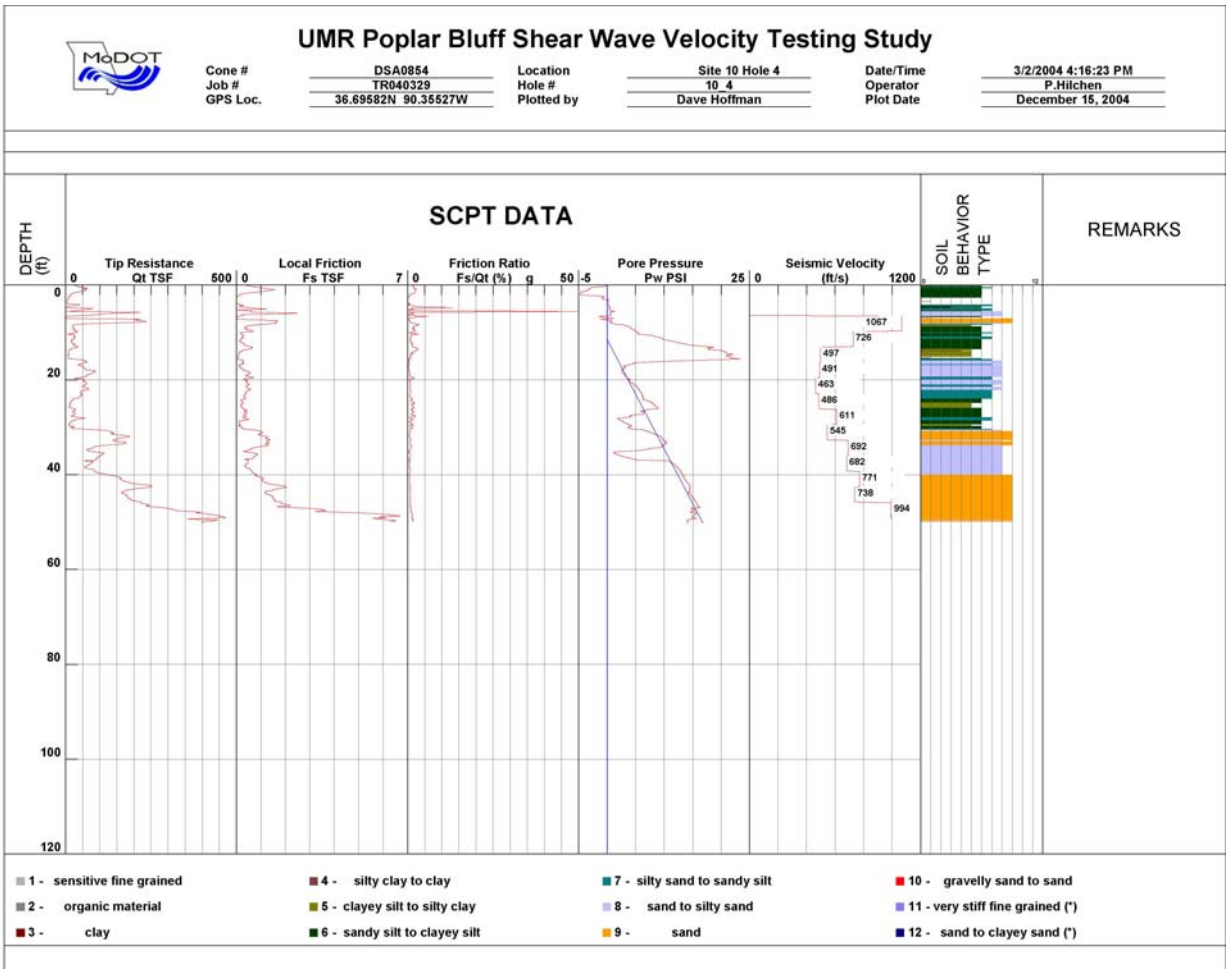

Figure D.11: SCPT data for SCPT Test Site #10-4 (Figure 2.4).

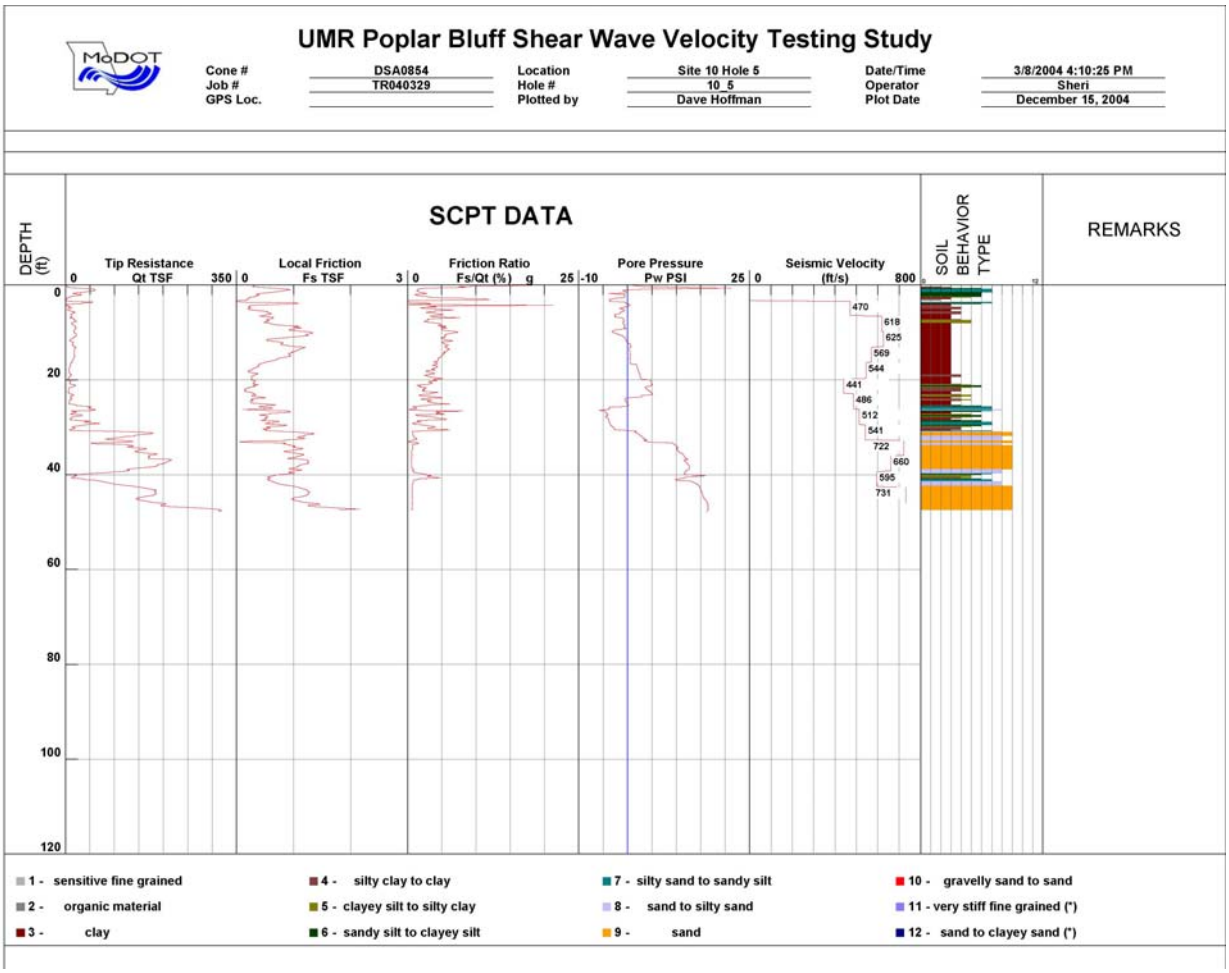

Figure D.12: SCPT data for SCPT Test Site #10-5 (Figure 2.4).

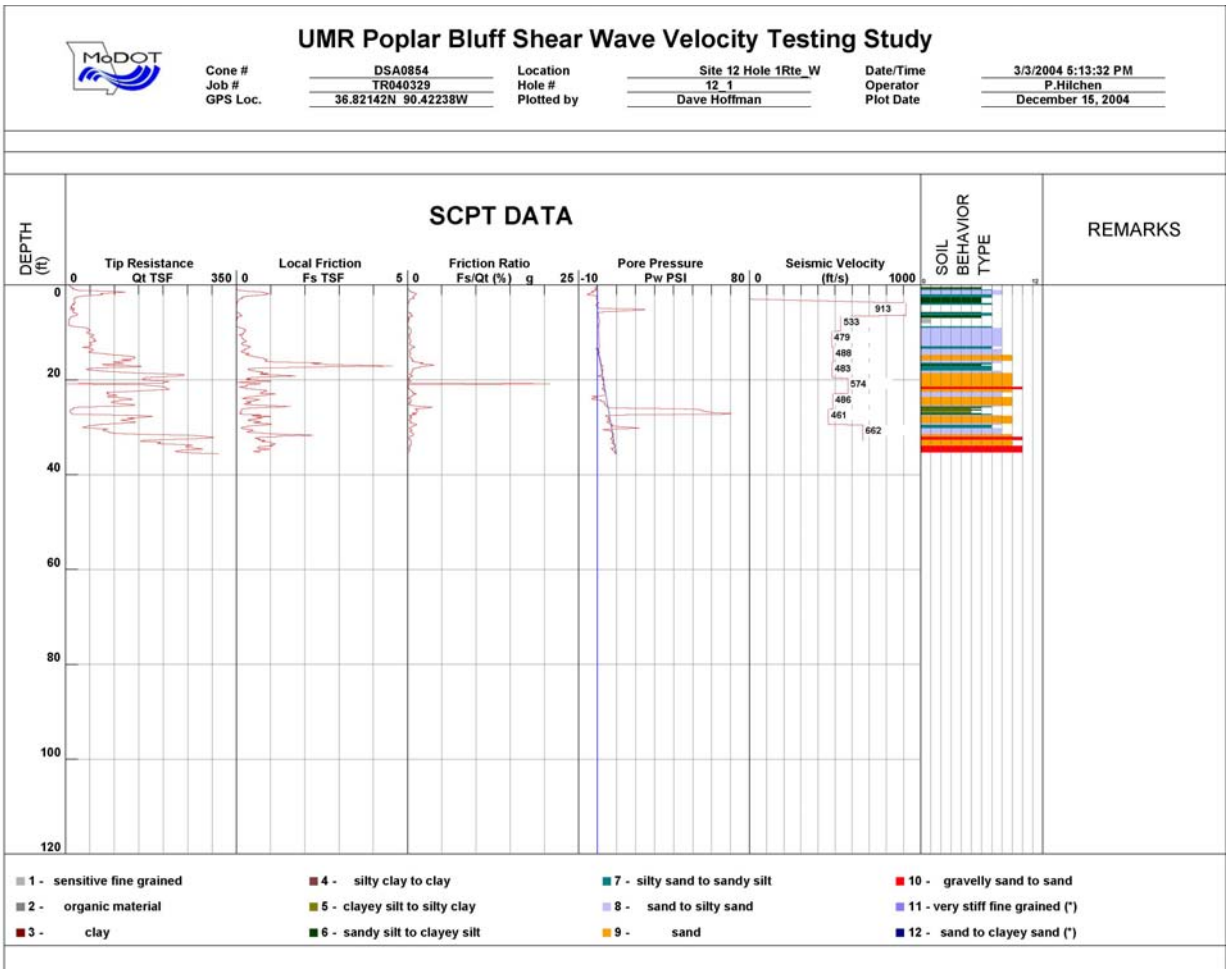

Figure D.13: SCPT data for SCPT Test Site #12-1 (Figure 2.4).

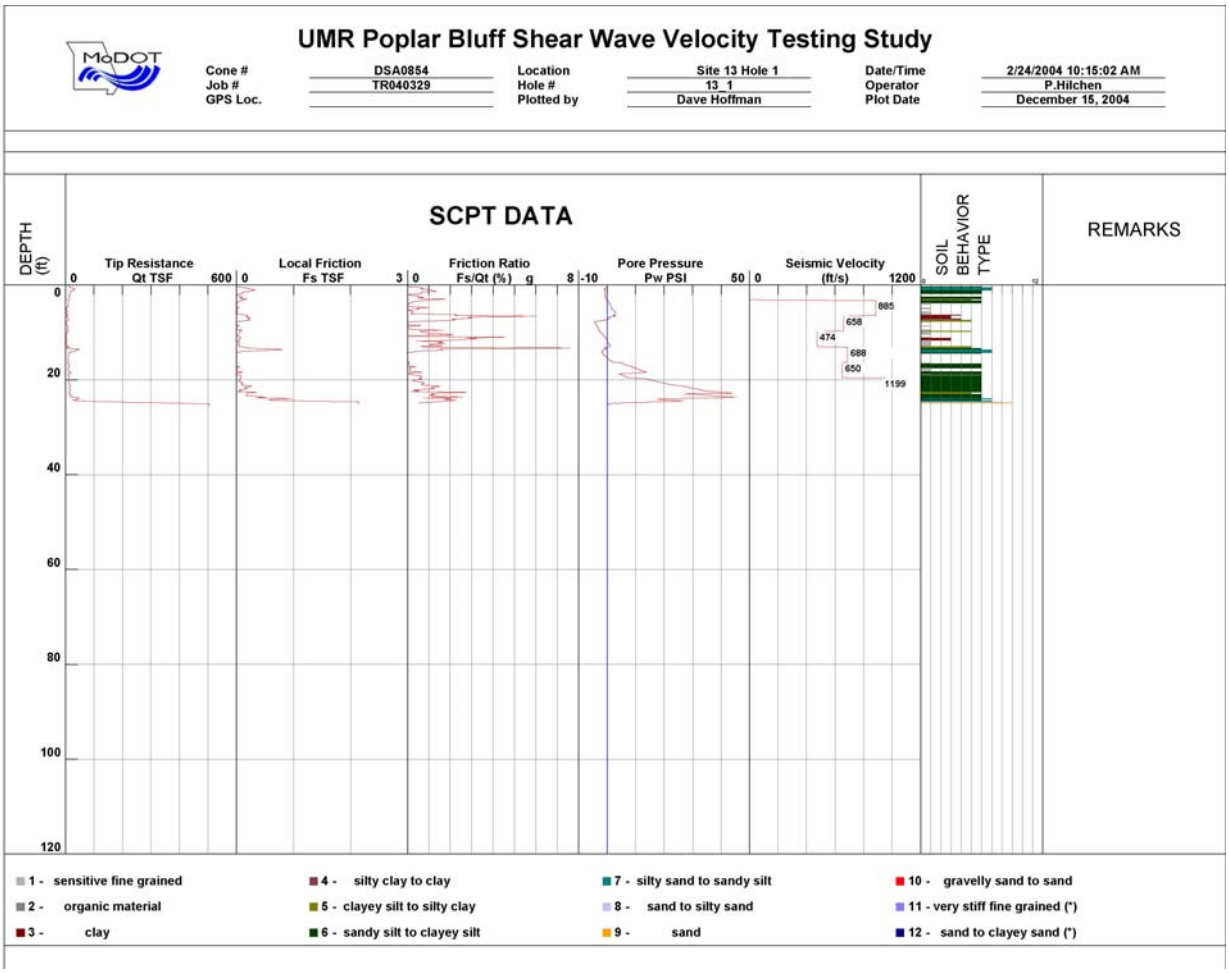

Figure D.14: SCPT data for SCPT Test Site #13-1 (Figure 2.4).

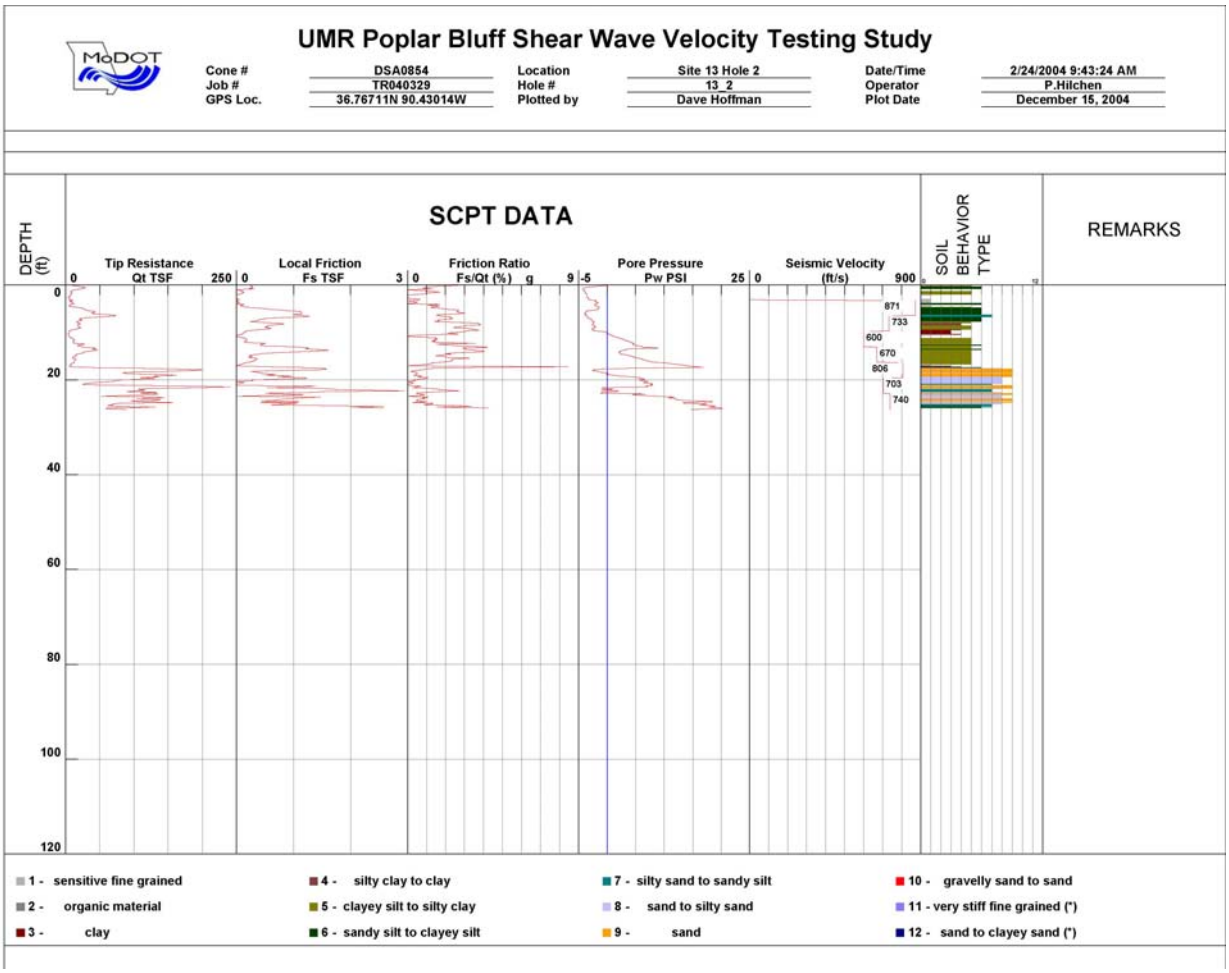

Figure D.15: SCPT data for SCPT Test Site #13-2 (Figure 2.4).

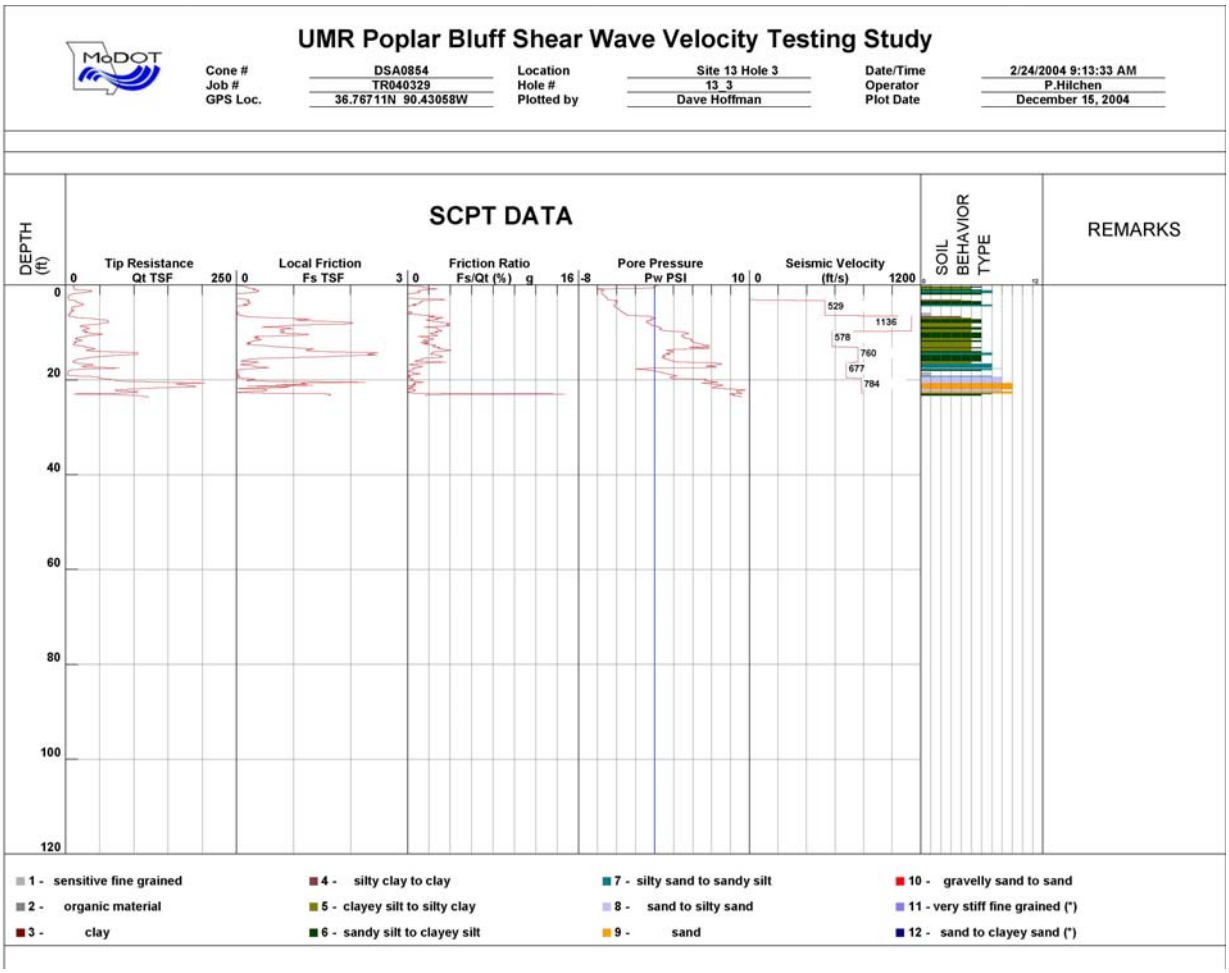

Figure D.16: SCPT data for SCPT Test Site #13-3 (Figure 2.4).

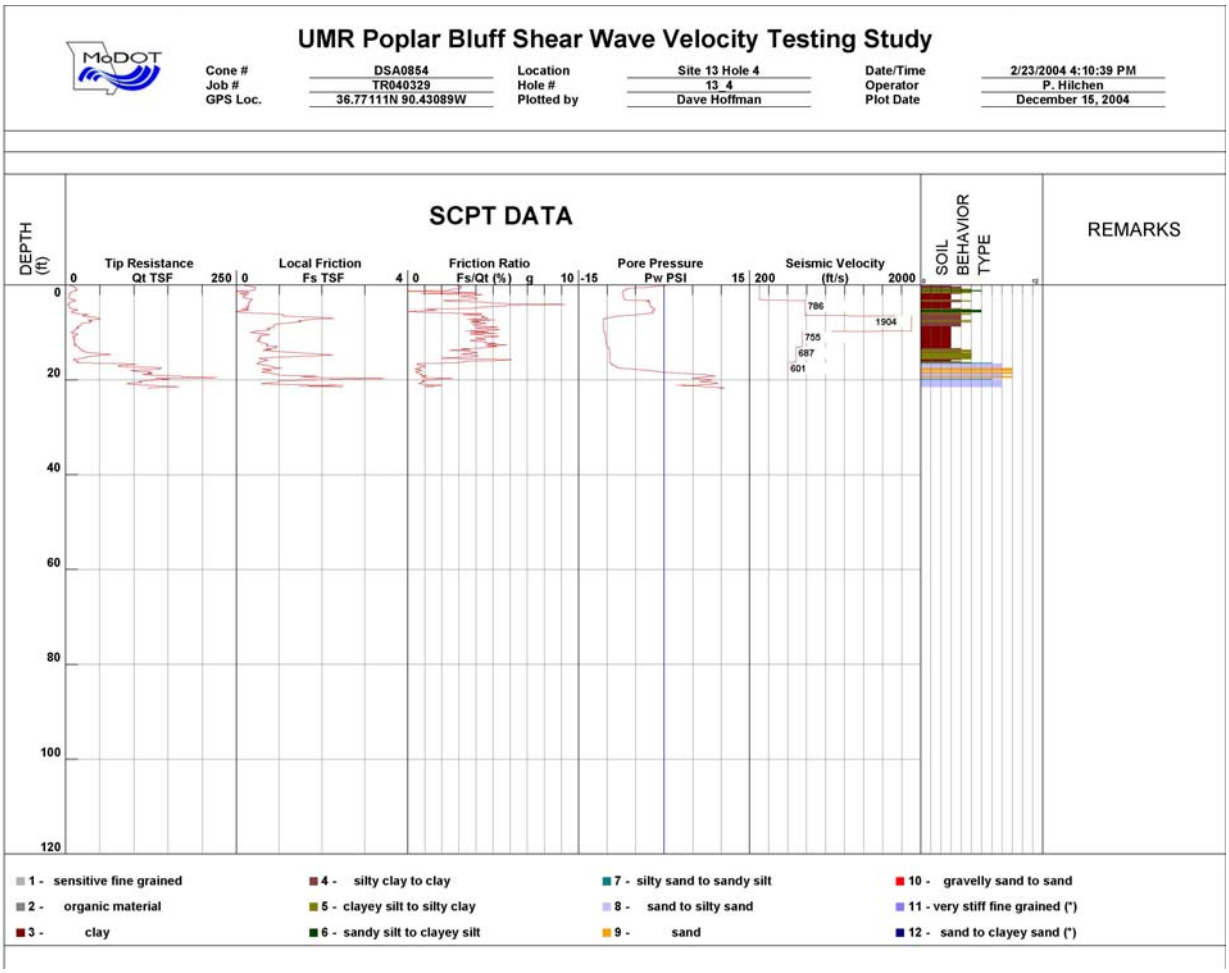

Figure D.17: SCPT data for SCPT Test Site #13-4 (Figure 2.4).

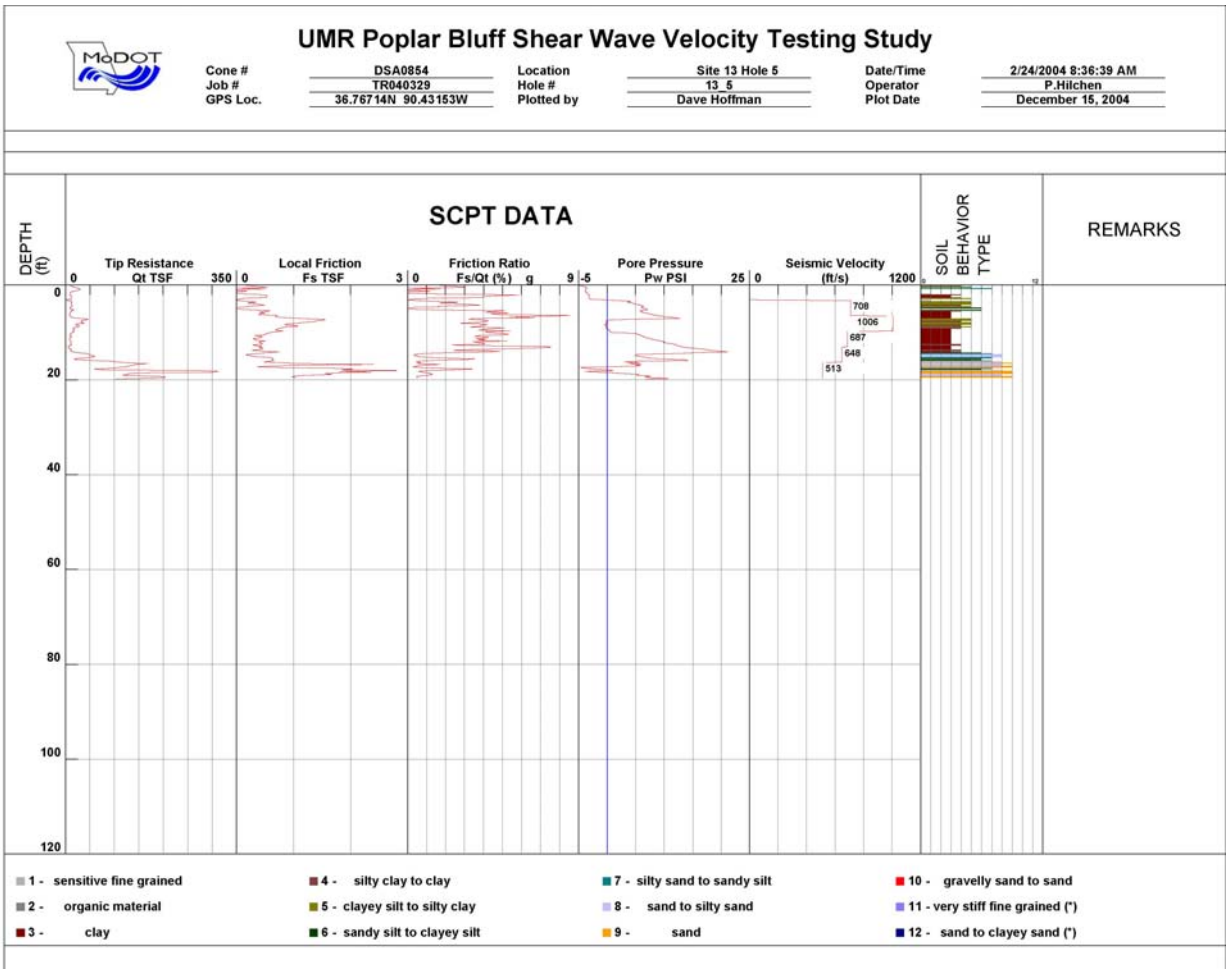

Figure D.18: SCPT data for SCPT Test Site #13-5 (Figure 2.4).

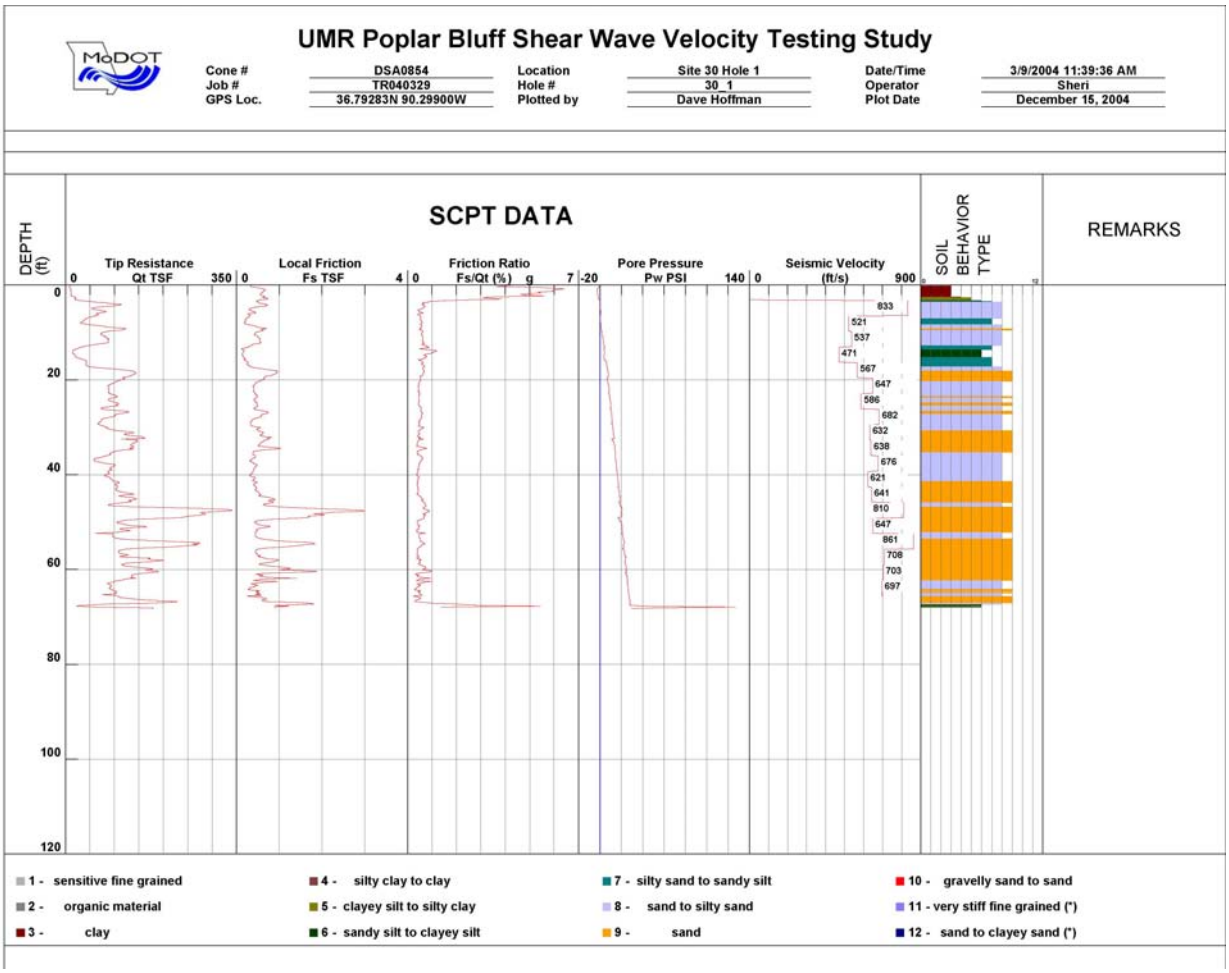

Figure D.19: SCPT data for SCPT Test Site #30-1 (Figure 2.4).

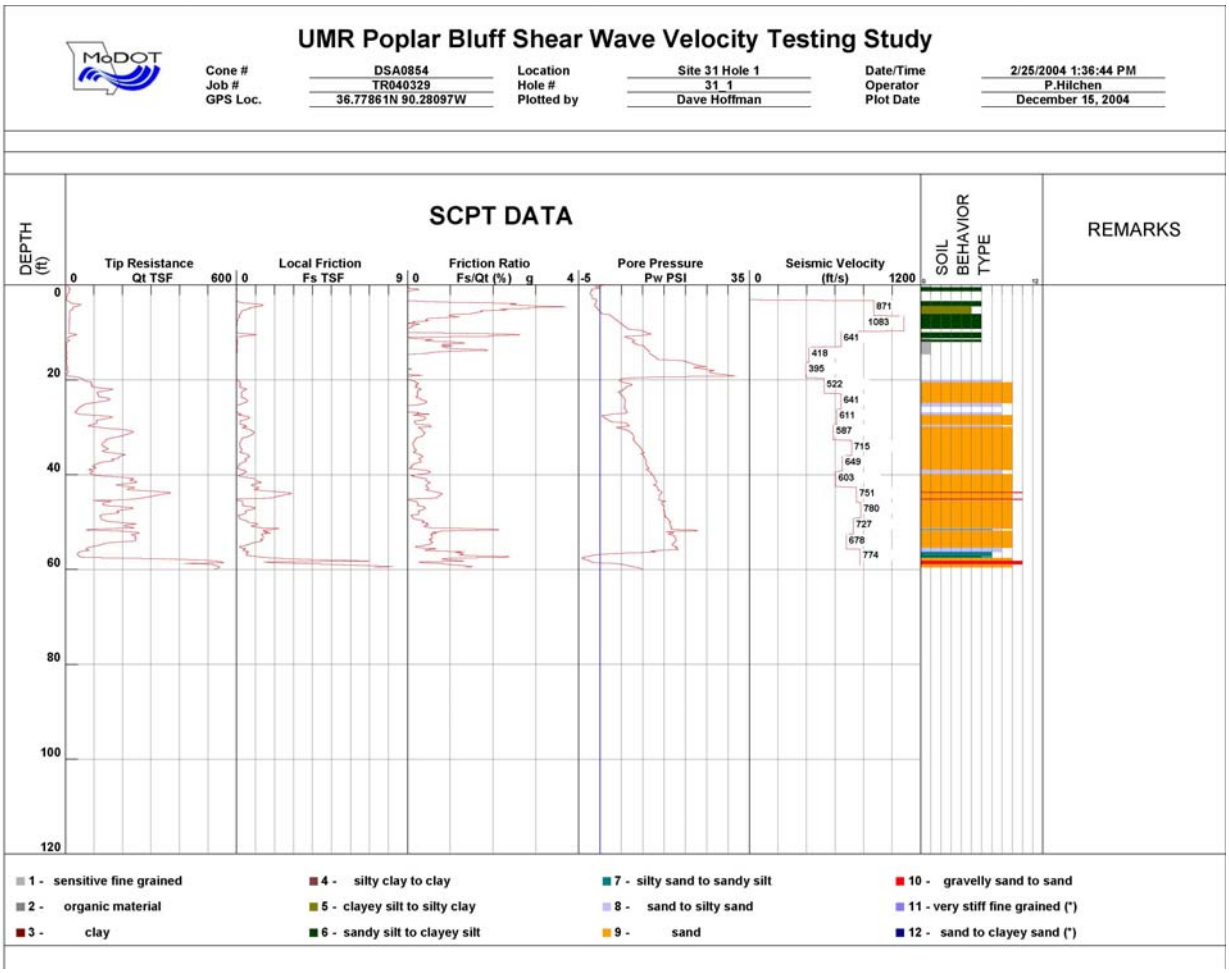

Figure D.20: SCPT data for SCPT Test Site #31-1 (Figure 2.4).

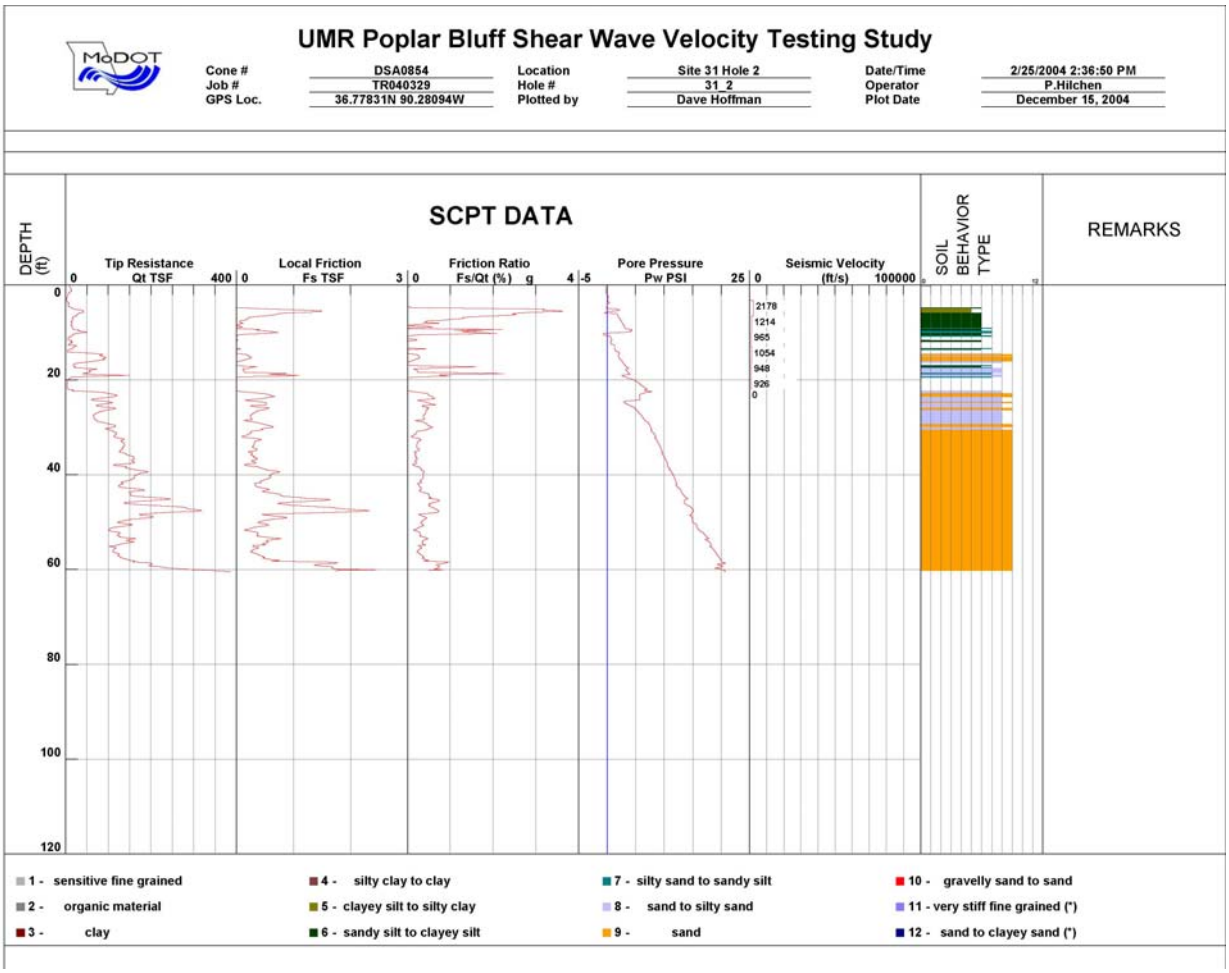

Figure D.21: SCPT data for SCPT Test Site #31-2 (Figure 2.4).

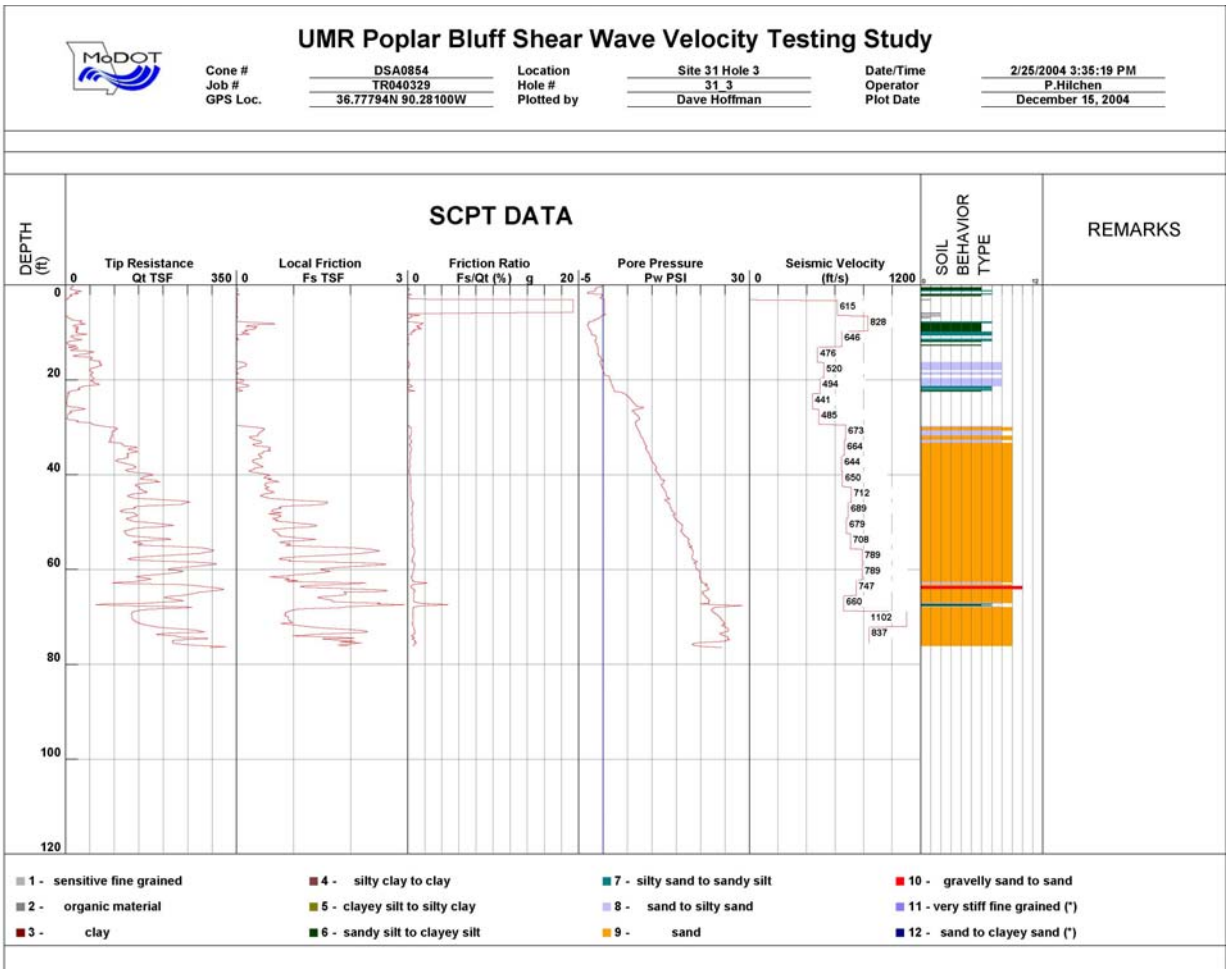

Figure D.22: SCPT data for SCPT Test Site #31-3 (Figure 2.4).

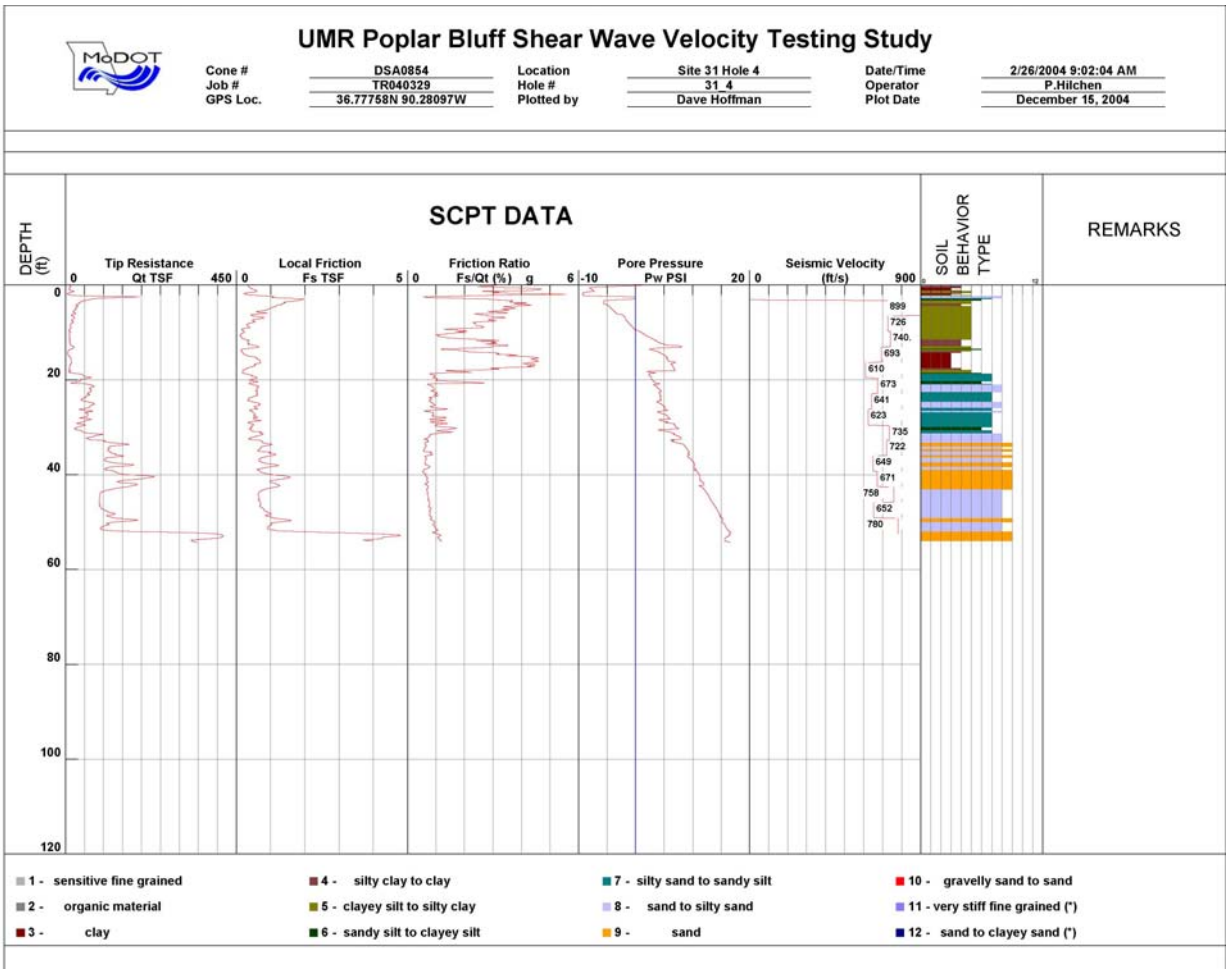

Figure D.23: SCPT data for SCPT Test Site #31-4 (Figure 2.4).

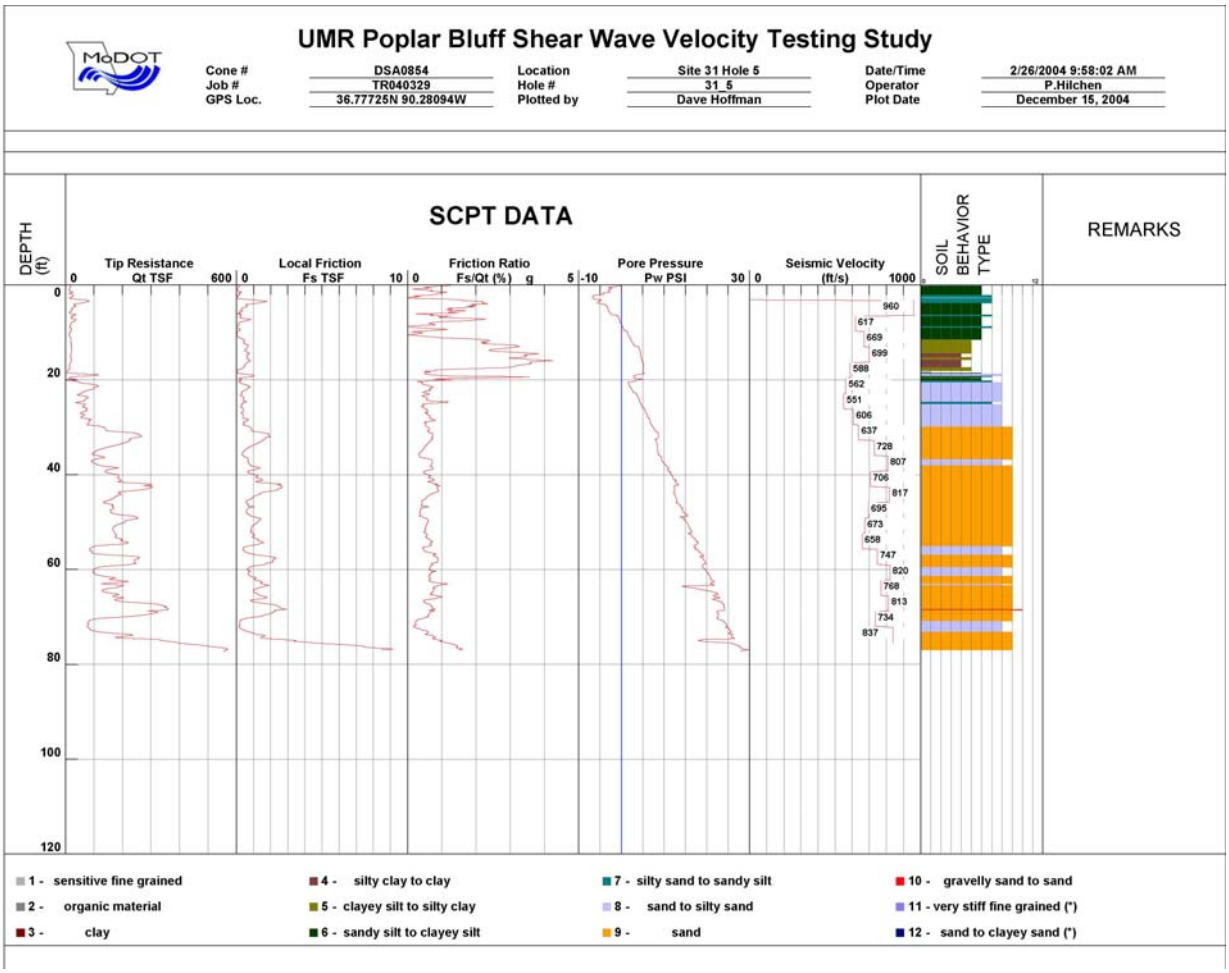

Figure D.24: SCPT data for SCPT Test Site #31-5 (Figure 2.4).

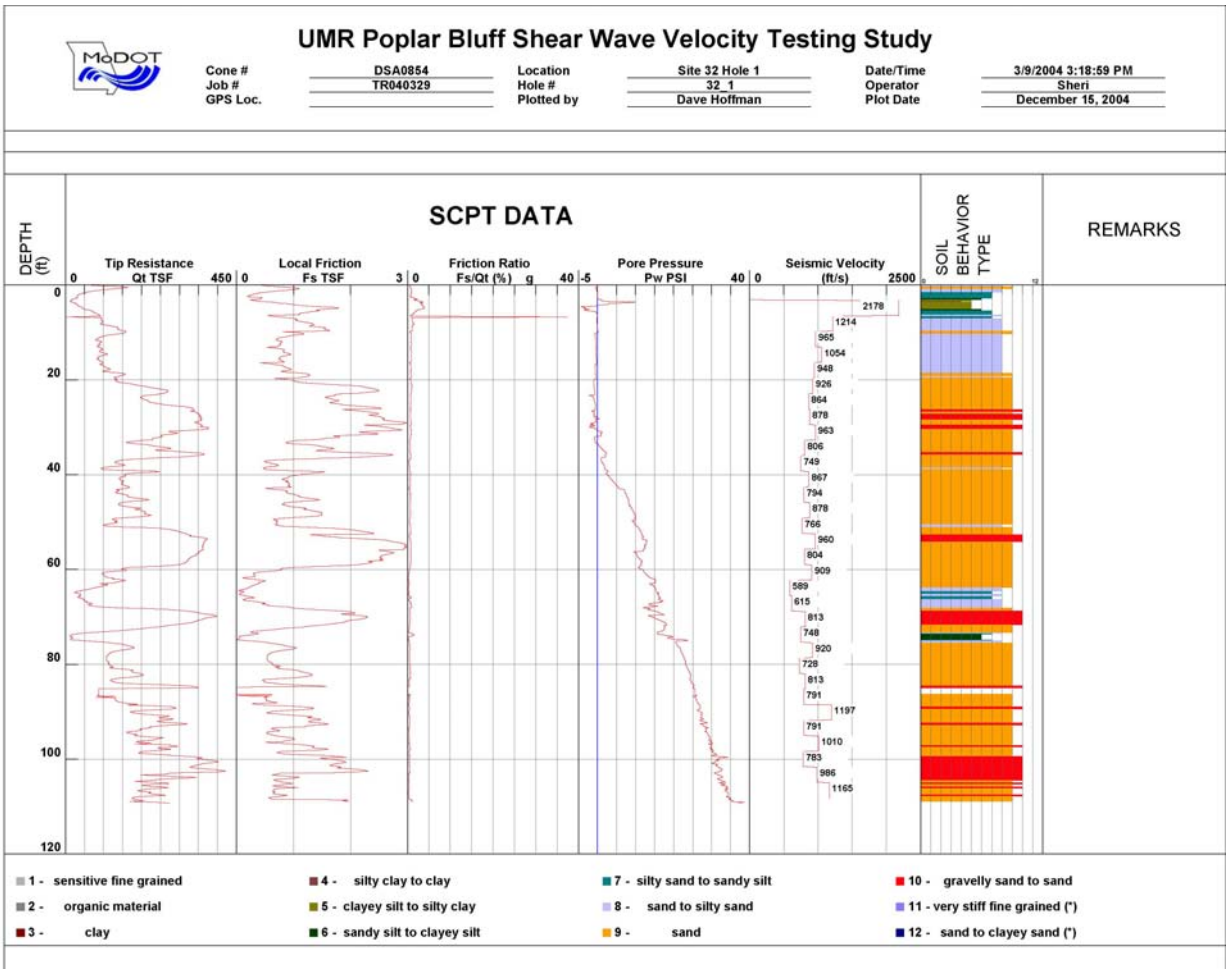

Figure D.25: SCPT data for SCPT Test Site #32-1 (Figure 2.4).

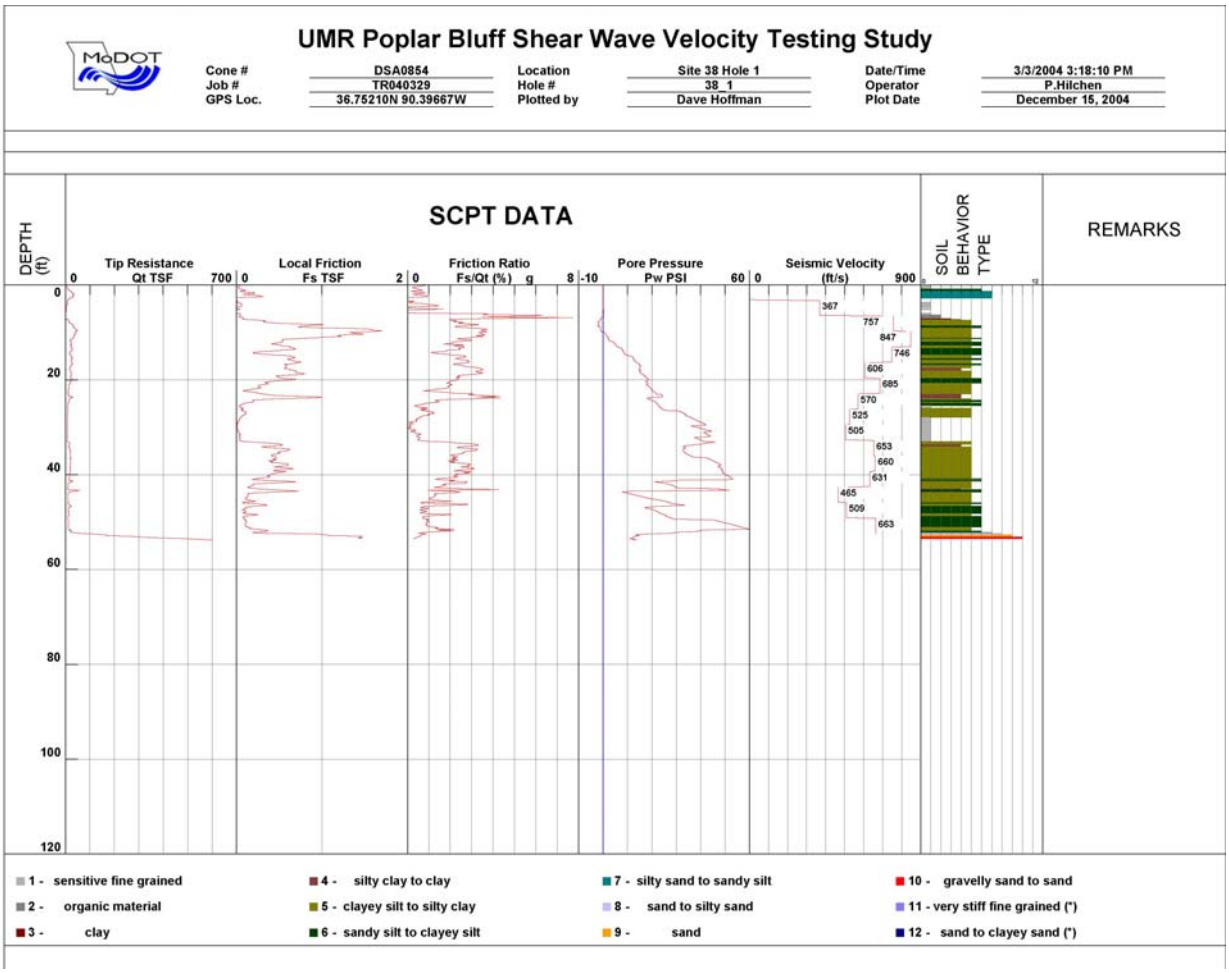

Figure D.26: SCPT data for SCPT Test Site #38-1 (Figure 2.4).

APPENDIX E: MASW SENSITIVITY ANALYSES

E.1 Overview

The transformation of field-recorded Rayleigh-wave data into shear-wave velocity data is based on two fundamental assumptions. The first assumption is that a reliable dispersion curve can be extracted from the field-recorded Rayleigh-wave data. The second assumption is that reliable shear-wave velocities can be extracted from a Rayleigh-wave dispersion curve, even though the dispersion curve is principally a function of two unknowns: the shear-wave velocity of the subsurface and the compression-wave velocity of the subsurface.

In order to evaluate the reasonableness of these two assumptions, we conducted two sensitivity analyses. In the first sensitivity study, we analyzed the qualitative processes involved in the extraction of a dispersion curve from field-recorded Rayleigh-wave data. We concluded that a trained interpreter will consistently extract reliable dispersion curve data from good-quality field-recorded Rayleigh-wave data. In the second sensitivity study, we examined the inter-relationships between Rayleigh-wave velocities, shear-wave velocities and compression-wave velocities. We concluded that the inversion of Rayleigh-wave dispersion data (i.e., generation of a shear-wave velocity curve) is a robust and reliable process even though Rayleigh-wave velocities are also a function of compression-wave velocities. This is because the velocities of high-frequency (5 Hz+) Rayleigh waves are relatively insensitive to variations in the compression-wave velocity of the subsurface.

E.2 Sensitivity Study #1: Extraction of Dispersion Curve Data

The extraction of dispersion data from field-recorded Rayleigh-wave data is a standard, established mathematical process that does not require any interactive input from the interpreter (Figure E.1). The analysis of the output dispersion data and the selection of optimum phase velocities (dispersion curve), in contrast, requires qualitative input from the interpreter. Hence, there is potential for human error.

The selection of optimum phase velocities from dispersion data is usually straightforward if good quality Rayleigh-wave data are acquired in the field. If the field data are good quality, the dispersion data will be characterized by a narrow, well-defined peak (Figure E.1). In this case, the interpreter merely selects phase velocities that fall along the well-defined peak. Numerous modeling studies and field tests have confirmed that these phase velocities are “optimum” (Xia et al., 1999). The “optimum” dispersion curve has been superposed on the dispersion data of Figure E.1c and plotted separately in Figure E.2a. The corresponding 1-D shear-wave velocity curve is plotted in Figure E.2b. This shear-wave velocity curve is also considered to be “optimum”.

In order to demonstrate the sensitivity of the dispersion curve extraction process, we intentionally extracted two non-optimum dispersion curves (Figures E.1b and E.1d). These two curves are non-optimum because their phase velocities do not fall on the well-defined peak on the dispersion data. More specifically, the phase velocities selected in Figure E.1b are greater than optimum; the phase velocities selected in Figure E.1d are lower than optimum (Figures E.1

and E.2). The velocity values on the corresponding 1-D shear-wave velocity curves are similarly too low and too high, respectively (Figure E.2).

As previously mentioned, the selection of optimum phase velocities from good quality dispersion data is usually straightforward over the dominant bandwidth of the data. Trained interpreters will usually select similar phase velocities and generate similar 1-D shear-wave velocity profiles. However, difficulties (and differences of opinion) can arise when the interpreter selects phase velocities at frequencies near the low end of those that were actually generated by the source in the field.

The nature of this problem is illustrated by the dispersion data in Figure E1. These dispersion data are characterized by a well-defined peak at frequencies above 7 Hz. This "peak" has widened considerably at 6 Hz and is almost absent at 5 Hz. (Data quality at low frequencies is variable being a function of both source size and ground conditions.) The selection of phase velocities at the low frequency 5-6 Hz range (in a genuine attempt to extract velocity control at greater depth) requires judicious extrapolation. If the selected phase velocities are too low, the *shear-wave velocities assigned to the deepest layers in the output model will be too low. Conversely, if the selected phase velocities are too high, the assigned shear-wave velocities will also be too high. This can also result in the underestimation or overestimation of depths, respectively.

E.3 Sensitivity Study #2: Inversion of Surface (Rayleigh) Wave Data

Rayleigh-wave velocities are a function of both the shear-wave velocity of the subsurface and the compression-wave velocity of the subsurface. The inter-relationships between Rayleigh-wave velocities, shear-wave velocities and compression-wave velocities in a uniform half-space are expressed in Equation 1.

$$\mathbf{V_R^6 - 8\beta^2 V_R^4 + (24 - 16\beta^2/\alpha^2)\beta^4 V_R^2 + 16(\beta^2/\alpha^2 - 1)\beta^6 = 0} \qquad \text{Equation 1}$$

where:

$\mathbf{V_R}$ is the Rayleigh-wave velocity within the uniform medium,
$\boldsymbol{\beta}$ is the shear-wave velocity within the uniform medium (also denoted Vs),
$\boldsymbol{\alpha}$ is the compression-wave velocity within the uniform medium (also denoted Vp).

As indicated in Equation 1, Rayleigh-wave velocities are a function of both the shear-wave velocity of the subsurface and the compression-wave velocity of the subsurface. This fact that Equation 1 contains two unknowns (shear and compression-wave velocities) might initially suggest that it would be difficult to extract reliable shear-wave velocity information from field-recorded Rayleigh waves. Fortunately, this is not the case.

Sensitivity studies conducted by several authors including Xia et al. (1999) and Stokoe et al. (1994) have concluded that Rayleigh-wave phase velocities are influenced much less by changes in compression-wave velocity than by changes in shear-wave velocity. Stokoe (1994), for

example, indicates that Rayleigh-wave velocity and shear-wave velocity in a uniform half-space are related by the following equation:

$$\boldsymbol{\beta} = \mathbf{V_R} / \mathbf{C} \qquad \text{Equation 2}$$

where:

$\mathbf{V_R}$ is the Rayleigh-wave velocity within the uniform layer,
$\boldsymbol{\beta}$ is the shear-wave velocity within the uniform medium,
C is a constant ranging from 0.874 to 0.955 for Poisson's ratio ranges from 0.0 to 0.5.

Equation 2 indicates that the ratio of shear-wave velocity to Rayleigh-wave velocity does not change significantly even with extreme variations in Poisson's ratio.

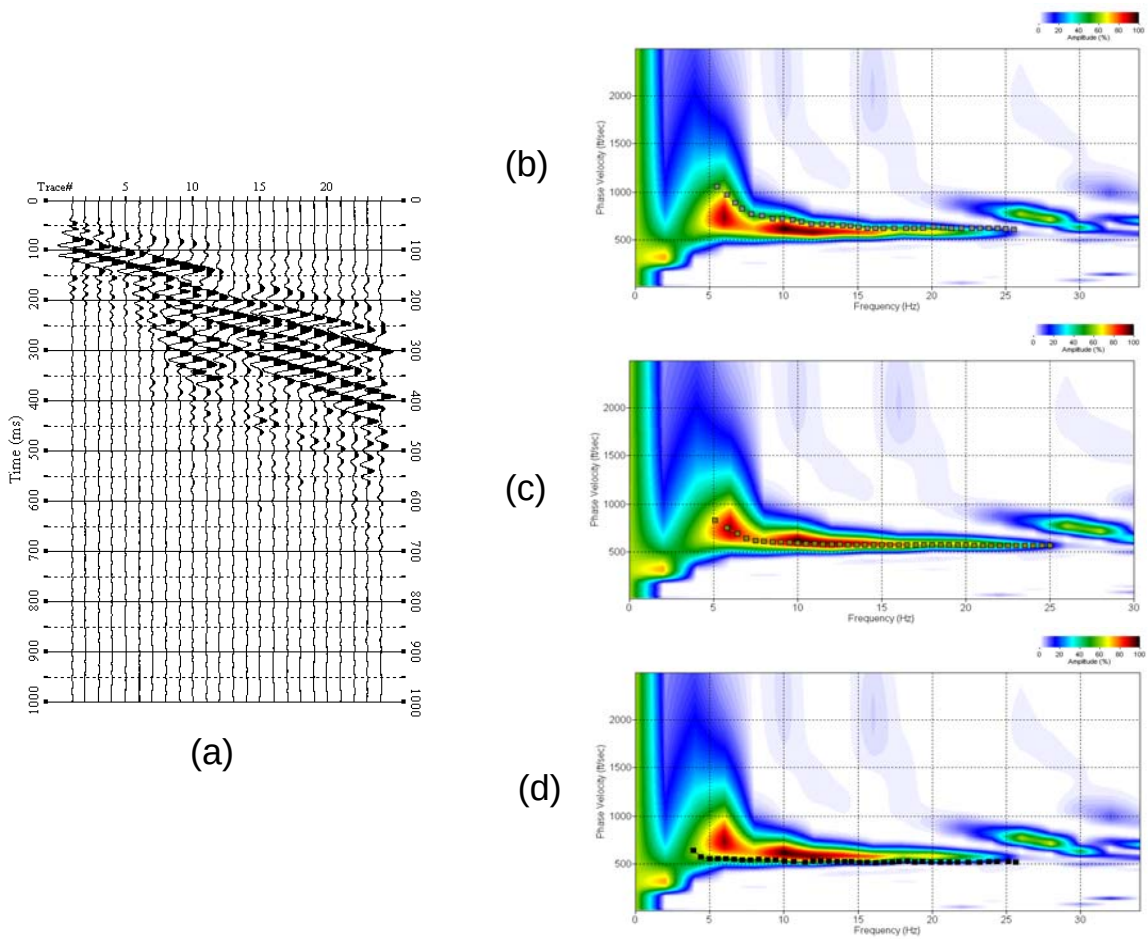

+

Figure E.1: Field record and three interpreted dispersion curves.

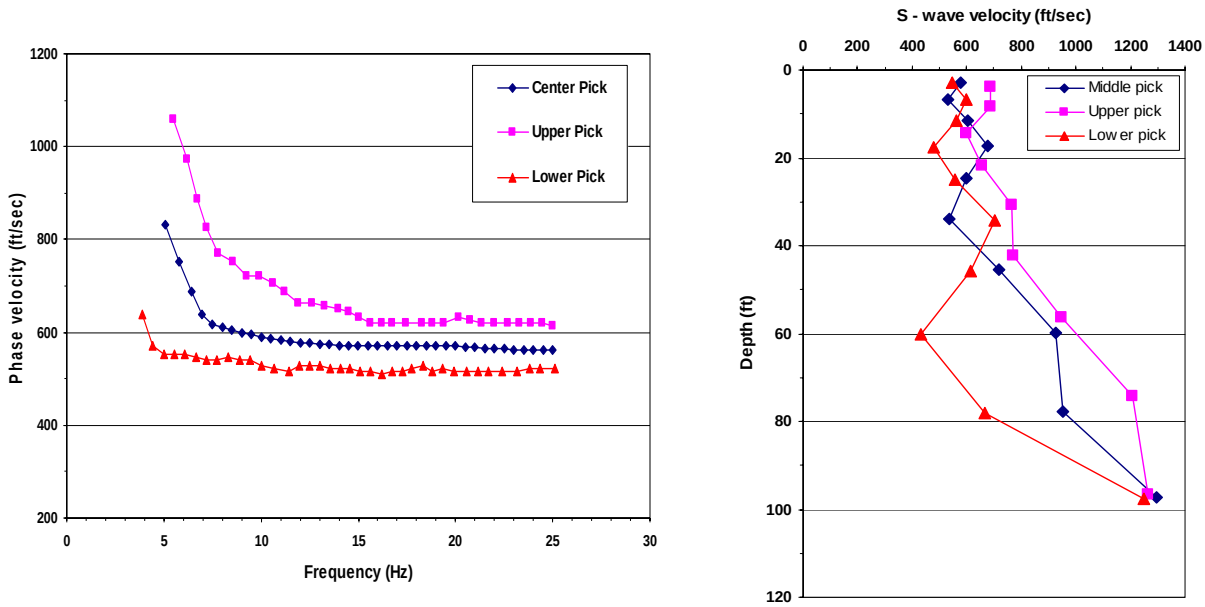

Figure E.2: Three interpreted dispersion curves and corresponding 1-D shear-wave velocity profiles.

Xia et al. (1999) conducted multiple model analyses and arrived at a similar conclusion. Xia et al. use a 6-layered earth model to illustrate the significance of this finding. They demonstrate that if the compression-wave velocity of each layer in their 6-layered model is increased by 25%, the Rayleigh-wave phase velocities are increased by less than 3%. In contrast, if the shear-wave velocity of each layer is increased by 25%, the Rayleigh-wave phase velocities are increased by 39%. Clearly, shear-wave velocity is the dominant parameter influencing changes in Rayleigh-wave phase velocity. They conclude that Rayleigh-wave phase velocity data can be reliably inverted and used to generate corresponding shear-wave data.

Xia et al. (1999) also discuss the Rayleigh-wave dispersion curve inversion program incorporated into the SURFSEIS MASW software package. (This software was used to process the MASW data collected as part of the Poplar Bluff study.) Xia et al. (1999) state that for the purposes of inversion, Poisson's ratio and therefore the constant **C** in Equation 2, can be assumed to be known. Based on multiple modeling studies using realistic compression-and shear-wave velocities, the value of the constant C (Equation 2) used in the SURFSEIS MASW software package has been preset to 0.88. Xia et al. (1999) state that this assumption introduces minimal error (generally <3%) into the output shear-wave velocity data.

APPENDIX F: RESONANT COLUMN TEST RESULTS

To obtain the shear modulus reduction curve over different strain levels ranging from 10^{-6} to 1, additional resonant column tests were conducted. Three samples were selected from three different types of soils. They are sand (BHUMR1-32), residuum (CHUMR3), and silt/clay (CHUMR3-141). The sand and residuum samples were remolded to the same density used for ultrasonic and cyclic triaxial tests with same confining pressure. The silt/clay sample is the disturbed samples from same Shelby tube used for ultrasonic and cyclic triaxial tests. The same confining pressure was employed. The different strain levels were obtained by changing the torque output amplitude to driving system. The shear strain ranges about from $10^{-5} \sim 10^{-2}$. The shear modulus variation with shear strain for these three samples is shown in Figure F.1. Figure F.2 illustrates the normalized shear modulus reduction curves for the three samples. The shear modulus deceases with shear strain increasing for all three types of soils, which implicates the behavior of soils become nonlinear at high strain levels. For these three soil samples their shear moduli dramatically decreased even at shear strain higher than 10^{-5}. All these results are comparable and within the range in the foregoing literature. The resonant frequency and test results using different torque output amplitudes are presented as Figures F.3 – F.5.

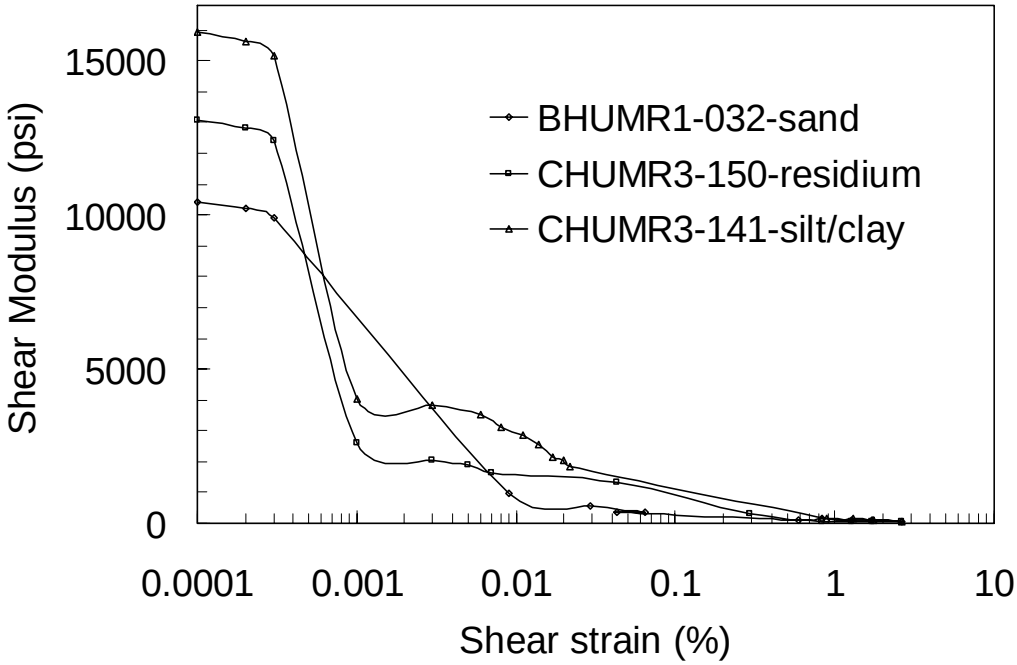

Figure F.1: Shear modulus variation with shear strain.

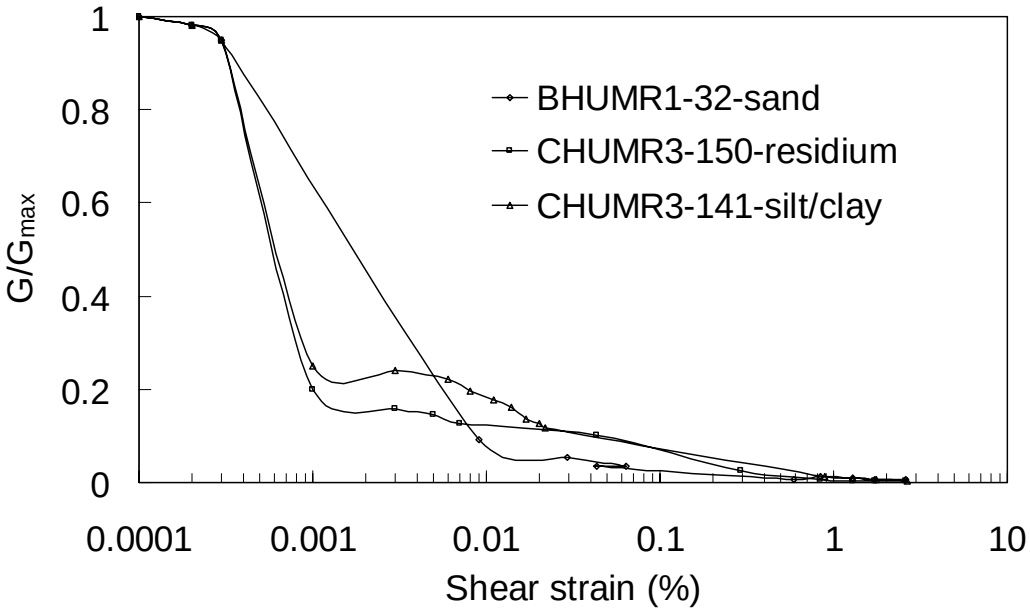

Figure F.2: Normalized shear modulus reduction with shear strain.

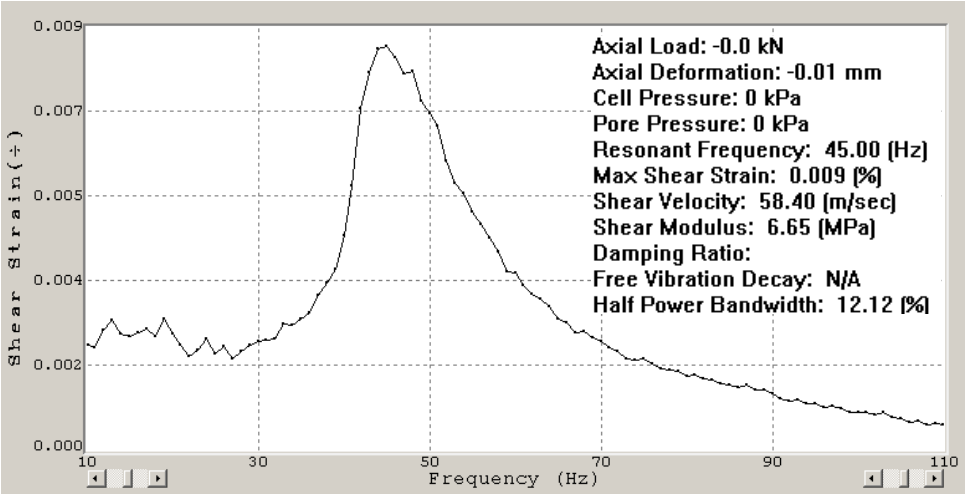
Axial Load: -0.0 kN
Axial Deformation: -0.01 mm
Cell Pressure: 0 kPa
Pore Pressure: 0 kPa
Resonant Frequency: 45.00 (Hz)
Max Shear Strain: 0.009 (%)
Shear Velocity: 58.40 (m/sec)
Shear Modulus: 6.65 (MPa)
Damping Ratio:
Free Vibration Decay: N/A
Half Power Bandwidth: 12.12 (%)
Shear Strain(÷)
Frequency (Hz)

(a)

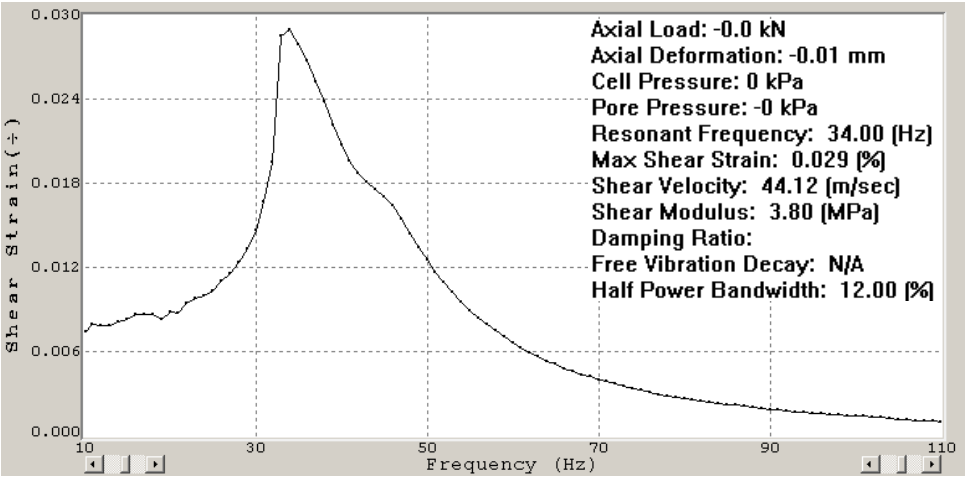
Axial Load: -0.0 kN
Axial Deformation: -0.01 mm
Cell Pressure: 0 kPa
Pore Pressure: -0 kPa
Resonant Frequency: 34.00 (Hz)
Max Shear Strain: 0.029 (%)
Shear Velocity: 44.12 (m/sec)
Shear Modulus: 3.80 (MPa)
Damping Ratio:
Free Vibration Decay: N/A
Half Power Bandwidth: 12.00 (%)
Shear Strain(÷)
Frequency (Hz)

(b)

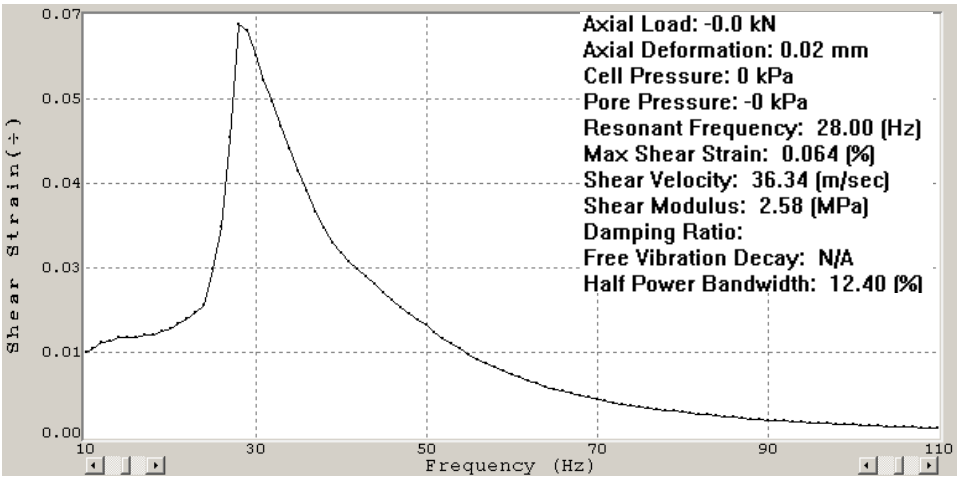
Axial Load: -0.0 kN
Axial Deformation: 0.02 mm
Cell Pressure: 0 kPa
Pore Pressure: -0 kPa
Resonant Frequency: 28.00 (Hz)
Max Shear Strain: 0.064 (%)
Shear Velocity: 36.34 (m/sec)
Shear Modulus: 2.58 (MPa)
Damping Ratio:
Free Vibration Decay: N/A
Half Power Bandwidth: 12.40 (%)
Shear Strain(÷)
Frequency (Hz)

(c)

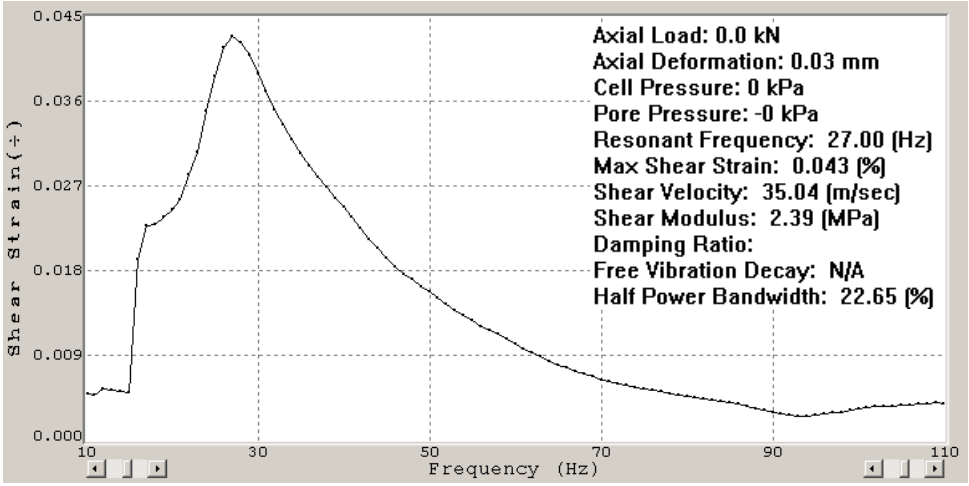

(d)

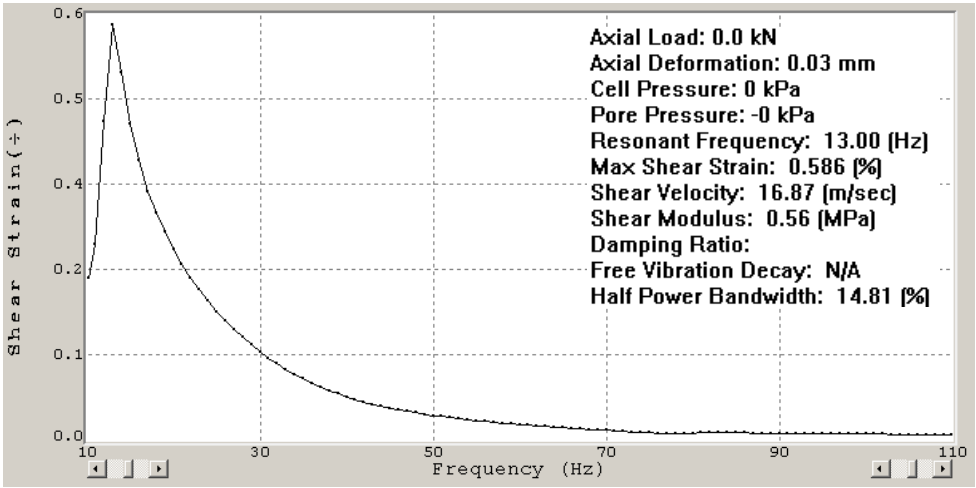

(e)

Figure F.3: Resonant frequency and shear modulus of sample CHUMR3-150 at different shear strain levels (a) psf=1%; (b) psf=2%; (c) psf=3%; (d) psf=4%; (e) psf=10%.

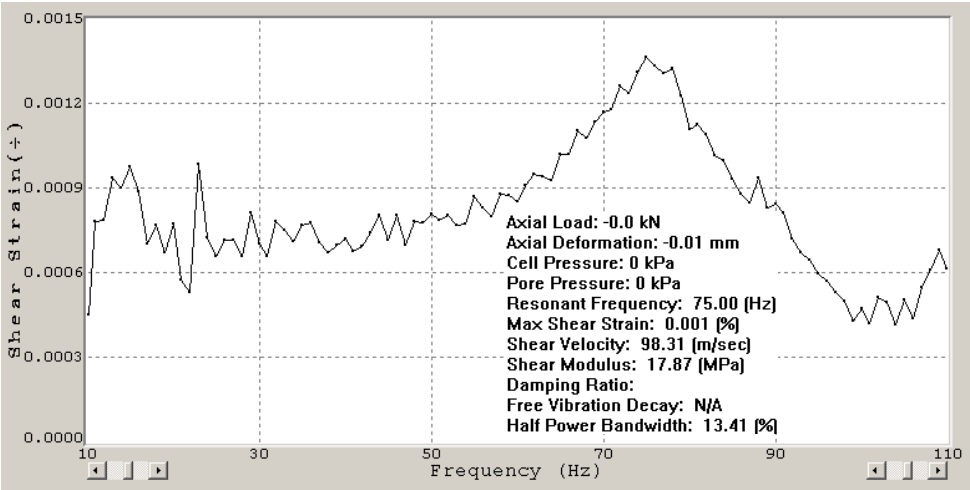
Shear Strain(÷)
0.0015
0.0012
0.0009
0.0006
0.0003
0.0000
10
30
50
70
90
110
Frequency (Hz)
Axial Load: -0.0 kN
Axial Deformation: -0.01 mm
Cell Pressure: 0 kPa
Pore Pressure: 0 kPa
Resonant Frequency: 75.00 (Hz)
Max Shear Strain: 0.001 (%)
Shear Velocity: 98.31 (m/sec)
Shear Modulus: 17.87 (MPa)
Damping Ratio:
Free Vibration Decay: N/A
Half Power Bandwidth: 13.41 (%)

(a)

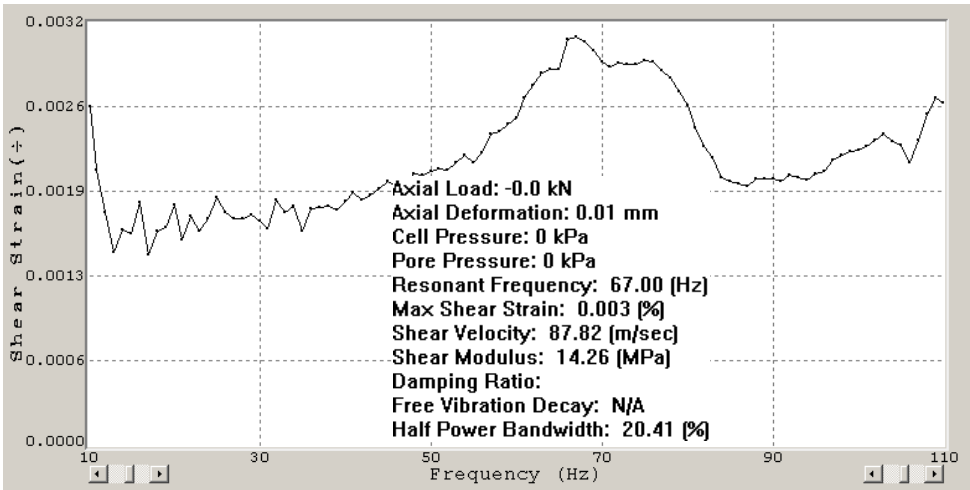
Shear Strain(÷)
0.0032
0.0026
0.0019
0.0013
0.0006
0.0000
10
30
50
70
90
110
Frequency (Hz)
Axial Load: -0.0 kN
Axial Deformation: 0.01 mm
Cell Pressure: 0 kPa
Pore Pressure: 0 kPa
Resonant Frequency: 67.00 (Hz)
Max Shear Strain: 0.003 (%)
Shear Velocity: 87.82 (m/sec)
Shear Modulus: 14.26 (MPa)
Damping Ratio:
Free Vibration Decay: N/A
Half Power Bandwidth: 20.41 (%)

(b)

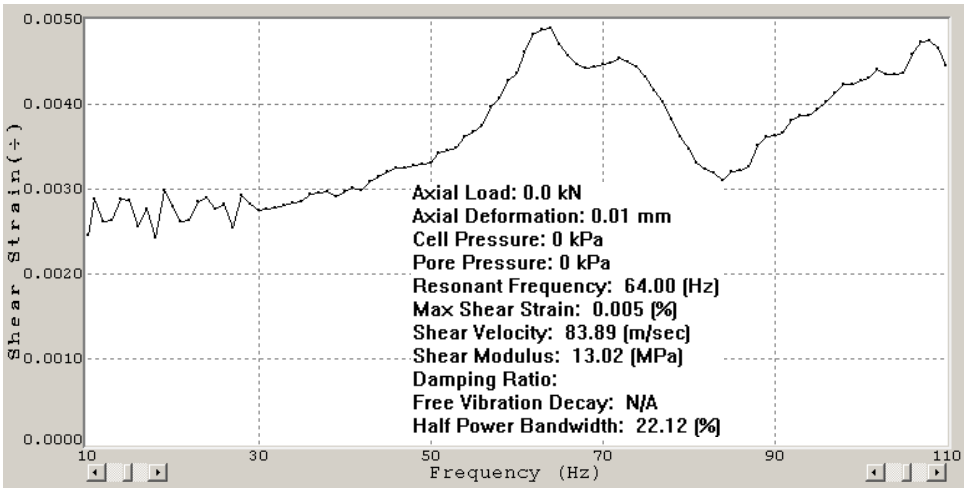
Shear Strain(÷)
0.0050
0.0040
0.0030
0.0020
0.0010
0.0000
10
30
50
70
90
110
Frequency (Hz)
Axial Load: 0.0 kN
Axial Deformation: 0.01 mm
Cell Pressure: 0 kPa
Pore Pressure: 0 kPa
Resonant Frequency: 64.00 (Hz)
Max Shear Strain: 0.005 (%)
Shear Velocity: 83.89 (m/sec)
Shear Modulus: 13.02 (MPa)
Damping Ratio:
Free Vibration Decay: N/A
Half Power Bandwidth: 22.12 (%)

(c)

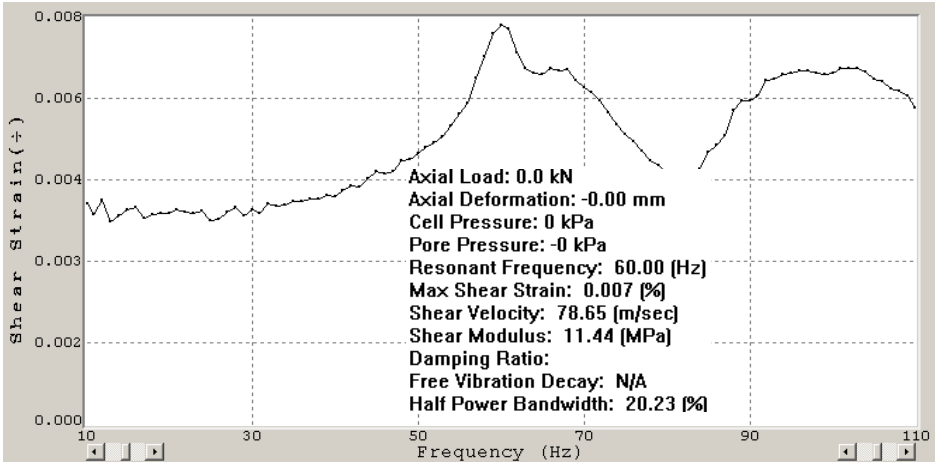

(d)

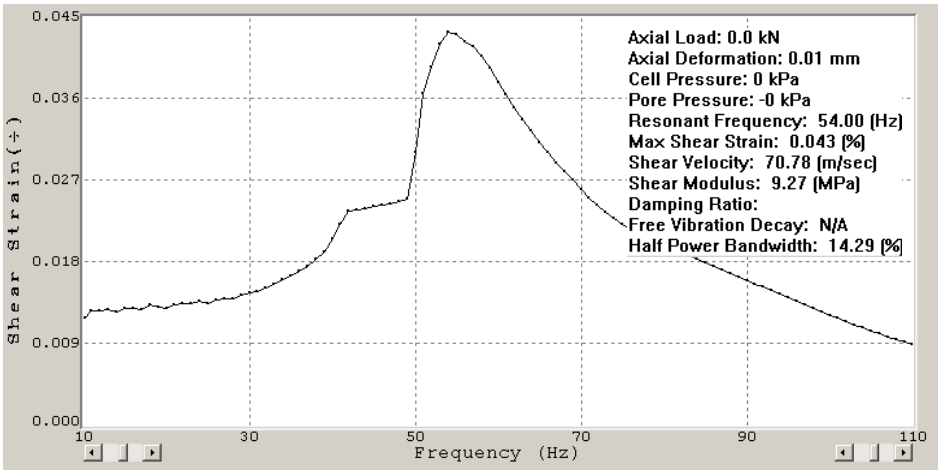

(e)

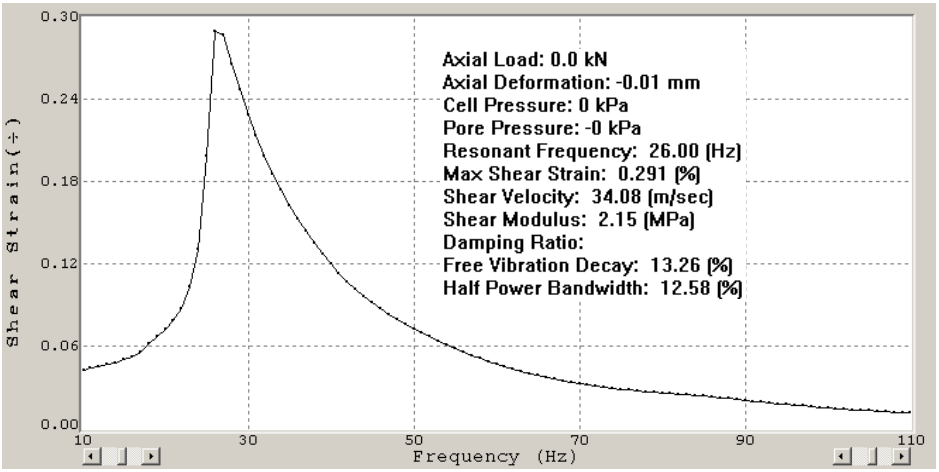

(f)

Figure F.4: Resonant frequency and shear modulus of sample BHUMR1-032 at different strain levels (a) psf=1%; (b) psf=2%; (c) psf=3%; (d) psf=4%; (e) psf=10%; (f) psf=20%.

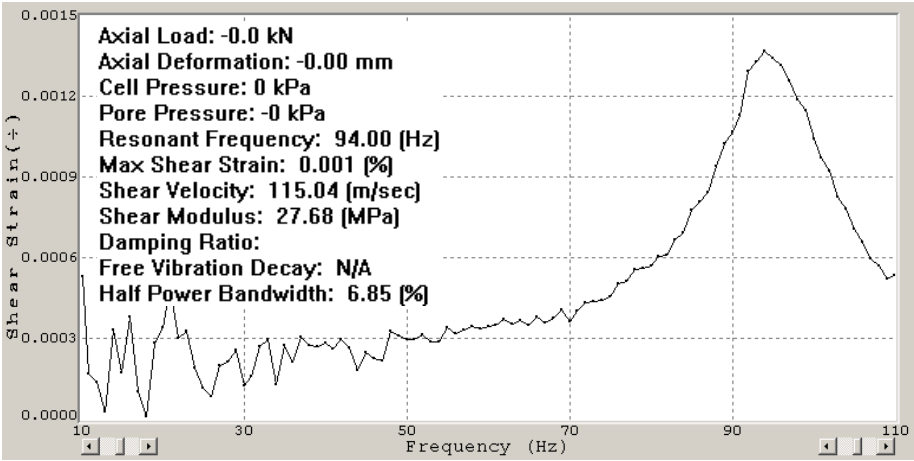
Axial Load: -0.0 kN
Axial Deformation: -0.00 mm
Cell Pressure: 0 kPa
Pore Pressure: -0 kPa
Resonant Frequency: 94.00 (Hz)
Max Shear Strain: 0.001 (%)
Shear Velocity: 115.04 (m/sec)
Shear Modulus: 27.68 (MPa)
Damping Ratio:
Free Vibration Decay: N/A
Half Power Bandwidth: 6.85 (%)
Shear Strain(÷)
0.0015
0.0012
0.0009
0.0006
0.0003
0.0000
10
30
50
70
90
110
Frequency (Hz)

(a)

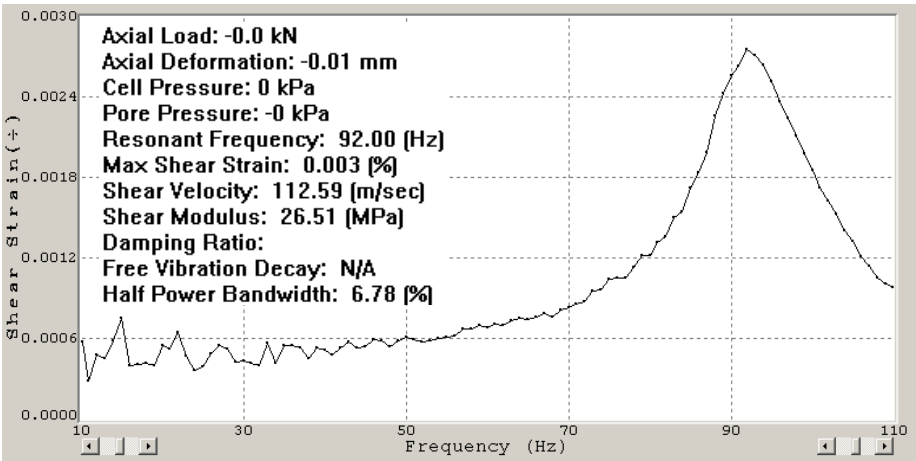
Axial Load: -0.0 kN
Axial Deformation: -0.01 mm
Cell Pressure: 0 kPa
Pore Pressure: -0 kPa
Resonant Frequency: 92.00 (Hz)
Max Shear Strain: 0.003 (%)
Shear Velocity: 112.59 (m/sec)
Shear Modulus: 26.51 (MPa)
Damping Ratio:
Free Vibration Decay: N/A
Half Power Bandwidth: 6.78 (%)
Shear Strain(÷)
0.0030
0.0024
0.0018
0.0012
0.0006
0.0000
10
30
50
70
90
110
Frequency (Hz)

(b)

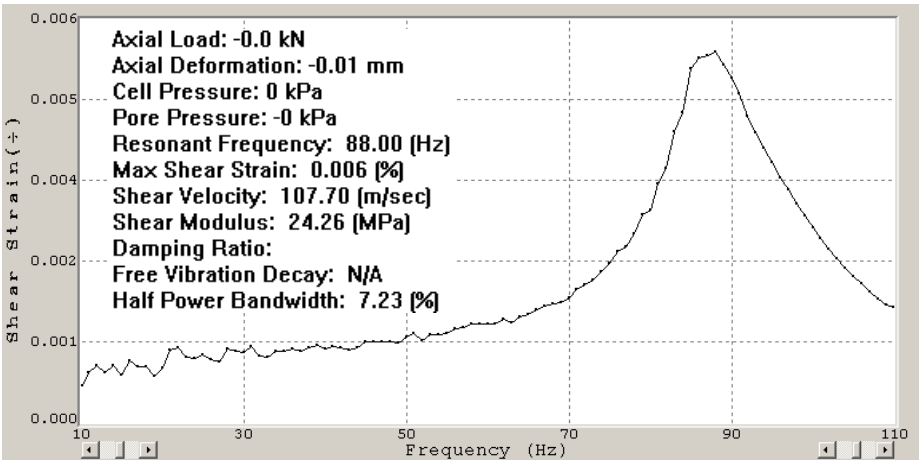
Axial Load: -0.0 kN
Axial Deformation: -0.01 mm
Cell Pressure: 0 kPa
Pore Pressure: -0 kPa
Resonant Frequency: 88.00 (Hz)
Max Shear Strain: 0.006 (%)
Shear Velocity: 107.70 (m/sec)
Shear Modulus: 24.26 (MPa)
Damping Ratio:
Free Vibration Decay: N/A
Half Power Bandwidth: 7.23 (%)
Shear Strain(÷)
0.006
0.005
0.004
0.002
0.001
0.000
10
30
50
70
90
110
Frequency (Hz)

(c)

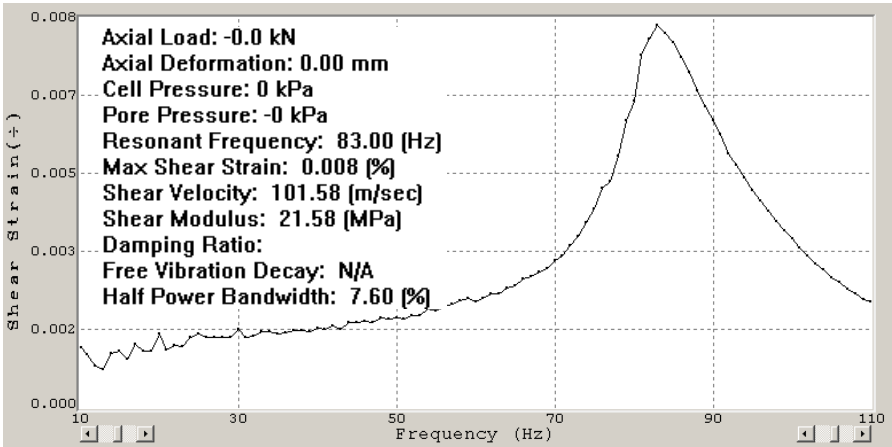
Axial Load: -0.0 kN
Axial Deformation: 0.00 mm
Cell Pressure: 0 kPa
Pore Pressure: -0 kPa
Resonant Frequency: 83.00 (Hz)
Max Shear Strain: 0.008 (%)
Shear Velocity: 101.58 (m/sec)
Shear Modulus: 21.58 (MPa)
Damping Ratio:
Free Vibration Decay: N/A
Half Power Bandwidth: 7.60 (%)
Shear Strain(÷)
0.008
0.007
0.005
0.003
0.002
0.000
10
30
50
70
90
110
Frequency (Hz)

(d)

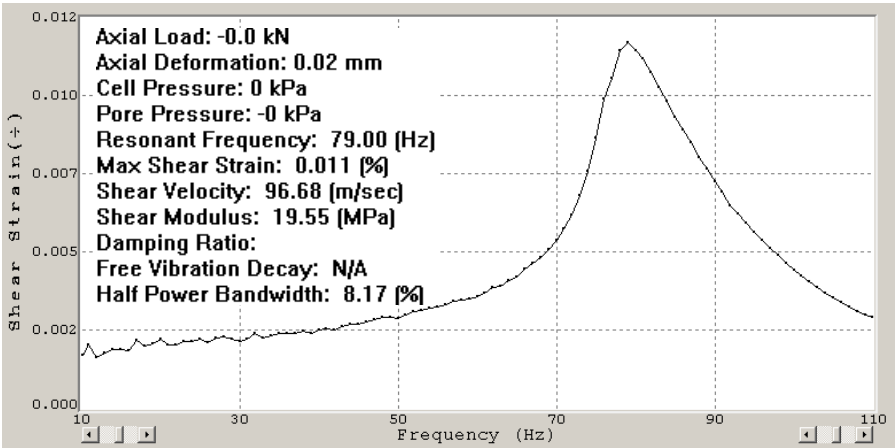
Axial Load: -0.0 kN
Axial Deformation: 0.02 mm
Cell Pressure: 0 kPa
Pore Pressure: -0 kPa
Resonant Frequency: 79.00 (Hz)
Max Shear Strain: 0.011 (%)
Shear Velocity: 96.68 (m/sec)
Shear Modulus: 19.55 (MPa)
Damping Ratio:
Free Vibration Decay: N/A
Half Power Bandwidth: 8.17 (%)
Shear Strain(÷)
0.012
0.010
0.007
0.005
0.002
0.000
10
30
50
70
90
110
Frequency (Hz)

(e)

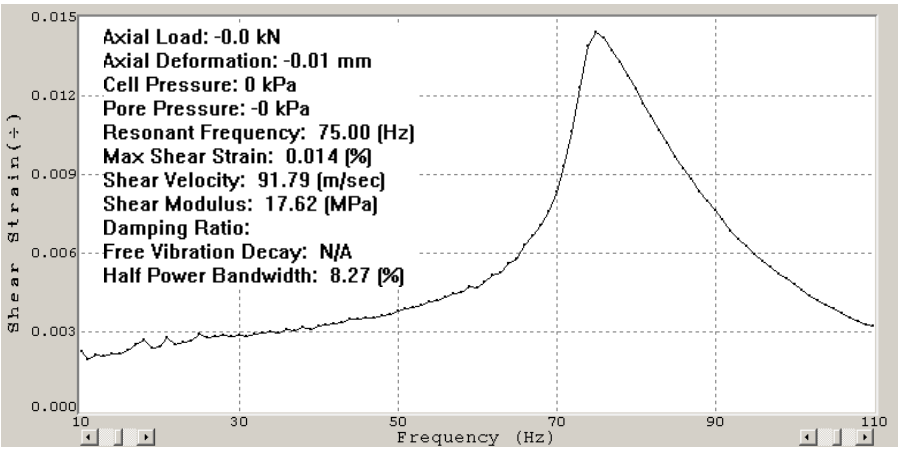
Axial Load: -0.0 kN
Axial Deformation: -0.01 mm
Cell Pressure: 0 kPa
Pore Pressure: -0 kPa
Resonant Frequency: 75.00 (Hz)
Max Shear Strain: 0.014 (%)
Shear Velocity: 91.79 (m/sec)
Shear Modulus: 17.62 (MPa)
Damping Ratio:
Free Vibration Decay: N/A
Half Power Bandwidth: 8.27 (%)
Shear Strain(÷)
0.015
0.012
0.009
0.006
0.003
0.000
10
30
50
70
90
110
Frequency (Hz)

(f)

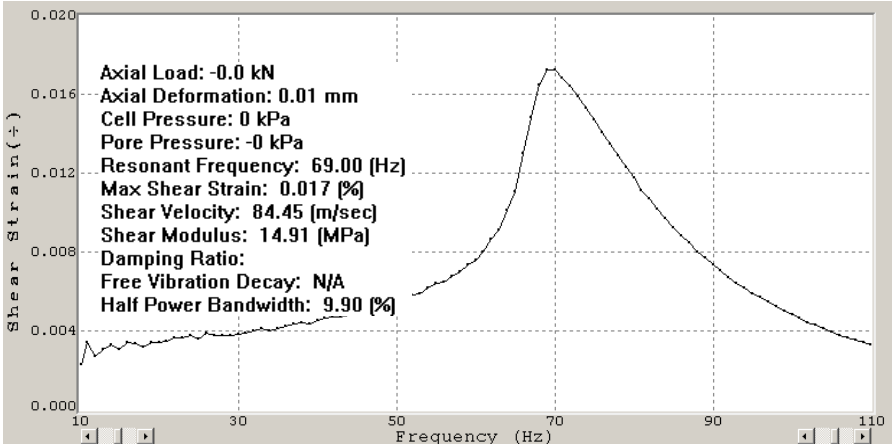

(g)

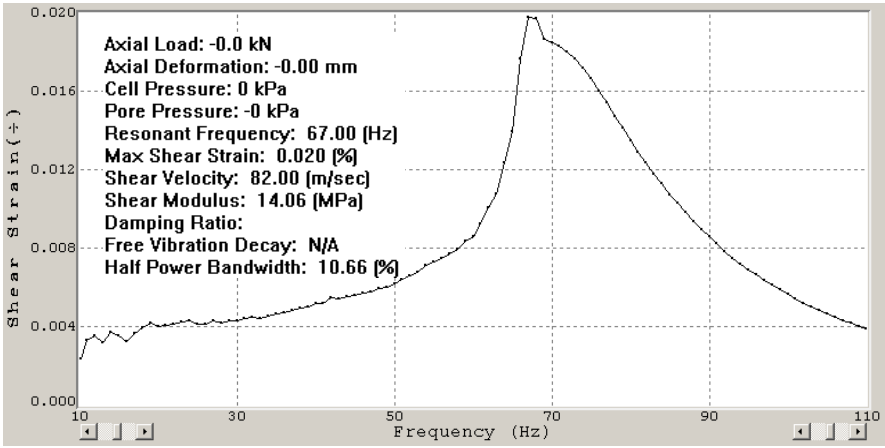

(h)

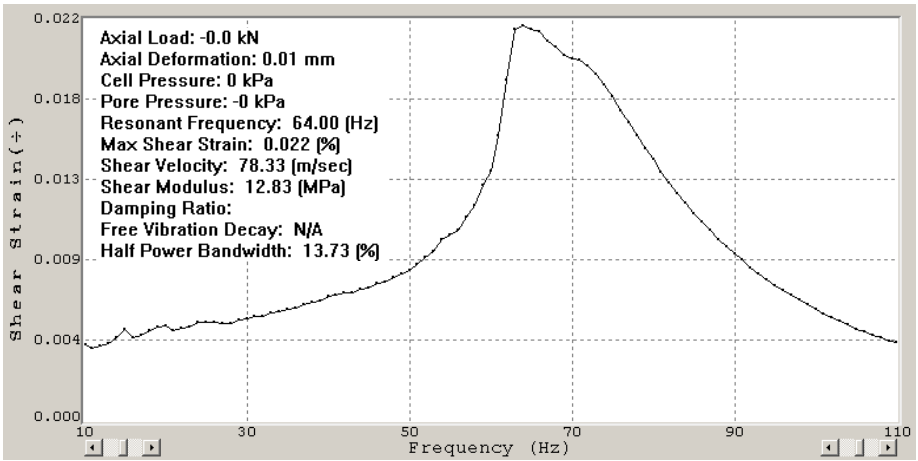

(i)

Figure F.5: Resonant frequency and shear modulus of sample CHUMR3-141 at different shear strain levels (a) psf=5%; (b) psf=10%; (c) psf=20%; (d) psf=30%; (e) psf=40%; (f) psf=50%; (g) psf=60%; (h) psf=70%; (i) psf=80%.